Rational Design, Manufacture and Evaluation of Respirable TB Subunit Vaccines

Shuai Shi

A dissertation submitted to the faculty of the University of North Carolina at Chapel Hill in partial fulfillment of the requirements for the degree of Doctor of Philosophy in the Eshelman School of Pharmacy.

Chapel Hill
2010

Approved by,

Dissertation advisor: Anthony J. Hickey, PhD, D.Sc

Committee chair: Jian Liu, PhD

Committee member: Xiao Xiao, PhD

Committee member: Miriam Braunstein, PhD

Committee member: Lucila Garcia-Contreras, PhD

ABSTRACT

Shuai Shi

Rational Design, Manufacture and Evaluation of Respirable TB Subunit Vaccines

(Under the direction of Dr. Anthony J. Hickey, PhD, D.Sc)

The purpose of this dissertation is to compare the *in vitro* immune response of newly designed respirable TB subunit vaccines based on Ag85B/TB10.4 and their different combinations in order to make a recommendation of the best antigen/antigen combination for future animal protection study. The second goal is to develop a particle size comparator to evaluate the batch-to-batch reproducibility of inhalation products.

Antigens were expressed and purified as soluble recombinants. The solubility of TB10.4 and TB10.4-Ag85B was dramatically improved by recombinant fusion to the C-terminal of a bacterial protein thioredoxin. A purification method involving three chromatographic steps and one enzymatic treatment was successfully developed to purify soluble TB10.4 and TB10.4-Ag85B to homogeneity. The secondary structure and melting temperature of Ag85B, TB10.4 and TB10.4-Ag85B were characterized by circular dichroism.

Purified soluble recombinant antigens were encapsulated into polylactide-co-glycolide (PLGA) microparticles by emulsion/spray-drying. By employing the concept of Quality-by-Design (QbD), the spray-drying parameters were successfully optimized to give the desired particle properties. Particle size was optimized to a target of 3 μm with a single mode and narrow size distributions. A mass median aerodynamic diameter (MMAD) of 3.3μm and a

fine particle fraction of 61.5% suggested that these particles are suitable for pulmonary delivery. PLGA microparticles encapsulating different antigens or antigen combination showed highly reproducible physicochemical properties such as size, surface charge and glass transition temperature. Moreover, antigen encapsulation did not compromise its integrity.

In vitro evaluation of TB subunit vaccines demonstrated that antigens encapsulated into PLGA microparticles induced much stronger and sustained Ag85B specific MHC II immune response compared to antigen solution formulations. Moreover, our data suggested that antigen blend of Ag85B and TB10.4 induced much better Ag85B response than antigen fusion TB10.4-Ag85B.

We also developed a particle size comparator to evaluate the batch-to-batch reproducibility of inhalation products based on orthogonal partial least square analysis (OPLS). It was shown that OPLS coupled with Pareto scaling gave the best performance in terms of consistency with the Product Quality Research Institute (PQRI) working group evaluation. In addition, OPLS-based comparator showed better performance than that based on chi-square ratio statistics proposed by PQRI.

ACKNOWLEDGEMENTS

In the past three years, many people have kindly offered me generous support. I want to thank everyone who helped me during my studies at University of North Carolina-Chapel Hill.

First, I would like to cordially thank each of my committee members. Dr. Jian Liu is my committee chair who offered me tremendous support during my PhD study. He offered me his lab equipment such as FPLC to purify antigens and gave me a platform to perform my early part of research. He also supported me with his intelligence. I learnt a lot after helpful discussions with him. He is also a good mentor who points the direction I would like to pursue. Dr. Miriam Braunstein gave me a lot of help on cell culture. She strengthened my understanding of immunology. Dr. Lucila Garcia-Contreras helped me understand spray-drying technique. Without her assistance, I can't imagine I can make a success with particle manufacturing. Dr. Xiao Xiao is always nice to me. He continuously stimulated my research interest. Discussion with him is always helpful to me.

I would not get this far without the guidance of my advisor, Dr. Anthony J. Hickey. First, he offered me an opportunity to work with him three years ago when I was in a tough time. Second, he offered me enough research freedom to select my interested research project. Third, he continuously supported my project with research funding. His willingness to talk with me through every situation made my PhD life much easier. Without his generous support, I can't achieve such progress in this short period of time. Moreover, his positive

attitude towards science and life will definitely influence my professional career.

I also want to thank some people who gave me technical assistance. I am indebted to Dr. Laleh Majlessi at Pasteur Institute, who kindly offered me the YB8 CD8 T-hybridoma, without which studying TB10.4 response was impossible. Dr. Majlessi also helped me learn immunology. I also want to acknowledge Dr. Henry Boom from Case Western Reserve University, who provided us a CD4 T-hybridoma to study Ag85B specific immune response. I greatly appreciate the technical assistance offered by Amar Kumbhar for SEM imaging and Dr. Ashutosh Tripathy for circular dichroism analysis. I want to thank Dr. Thomas O'Connell for helping me learn orthogonal partial least square analysis.

I also want to acknowledge a number of my friends here. They are Yang Zhou, Pingjie Xiao, Ping Ma, Dongyun Liu, Lan Feng, Kai Li, Yongmei Yu, Lan Yu, Chenchen Wang, Zhen Xu, Hailing Wang, and Bo He. They all contribute to my progress and achievement.

Finally, I am grateful to my family. My wonderful wife, Dengyun Sun, has supported my PhD study all way through. Without her encouragement, assistance and understanding, I would not achieve this rapid progress. My father and mother have been very supportive in the past three years. Thank you to all of them!!!

TABLE OF CONTENTS

LIST OF TABLES xiii

LISTOF FIGURES xiv

LIST OF ABBREVIATIONS AND SYMBOLS xvi

Chapter

1 INTRODUCTION 1

1.1 General introduction 1

1.1.1 *Mycobacterium tuberculosis* (*MTB*): the pathogen of tuberculosis 2

1.1.1.1 Physiology of *MTB* 2

1.1.1.2 Transmission of *MTB* 3

1.1.1.3 Infection of *MTB* 4

1.1.2 Alveolar macrophage host defense against *Mycobacterium tuberculosis* 5

1.1.2.1 Recognition of *M. tuberculosis* by alveolar macrophage 5

1.1.2.2 Macrophage defense mechanisms against *M. tuberculosis* 6

1.1.2.3 Effect of cytokines on macrophages 7

1.1.3 Interaction of *Mycobacterium tuberculosis* with dendritic cells 8

1.1.3.1 Recognition of *M. tuberculosis* by dendritic cells 8

1.1.3.2 Activation of dendritic cells 9

1.1.3.3 Immune activation by *M. tuberculosis* infected dendritic cells 9

1.1.4 Bacillus Calmette-Guérin (BCG) and its drawbacks 10

1.1.5 Advances in tuberculosis vaccine strategies 11

1.1.5.1 Modified BCG 11

1.1.5.2 Modified *MTB* 13

1.1.5.3 Naked DNA and viral-vectored vaccines 14

1.1.5.4 Subunit vaccines..... 15

1.1.6 Antigen candidates for TB subunit vaccine 16

1.1.6.1 Ag85B 16

1.1.6.2 TB10.4..... 17

1.1.7 Rationale for pulmonary vaccine delivery 18

1.1.7.1 Immune responses induced by pulmonary vaccination 19

1.1.7.2 Current status of pulmonary vaccine delivery 21

1.1.8 Pulmonary vaccine delivery by aerosol technology..... 22

1.1.9 Dry-powder vaccine formulation 23

1.1.9.1 Antigens: the active ingredient of a dry-powder formulation 24

1.1.9.2 Adjuvants: the active excipient of a dry-powder formulation 24

1.1.9.3 Particulate systems 25

1.1.9.4 Dispersion of vaccines with carrier excipient 29

1.1.10 Particle size characterization of dry powders..... 30

1.1.11 Particle size comparator to evaluate batch-to-batch reproducibility of inhalation products..... 33

1.2 Problem statement 34

1.3 Hypotheses and specific aims..... 36

1.3.1 Research goals..... 36

1.3.2 Hypotheses 36

1.3.3 Specific aims 36

1.4 Summary 38

2 RECOMBINANT ANTIGEN DESIGN, EXPRESSION, PURIFICATION AND CHARACTERIZATION 43

2.1 Introduction 44

2.2 Materials and Methods 46

2.3 Results 51

2.3.1 Production of soluble Trx-TB10.4 and TB10.4 51

2.3.2 TB10.4 exists as an oligomer 51

2.3.3 Effect of pH on Trx-TB10.4 and TB10.4 stability 52

2.3.4 Production of soluble Trx-TB10.4-Ag85B and TB10.4-Ag85B 52

2.3.5 Increasing the yield of Trx-TB10.4-Ag85B by co-expression of chaperon proteins 53

2.3.6 Purification of Trx-TB10.4-Ag85B and TB10.4-Ag85B from the inclusion body 53

2.3.7 Study antigen secondary structure and thermal stability by circular dichroism 53

2.4 Discussion 55

2.5 Summary 59

3 MANUFACTURE AND CHARACTERIZATION OF RESPIRABLE PLGA-rAg MICROPARTICLES 76

3.1 Introduction 77

3.2 Materials and Methods 82

3.3 Results 86

3.3.1 Half-factorial design for optimization of spray-drying parameters 86

3.3.2 Analysis of spray-drying parameters with respect to

size and yield respectively 87

3.3.3 Simultaneous optimization of spray-drying parameters 88

3.3.4 Morphology analysis of spray-dried microparticles 88

3.3.5 Particle size analysis of microparticles 89

3.3.6 Flow property of microparticles 89

3.3.7 Effect of scanning rate on the glass transition temperature of microparticles 90

3.3.8 Thermal characterization of PLGA-rAg formulations and MDP 91

3.3.9 Surface energy and charge characterization of microparticles 91

3.3.10 Effect of spray-drying on antigen integrity 91

3.3.11 Release profiles of microparticles 92

3.4 Discussion 92

3.5 Summary 95

4 STUDY OF *IN VITRO* IMMUNE RESPONSES INDUCED BY PLGA-rAg MICROPARTICLES 111

4.1 Introduction 112

4.2 Materials and Methods 114

4.3 Results 117

4.3.1 PLGA-rAg induced Ag85B specific MHC II immune response 117

4.3.2 Kinetic study of PLGA-rAg induced Ag85B specific MHC II immune response 117

4.3.3 Study of TB10.4 specific MHC I immune response 118

4.4 Discussion 119

4.5 Summary 122

5 DEVELOPMENT OF A PARTICLE SIZE COMPARATOR

TO EVALUATE BATCH-TO-BATCH REPRODUCIBILITY OF INHALATION PRODUCTS 128

5.1 Introduction 129

5.2 Methods 132

5.3 Results and Discussion 133

5.3.1 Monte Carlo simulation to recover 55 realistic scenarios of aerodynamic particle size distribution profiles 133

5.3.2 Comparison of chi-square ratio statistics and orthogonal partial least square analysis with respect to profile comparison 134

5.3.3 Orthogonal partial least square analysis of test and reference profiles 135

5.3.4 Studying 55 realistic scenarios with orthogonal partial least square analysis 136

5.3.5 Effect of different data pretreatment methods on the performance of orthogonal partial least square analysis 137

5.3.6 Three scenarios mis-predicted by orthogonal partial least square analysis 139

5.3.7 Orthogonal partial least square analysis of mass deposition on partial deposition sites 139

5.4 Summary 140

6 DISCUSSION AND FUTURE STUDIES 154

6.1 Milligram quantities of soluble recombinant antigens can be obtained by rational design of the expression constructs 156

6.2 Respirable PLGA-rAg microparticles can be manufactured with a target size by optimizing the spray-drying parameters 157

6.3 PLGA-rAg microparticles can induce stronger and prolonged immune response *in vitro* compared to antigen solutions 159

6.4 Particle size comparator constructed on the basis of orthogonal partial least square analysis has a better performance than that developed on the basis of chi-square ratio statistics 159

6.5 General conclusions..... 159

6.6 Future studies..... 161

6.7 Concluding remarks..... 165

REFERENCES 167

LIST OF TABLES

Table 1.1 Summary of new-generation tuberculosis vaccines 40

Table 1.2 Expression of four proteins belonging to the ESAT6 family in different mycobacterium strains 41

Table 2.1 Summary of recombinant antigens 61

Table 3.1 Half-factorial design (2^{5-1}) to optimize spray-drying parameters 96

Table 3.2 Particle size and surface charge characterization of spray-dried microparticles 97

Table 3.3 Thermal characterization of spray-dried microparticles 98

Table 5.1 Equivalence value determined from different analysis methods and the working group evaluation 142

LIST OF FIGURES

Figure 1.1 Particle size characterization of micafungin aerosol by Anderson cascade impactor... 42

Figure 2.1 Construct design for recombinant antigens 62

Figure 2.2 Purification of TB10.4 by nickel-affinity and size-exclusion chromatography. 63

Figure 2.3 SDS-PAGE and native-PAGE analysis of recombinant antigens 65

Figure 2.4 Effect of buffer pH on antigen stability 66

Figure 2.5 SDS-PAGE analysis of recombinant fusion antigens 67

Figure 2.6 Purification of TB10.4-Ag85B by nickel-affinity and size-exclusion chromatography 68

Figure 2.7 Comparison of the yield of two recombinant antigens with or without the co-expression of chaperons 69

Figure 2.8 Purification of Trx-TB10.4-Ag85B from inclusion body 70

Figure 2.9 Structures of Ag85B and TB10.4 71

Figure 2.10 Study antigen secondary structure and thermal stability by circular dichroism. 72

Figure 3.1 Optimization of spray-drying parameters 99

Figure 3.2 Morphology analyses of spray-dried microparticles 101

Figure 3.3 Aerodynamic particle size analysis of spray-dried microparticles prepared under optimized conditions 103

Figure 3.4 Effect of scanning rate on the glass transition temperature (Tg) of three PLGA formulations 104

Figure 3.5 Thermal characterization of different PLGA-rAg formulations and MDP by DSC 107

Figure 3.6 Characterization of surface free energy of microparticles. 108

Figure 3.7 SDS-PAGE analysis of antigen integrity after spray drying. 109

Figure 3.8 Release profile of microparticles. 110

Figure 4.1 Schematic description of two *in vitro* antigen presentation assays. 123

Figure 4.2 Comparison of Ag85B specific MHC II immune response induced by different formulations after 1-day antigen exposure 124

Figure 4.3 Kinetic study of Ag85B specific MHC II immune response 125

Figure 4.4 Titration of TB10.4 specific MHC I response with various concentrations of homologous TB10.4 peptide 126

Figure 4.5 MHC I and II antigen presentation pathways 127

Figure 5.1 Reconstituted aerodynamic particle size distribution profiles for scenario 13c and scenario 2bb2 144

Figure 5.2 Comparison of chi-square ratio statistics and orthogonal partial least square analysis 145

Figure 5.3 Score plot of orthogonal partial least square analysis to compare reference and test profiles generated by Monte Carlo simulation 147

Figure 5.4 Differences between the working group (WG) assessment and statistical analyses based on different methods and data pretreatment 150

Figure 5.5 Comparison of the performance of the combination test (chi-square plus ISM-PBE) with that of orthogonal partial least square analysis based on Pareto scaling 153

LIST OF ABBREVIATIONS AND SYMBOLS

APC	antigen presenting cell
APSD	aerodynamic particle size distribution
BCG	Bacillus Calmette-Guérin
BSA	bovine serum albumin
CARD	caspase activation and recruitment domain
CCI	Carr's compressibility index
CD	circular dichroism
CFA	complete Freund's adjuvant
CMD	count median diameter
CMI	cell mediated immune
CR3	complement receptor 3
CT	cholera toxoid
DC	dendritic cells
DLS	dynamic light scattering
DPI	dry-powder inhaler
DSC	differential scanning calorimetry
E. coli	*Escherichia coli*
FDA	Food and Drug Administration
FPLC	fast protein liquid chromatography

GSD	geometric standard deviation
HIV	human immunodeficiency virus
IB	inclusion body
IFN-γ	interferon-gamma
IGC	inverse gas chromatography
IL-2	interleukin-2
iNOS	inducible nitric oxide synthease
IPTG	isopropyl-β-thiogalactopyranoside
ISM	impactor-sized mass
LB	Luria-Bertani
LMD	length median diameter
LPS	lipopolysaccharide
MALT	mucosa-associated lymphoid tissue
M-cell	microfold cell
MDP	muramyl dipeptide
MDR-TB	multidrug-resistant tuberculosis
MHC	major histocompatibility complex
MMAD	mass median aerodynamic diameter
MPL	monophosphoryl lipid A
MR	mannose receptor
MTB	*Mycobacterium tuberculosis*

OINDP	orally inhaled and nasal drug product
OPLS	orthogonal partial least square analysis
PBE	population bioequivalence
PBS	phosphate buffered saline
PCS	photon correlation spectrometry
PEI	polyethyleneimine
PLGA	polylactide-co-glycolide
pMDI	pressurized metered-dose inhaler
PMN	polymorphonuclear leukocyte
PMSF	phenylmethylsulphonyl fluoride
PNAP	porous nanoparticle-aggregate particle
PQRI	Product Quality Research Institute
PrP	prion protein
QbD	Quality-by-Design
SDS	sodium dodecyl sulfate
SMD	surface median diameter
TB	tuberculosis
Tg	glass transition temperature
THF	tetrahydrofuran
TLR	Toll-like receptors
TMM	trehalose 6-monomycolate

TNF-α	tumor necrosis factor-α
Trx	thioredoxin
UV	unit-variance
VMD	volume median diameter
WG	working group
WHO	World Health Organization

CHAPTER 1: INTRODUCTION

1.1 General introduction

Tuberculosis (TB) poses a significant risk to the global public health. According to the World Health Organization (WHO) report 2009 (1), there were an estimated 9.27 million cases of TB in 2007. Most of the cases were from Asia (55%) and Africa (31%), with small proportions from the European region (5%) and the regions of Americas (3%). Although the number of cases per capita has been falling since 2004, the total number of TB cases increased in absolute terms due to population growth (1).

Among the 9.27 million cases in 2007, it was estimated that 1.37 million (14%) were HIV-positive with majority of these cases in the African region and the Southeast Asia region. Of HIV-negative cases of TB in 2007, there were an estimated 1.3 million deaths. An additional 456, 000 deaths occurred among HIV-positive incident TB cases (1). TB is a major cause of death for people who are also infected by HIV and HIV is the main reason for the failure of TB control in high HIV settings (2).

TB treatment requires a lengthy drug therapy which employs a combination of antibiotics such as rifampicin, isoniazid, ethambutol and pyrazinamide (3). Most TB regimens have an initial high-intensity phase followed by a continuation phase (4). Improper use of antibiotics is the main reason for the emergence of multidrug-resistant tuberculosis (MDR-TB) and extensively drug-resistant tuberculosis (XDR-TB) (3, 5). There is evidence for the evolution from susceptible strain to MDR and then to XDR tuberculosis over a period of slightly more than a decade (6). Acquisition of resistance results from genetic mutations in

specific resistance-determining regions in the genome of *Mycobacterium tuberculosis* (*MTB*) (7, 8). Chan *et al.* suggested a multifaceted approach to prevent a more widespread epidemic of MDR-TB and XDR-TB, which includes a) rapid diagnostic assays to detect drug-resistant TB and b) development of new drugs to treat all forms of TB in a shorter period of time (9).

Approximately 2 billion people are currently infected by *MTB*. In the next 10 years, it is estimated that nearly 1 billion people will be infected by *MTB* and develop the latent form of TB, 200 million people will exhibit the active disease, and 35 million people will die from infection (1). Unfortunately, the only commercially available vaccine against TB, Bacillus Calmette-Guérin (BCG), does not afford complete protection (10). Protection conferred by BCG during childhood wanes after approximately 10 to 15 years (11). Even more discouragingly, boosters of BCG with repeated doses did not provide additional protection as demonstrated in a clinical trial (12). In light of the drawbacks of BCG, a spectrum of new-generation TB vaccines have been developed and studied, including modified BCG (13, 14), modified *MTB* (15, 16), naked DNA vaccine (17), viral-vectored vaccine (18), and subunit vaccine (19).

1.1.1 *Mycobacterium tuberculosis* (*MTB*): the pathogen of tuberculosis

1.1.1.1 Physiology of *MTB*

Mycobacterium tuberculosis (*MTB*), the causative organism of tuberculosis, is a rod-shaped bacterium that is 0.2-0.3 μm in width and 2-5μm in length (20). This bacterium requires oxygen to grow and is classified as an obligate aerobe. Therefore, in the classic case of tuberculosis, *MTB* is always found in the well-aerated upper lobes of the lung. *MTB* has very slow multiplication time of 15-20 hours, which is extremely slow compared to other bacteria (e.g. *Escherichia coli* (*E. coli*) divides roughly every 20 minutes).

The cell wall structure of *MTB* is very unique among other prokaryotes. *MTB* is surrounded by a thin layer of cytoplasmic membrane and a second layer of peptidoglycan and lipids (21). The lipid fraction of cell wall mainly consists of three components: 1) mycolic acids, 2) cord factor and 3) wax-D. Mycolic acids are unique alpha-branched fatty acids, which can make up 50% of the dry weight of *MTB* cell wall (22). The lipid shell formed by the strong hydrophobic mycolic acid regulates the permeability properties at the cell surface of *MTB* and affects the outcome of Gram staining. It is believed that mycolic acids are pivotal determinant of *MTB* virulence probably by preventing *MTB* from attack by oxygen radicals, cationic proteins, and lysozyme in the phagocytic granules of macrophages (23). Mycolic acids may also protect extracellular mycobacteria from complement deposition in blood (23). Cord factor was first associated with virulent strains of *MTB* by Robert Koch, who observed that cells in smears made from *in vitro*-grown colonies often formed distinctive serpentine cords. Trehalose dimycolate (cord factor) is responsible for the serpentine cording mentioned above. Cord factor, produced mostly abundantly by virulent strains of *MTB*, is also toxic to mammalian cells and is an inhibitor of polymorphonuclear leukocytes (PMN) migration (24). Wax-D is the major component of Freund's complete adjuvant (CFA) (24). Generally, many properties of *MTB* have been associated with the high concentration of lipids in the cell wall including 1) impermeability to stains, 2) resistance to antibiotics, 3) resistance to acidic and alkaline compounds, 4) resistance to complement deposition, and 5) resistance to lethal oxidations in macrophages.

1.1.1.2 Transmission of *MTB*

Tuberculosis (TB) transmits through the air. People who are afflicted with active TB in their lungs are infectious. When these people sneeze, cough or spit, they expel infectious

aerosol droplets containing TB microorganisms, known as bacilli, into the air. Once a small number of these droplets are inhaled by healthy individuals, they may become infected because the dose of *MTB* to produce infections in human is very low. People with frequent and prolonged contact with TB patients have a higher risk of becoming infected, with an estimated infection rate of 22% (25). People at high risk also include those who inject drugs using unsanitary needles, patients in immunocompromised conditions such as HIV-positive patients, people who use immunosuppressant drugs, and children exposed to adults in high-risk categories (1).

1.1.1.3 Infection of *MTB*

It has been shown in single case contact studies that only 20-50% of individuals that are exposed to *MTB* become infected (26). Around 5% of these infected people develop pulmonary disease or other clinical form of TB over a period of 2-5 years. However, the other 95% of infected people develop latent TB infection. Individuals with latent TB infection have an approximately 5% lifetime chance of reactivation, leading to the development of clinical TB (26). When the infection becomes active, 75% of the cases are pulmonary TB and the other 25% of the cases are collectively denoted extrapulmonary TB (25). The infection sites of extrapulmonary TB include the central nervous system in meningitis, the genitourinary system in urogenital tuberculosis, and bones and joints in Pott's disease. In the most serious TB infection, miliary tuberculosis, the bacteria are disseminated throughout the system.

The development of pulmonary TB can be characterized by several stages. In the first stage, inhaled *MTB* may multiply or may be eliminated by alveolar macrophages before the emergence of any lesion. Second, small caseous lesions may heal or stabilize before

detectable or may progress to the next stage. Third, large caseous lesions may grow locally or shed bacteria into the lymph and blood leading to secondary lung lesions, or they may heal or stabilize. Alternatively, caseous lesions may liquefy and introduce bacteria into the bronchial tree, making disease control more difficult (27). Generally speaking, the disease progress from one stage to the next is associated with weaker host defense.

1.1.2 Alveolar macrophage host defense against *Mycobacterium tuberculosis*

1.1.2.1 Recognition of *M. tuberculosis* by alveolar macrophage

M. tuberculosis infects alveolar macrophages and multiplies inside the cellular compartment of macrophages (28). Meanwhile, the macrophage plays a very important role in host innate immune response against *M. tuberculosis* infection.

In human macrophages, the primary receptors for *MTB* are the mannose receptor (MR), the complement receptor 3 (CR3) and the Toll-like receptors (TLR) (29, 30). Among them, TLRs are mostly studied. TLRs constitute a family of proteins, known as pattern recognition receptors, for the detection of *MTB* ligands and initiation of subsequent inflammatory immune responses (31, 32). TLR 2, as a heterodimer with TLR 1 or TLR 6, recognizes a triacylated lipoprotein from *MTB*; whereas TLR9 recognizes bacterial CpG DNA. It has been shown by several studies that TLR2 played a central role in *MTB* recognition (33-35). Recognition of *MTB* by TLRs ultimately activates NF-κB leading to the production of inflammatory cytokines and generation of antimicrobial activity (36-38).

In contrast to cell surface pattern recognition molecules such as TLRs, the nucleotide oligomerization domain (NOD)-like receptor, NOD 2, serves as a cytoplasmic sensor for *MTB* (39). NOD 2 is a cytoplasmic protein containing a central nucleotide-binding domain, a leucine-rich region, and two caspase activation and recruitment domains (CARD). NOD 2

recognizes intracellular muramyl dipeptide (MDP), which is a peptidoglycan found on *MTB* (40, 41). Upon recognition, NOD 2 mediates the production of cryptdins or α-4 defensins (42), which exert bactericidal effect against *MTB*. In addition, NOD 2 also induces inflammatory response against *MTB* infection. It has been shown that NOD 2 plays a non-redundant role in *MTB* recognition (43).

1.1.2.2 Macrophage defense mechanisms against *M. tuberculosis*

Alveolar macrophages employ several defense mechanisms to combat *MTB*. Nitric oxide, produced by the inducible nitric oxide synthase (iNOS), has powerful and necessary antimycobacterial activity in the mouse model of tuberculosis infection (44-46). However, the importance of iNOS and nitric oxide in killing *MTB* is still questionable in human macrophages (37, 47). It has been shown in one study that TLR induced antimicrobial activity in human macrophages was not dependent on iNOS activity and nitric oxide could not be detected in these infected cells (37). This suggests that human macrophages may employ a nitric oxide independent antimicrobial mechanism to combat *MTB*.

Autophagy is another defense mechanism employed by macrophages (48). Macrophages stimulated with key cytokines such as interferon-gamma (IFN-γ) undergo autophagy which is necessary for the antimicrobial activity against *MTB* (48). In a separate study, hydrolyzed ubiquitin peptides showed direct antimicrobial activity against *MTB* (49). This activity was delivered in an autophagy dependent manner to phagosomes sequestering *MTB* (49).

Vitamin D has also been suggested to induce antimicrobial activity in human macrophages. Treating *MTB* infected human macrophages with active vitamin D reduced the intracellular bacterial load; however, the concentration of vitamin D was above the

physiological concentrations in these experiments (50, 51). Further studies suggested that vitamin D induced antimicrobial activity was regulated by phosphatidylinositol-3 kinase and mediated by the production of oxygen intermediates *via* NADPH-dependent phagocyte oxidase (52).

1.1.2.3 Effect of cytokines on macrophages

Pro- and anti-inflammatory cytokines induced by innate and acquired immune response to *MTB* have distinct effects on macrophages. Successful outcome of *MTB* infection does not depend on a single cytokine but on cytokine networks established and maintained by macrophages and other immunocytes. Two important cytokines are reviewed below.

Tumor necrosis factor-α (TNF-α) is a pro-inflammatory cytokine produced by macrophages upon exposure to microbial products derived from *MTB* (53). TNF-α activates macrophages to produce nitric oxide synthase 2 (NOS 2), an enzyme catalyzing the synthesis of nitric oxide, assisting infected macrophages to kill intracellular *MTB* (54, 55). It has been shown that mice deficient in TNF-α or TNF-α receptor had increased susceptibility to *MTB* and impaired granuloma formation upon infection (56, 57). The importance of this cytokine has also been demonstrated in humans since patients treated with TNF-α inhibitors were more susceptible to tuberculosis (58).

Interferon-gamma (IFN-γ) is a prototypic cytokine of Th1 immune response. This cytokine plays an essential role in effective TB control (28). IFN-γ is produced by CD4+, CD8+ T cells and NK cells (28). It stimulates antimicrobial activity by two mechanisms: 1) the induction of NOS and subsequent release of nitric oxide in macrophages (28, 59), and 2) the induction of macrophage autophagy (48). Mice that failed to produce this cytokine had disseminated *MTB* infection upon aerosol or intravenous *MTB* challenge (60, 61). In humans,

the polymorphism in the IFN-γ promoter region is significantly associated with the susceptibility to develop active TB disease, which has been observed in several clinical studies (62-65).

1.1.3 Interaction of *Mycobacterium tuberculosis* with dendritic cells

1.1.3.1 Recognition of *M. tuberculosis* by dendritic cells

Although alveolar macrophages serve as the long-term hosts for mycobacterium, *MTB* infects dendritic cells (DCs) as well. This interaction is pivotal for the development of protective immunity against *MTB* (66, 67).

There is considerable evidence that mycobacteria and mycobacterial antigens can be phagocytosed by DCs (68). DCs lining the trachea may be one of the first cells that encounter *MTB*. A number of surface molecules have been considered to play an important role in the recognition of *MTB* by DCs including CD11b, CD11c, DEC-205, mannose receptor (MR) and DC-specific ICAM-3 Grabbing Non-integrin (DC-SIGN) (30, 69-72). DC-SIGN serves as a pattern recognition receptor for *MTB*. Depletion of this molecule with specific antibodies inhibits the interaction of DCs with mycobacteria, although other surface molecules are also expressed by DCs at high levels (73). This suggests that DC-SIGN is a preferred receptor on DCs for *MTB* recognition and interaction.

DCs also take up mycobacterial antigens in a process termed cross-priming (74). Apoptosis of *MTB* infected macrophages produces extracellular vesicles containing glycolipids and protein antigens derived from *MTB*. These vesicles are taken up by DCs and mycobacterial antigens are presented in the context of major histocompatibility complex (MHC) class I and MHC class II molecules produced by DCs.

1.1.3.2 Activation of dendritic cells

Phagocytosis of *MTB* by DCs results in the activation of NF-κB pathway which ultimately leads to the secretion of inflammatory cytokines and chemokines and the release of reactive oxygen and nitrogen intermediates (75, 76). Activation of NF-κB has also been implicated in the modulation of surface phenotype of infected DCs (77). *MTB* infection leads to increased surface expression of a number of molecules, for instance, MHC I, MHC II, CD40, CD54, CD 80 that are involved in the interaction with T cells (78-81).

Once being infected by *MTB* or cross-primed by *MTB* antigens, DCs migrate to the nearest draining lymph node. During migration, DCs undergo a process of 'maturation' characterized by reduced capability of phagocytosis yet increased surface expression of MHC I/II and costimulatory molecules (82).

1.1.3.3 Immune activation by *M. tuberculosis* infected dendritic cells

Infected DCs present class I and class II epitopes of *MTB* in the complex of MHC I and MHC II molecules. Presented epitopes are recognized by corresponding naïve CD8+ and CD4+ T cells which express specific T cell receptors. Upon this mutual recognition and with the help of cytokines and costimulatory molecules expressed by DCs, CD4+ and CD8+ T cells are activated through a cascade of signal transductions followed by clonal expansion of T cells (82).

Activated T cells circulate to the vicinity of infection sites and serve as effector cells by either activating diverse antimicrobial mechanisms inside infected macrophages (75, 76) or contributing to the formation of granuloma to contain the intracellular mycobacteria in a state of dormancy (83). It is generally accepted that CD4+ T cells are the pivotal component of protective immunity against tuberculosis since depletion of this cell population resulted in

loss of control of *MTB* growth (28). However, the contribution of CD8+ T cells to protective immunity against *MTB* is still controversial (84). Mice genetically deficient in β 2-microglobulin and, therefore, with impaired CD8+ T cells failed to control *MTB* infection in one study (85). However, in a recent study, knockout mice deficient in both CD4+ and CD8+ T cells, CD8+ T cells or CD4+ T cells were infected via aerosol *MTB* and monitored for survival rate and ability to control infection (86). The conclusion of this study suggested that CD8+ T cells were dispensable and not essential for the control of infection.

The importance of CD8+ T cells is again confounded by another factor: host differences (84). In one study, human CD8+ T cells recognizing *MTB*-infected macrophages had the ability to directly kill intracellular *MTB* by a granule-associated protein, granulysin, which is toxic to the mycobacteria (87, 88). However, mice do not have a granulysin homologue. Therefore, data from mice studies suggesting that CD8+ T cells are not essential for *MTB* control must take into account this missing mechanism.

1.1.4 Bacillus Calmette-Guérin (BCG) and its drawbacks

BCG is the only commercially available vaccine against tuberculosis that is prepared from a strain of attenuated live bovine bacillus, *Mycobacterium bovis*, which has lost its virulence by being cultured for generations in an artificial medium. The distribution of BCG for human use started since the 1920s and more than three billion people have received this vaccine. However, the continuing debate on the benefits and drawbacks of BCG never stopped since the early use of this vaccine. The major conclusion about the benefit of BCG is that it protects efficiently against leprosy (89) and against the childhood manifestations of TB (meningeal or miliary) (90). The drawbacks of BCG include safety concern as it cannot be used in immunocompromised patients, loss of sensitivity to tuberculin as a diagnostic marker,

efficacy decay over time, variable efficacy in different clinical trials, and in particular the failure of BCG in a number of trials in the third world.

One explanation of BCG failure is the mutation or loss of mycobacterial genes during culture. Since the first successful BCG vaccination, it has been distributed world-wide and propagated differently in various labs for several decades leading to both genotypic and phenotypic changes compared to the parent strain of BCG developed by Camille Guérin and Albert Calmette (91). These changes also exist among various daughter strains of BCG (91). These mutations may partly explain the variable protection efficacy of BCG. Berh and Small suggested that BCG may have lost important genes over time and gradually have been attenuated to impotence (92). Adding to this explanation are several other hypotheses including previous exposure to environmental mycobacteria (93); the deletion of protective antigens from BCG (94); failure of BCG to stimulate balanced CD4+ and CD8+ T- cell responses (95); age and route of administration (96); and lyophilization of vaccine (93).

1.1.5 Advances in tuberculosis vaccine strategies

Based on the understating of BCG, various new-generation tuberculosis vaccines have been developed to address one or more drawbacks of BCG. Theses vaccines underwent different development stages as listed in table 2.1 and will be discussed in detail below.

1.1.5.1 Modified BCG

Comparative genomics revealed the differences between BCG and *MTB*. A number of regions designated RD1-RD16 encompassing 129 reading frames have been identified (97). RD1 is the best characterized region of deletion, which is lost in all BCG substrains yet presents in all strains within the *MTB* complex (94). Reintroduction of RD1 led to a protein expression profile almost identical to that of virulent *M. bovis* and *M. tuberculosis* (94). By

extension, BCG::RD1 (with reintroduction of RD1 region) may improve the protection activity of BCG. There are ongoing pre-clinical studies scheduled to test this vaccine.

Recombinant BCG overexpressing already-existed genes was also developed. For instance, rBCG30 is BCG Tice engineered to overexpress Ag85B (13, 98, 99). The phase I trial in US was completed in 2004. The results suggested that rBCG30 promotes levels of protection greater than conventional BCG without causing serious adverse events (99). This study also suggests that modifying BCG by overexpressing important genes, even already existed gene, may be a promising approach to improve vaccine performance. Another example belonging to this category is rBCG-Aeras 403 with BCG Danish as the template overexpressing several proteins including Ag85A, Ag85B and TB10.4 (100).

Recombinant BCG with endosome-escaping capability was also developed to improve BCG performance based on the hypothesis that an optimal blend of both CD4+ and CD8+ T cell responses is critical to TB control. There is evidence suggesting that *MTB* antigens more readily gain access to the cytoplasmic compartment of host cells and, therefore, stimulate a more pronounced CD8+ T cell response compared to antigens derived from BCG (95). In support of this observation, *MTB* infection facilitated MHC I presentation of class I epitopes within ovalbumin while BCG infection was less effective in stimulating this process (101). In order for BCG to activate CD8+ T cells, BCG must either translocate from endosome to cytosol of the infected cells or induce apoptosis-mediated CD8+ T cell responses. Kaufmann's group developed an rBCG vaccine, rBCGΔUreC:Hly^{+}, with deleted BCG urease gene (*ureC*) and insertion of the *Listeria monocytogenes* Hly (listeriolysis) (102). UreC blocks the acidification of phagosome in infected cells and, therefore, deletion of this gene facilitates macrophage phagosome maturation. Hly is a sulphydryl-activated cytolysin that

creates pores in the membrane of early phagosomes and allows some leakage of rBCG from the phagosome to the cytosol of infected cells. In mouse-protection studies, vaccination with rBCGΔUreC:Hly^{+} induced better protective efficacy than with BCG (103). Also, it has been shown to protect significantly against the virulent *MTB* strain, Beijing/W (103). Both *MTB* and BCG produce various gene products to block apoptosis and, thus, inhibiting apoptosis-mediated CD8+ T cell responses. Following this reasoning, Jacobs suggested that a pro-apoptotic vaccine with deleted genes such as *nlaA*, which inhibits apoptosis of infected cells, may be superior to conventional BCG (104). Immunization with such vaccine may lead to apoptosis-mediated cross-priming and powerful cellular immune responses (105, 106).

1.1.5.2 Modified *MTB*

Virulent *MTB* is the cause of tuberculosis and, therefore, cannot be used as a vaccine. Molecularly attenuated *MTB* may have the desirable feature of effective vaccine which induces greater protective efficacy compared to BCG. One reason is that *MTB* contains over 120 *MTB* specific genes not found in BCG, which represent a reservoir of antigens available for immune activation (107-109). However, the biggest concern for attenuated *MTB* vaccine is the danger of reversion of live *MTB* to virulent state (110). Other concerns include the potential release of antibiotic-resistance gene markers from live *MTB* vaccine to the environment as well as the public perception and acceptance for such vaccine (110).

One example of attenuated *MTB* vaccine is developed by Soto's group (16). The virulence was attenuated by inactivating PhoP, which regulates the expression of many *MTB* proteins. This vaccine has shown promising animal protection in early study; however, a second, independent, non-reverting mutation is probably required to satisfy human safety concerns (110).

Other examples in this category include mc^{2}6020 (*panCpanDlysA*) and mc^{2}6030 (*panCpanDΔRD1*) (111, 112). In these mutants, gene products (PanC and PanD) involved in *MTB* lipid metabolism were disrupted, which greatly attenuated the growth of mutant *MTB*. Both attenuated *MTB* vaccines were safer than BCG in immunocompromised animals and offered similar levels of protection.

1.1.5.3 Naked DNA and viral-vectored vaccines

BCG immunization produced varying protective efficacy in different clinical trials, which may be explained in part by the hypothesis that previous exposure of human populations to environmental mycobacteria may bias the immune response towards a detrimental humoral response that cannot be overridden by a subsequent BCG vaccination (113). The consequence is that BCG induced immune response is limited whereas the immune response promoted by environmental mycobacteria is insufficient on its own to combat a subsequent *MTB* challenge. Vaccination with BCG, rBCG or attenuated *MTB* may not be ideal for people who have a significant risk of exposure to environmental mycobacteria, for instance, people in tropical regions (114). In this scenario, naked DNA or viral-vectored vaccines may be good alternatives. A recent study showed that immunization of mice with a recombinant adenoviral construct (Ad5) expressing the *MTB* antigen Ag85A (AdAg85A) by the intranasal route conferred protection superior to conventional BCG vaccination against an aerosol *MTB* challenge (115). Since Ad5 vector is prevalent in the environment, Aeras in collaboration with Crucell constructed Aeras 402 based on the less prevalent non-replicating Ad35 vector expressing multiple TB proteins including Ag85A, Ag85B and TB10.4 (116). A single dose vaccination of mice with this vaccine conferred protection against *MTB* challenge (110).

In the heterologous prime-boost vaccination strategy, DNA vaccines have been used as the booster for BCG prime immunization (110). There are two advantages to boost BCG with DNA vaccine: 1) existing BCG does not inhibit *MTB* antigen expression from DNA vaccine, and 2) DNA vaccines induce both CD4+ and CD8+ T cell responses rather than a biased CD4+ T cell response. In one study, mice were BCG primed followed by a booster with a DNA vaccine encoding Rv3407 (a 10-kDa protein of unknown function) (117). This study showed that mice were better protected with DNA booster compared to a single BCG vaccination.

1.1.5.4 Subunit vaccines

TB subunit vaccine consists of purified *MTB* antigens, adjuvants and delivery vehicles. Safety is one of the advantages of subunit vaccine; for instance, it can be used in immunocompromised patients such as HIV-positive patients and there is no concern of genome invasion with the use of subunit vaccine. Subunit vaccines may also serve as good booster for BCG in the prime-boost strategy.

Antigen identification is the first step to develop TB subunit vaccine since there is a whole repertoire of proteins expressed either by BCG or *MTB*. *MTB* antigens that can activate T cells in previously infected animals and humans are considered as promising vaccine candidates. Initially, several of the most abundant proteins have been identified by biochemical approaches including Ag85 complex, DnaK, PhoS, GroES, MPT32, MPT46, MPT53, MPT63, and the 19-kDa lipoprotein (118-120). Immunological dominant antigens in the low molecular mass range were identified subsequently, for example, the 6 kDa early secretory antigenic target (ESAT-6) protein family (121, 122). Serological expression cloning approaches identified several important *MTB* antigens such as Mtb32 (a serine

protease secreted by *MTB*) and Mtb39 (a member of the PPE (proline-proline-glumatic acid) protein family) (123, 124). Several promising antigens such as Rv3407 (117) have been identified by proteomic approaches.

Although each individual antigen has the potential to be developed as the subunit vaccine (e.g. a respirable TB subunit vaccine has been developed based on a single antigen Ag85B(125)), subunit vaccine consisting of antigen combinations may increase the opportunity for a better protection. Following this reasoning, recombinant fusion antigens were constructed by molecular engineering. For instance, Skeiky developed Mtb72F, which is a recombinant fusion of Mtb32 and Mtb39 (126); while Olsen developed Hybrid-1, a fusion of Ag85B and ESAT-6 (127). The efficacy of Mtb72F and Hybrid-1 have been tested in the mouse and guinea pig TB challenge models (126, 128-130), which demonstrated that once formulated in selected adjuvants both fusion antigens conferred protection as well as BCG.

1.1.6 Antigen candidates for TB subunit vaccine

1.1.6.1 Ag85B

Ag85 complex is composed of three major secretory proteins Ag85A, 85B and 85C. This protein complex accounts for 41% of the total culture filtrate protein. The antigen Ag85 proteins are homologous proteins that share very high sequence identity (68-79%). All three proteins contribute to *MTB* cell wall synthesis by catalyzing the transfer of one mycolic acid group from one trehalose 6-monomycolate (TMM) to another, giving rise to trehalose 6, 6'-dimycolate (TDM or cord factor) and free trehalose. The three proteins are expressed at a steady-state ratio of 2:3:1 (Ag85A: Ag85B: Ag85C). Ag85B (~30 kDa), among three proteins, is the most abundant isoform secreted which contributes to almost one-quarter of

the total extracellular protein; whereas it is the least active form as shown in one *in vitro* assay (131). Ag85B is also highly expressed in infected human macrophages. In the phagosomes of infected human macrophages, Ag85B is found in the phagosome space as well as on the bacterial cell wall (132-134).

Although Ag85B has been suggested as a drug target, searching Ag85B-specific inhibitors may not be a good idea since this enzyme shows least enzymatic activity compared to the other two Ag85 members (131). In one study, knockout of Ag85C from *MTB* resulted in a 40% decrease in the amount of cell wall linked mycolic acid, whereas knockouts of Ag85A and Ag85B had no noticeable effect (135). This study suggests that Ag85A and Ag85B have limited roles in *MTB* cell wall synthesis or their function can be compensated by Ag85C.

From the vaccine standpoint, Ag85B is a leading antigen candidate because it is an immunodominant antigen which interacts with the immune system at an early stage of *MTB* infection and induces both humoral and cell-mediated immune responses (125). Therefore, Ag85B has a great potential to be developed as a prophylactic vaccine. Indeed, this antigen has been incorporated into various novel TB vaccine strategies such as recombinant BCG, DNA vaccine, viral-vector vaccine, naked DNA vaccine and subunit vaccine. The efficacy of these Ag85B-based vaccines varies depending on the vaccine vector, the route of administration, and co-incorporated antigens.

1.1.6.2 TB10.4

TB10.4 is a peptide of 96 amino acids long, which is a member belonging to ESAT-6 protein family. The ESAT-6 family consists of 22 low molecular mass proteins, many of which are strongly immunogenic. TB10.4 has been found to be strongly recognized by BCG-

vaccinated donors and in infected TB patients (19). TB10.4 is an ideal candidate to replace ESAT-6 for two reasons: 1) in TB patients TB10.4 is much more strongly recognized than ESAT-6 and 2) use of TB10.4 leaves ESAT-6 as a potential diagnostic marker to distinguish BCG vaccinated vs. *MTB* infected individuals (table 1.2).

Majlessi's group identified an MHC class I epitope, GYAGTLQSL, from TB10.4 (136). This epitope can be efficiently recognized by cytotoxic T cells from *MTB* infected mice. A CD8+ T cell hybridoma restricted to this epitope, YB8, was also developed in this group. YB8 is able to recognize BCG infected macrophages and secrete interleukin-2 (IL-2). Billeskov identified another MHC I epitope of TB10.4, QIMYNYPAM (137). Their experiments showed that CD8+ T cells restricted to this epitope were induced at the onset of infection and were present throughout the infection at high numbers.

1.1.7 Rationale for pulmonary vaccine delivery

Vaccines are frequently administrated *via* the parenteral route such as intradermal and subcutaneous immunization. Pulmonary vaccine delivery represents an alternative route of immunization which has its unique advantages. Firstly, many pathogens utilize the respiratory tract as a portal of entry. For example, *MTB* is transmitted among individuals *via* the lungs, where the mycobacteria establish initial colonization. The mucosal surfaces lining the respiratory tract are the first defense system against pathogens. Therefore, immunity induced on mucosal surfaces by pulmonary vaccination is highly preferred at the early stage of infection with respect to pathogen neutralization. Secondly, pulmonary vaccination follows the natural route of infection for many pathogens and may induce immune responses mimicking the natural immunity produced by pathogens. Thirdly, a broader base of protection may be generated in the lungs considering the large surface areas in the deep lung,

where a large inter-related network of lymphoid tissues readily sharing antigenic information could be found. In addition to mucosal immunity, systemic immunity may also be activated *via* pulmonary vaccination. Fourthly, pulmonary vaccination is a noninvasive means of vaccine delivery, which eliminates the need for syringes and needles, ameliorates the pain and suffering associated with injections, improves patient compliance, and reduces waste disposal and the risk of transferring blood-borne infections. Fifthly, formulating vaccines into dry powders suitable for pulmonary delivery may possess a critical pharmaceutical advantage with respect to injectable vaccines, which is, increased stability. Liquid formulations or reconstitution of powder formulations for injection may cause potency loss of formulated antigens such as attenuated live bacteria, and purified protein antigens. (138-142). The advantage of lung immunization was shown in a recent publication where aerosol delivery of BCG significantly reduced lung pathology and bacterial burden both relative to untreated guinea pigs and to control guinea pigs vaccinated with the standard parenteral BCG (145). However, pulmonary BCG immunization only targets a specific population, i.e. neonates, because this population has a rare chance of prior exposure to environmental mycobacteria. Therefore, lung immunization by alternative vaccines such as TB subunit vaccine may benefit a larger population such as adults or immunocompromised patients.

1.1.7.1 Immune responses induced by pulmonary vaccination

In healthy humans, local immune system contributes 80% of all immunocytes. Local immunocytes are accumulated in different mucosa-associated lymphoid tissues (MALT), which form the largest lymphoid organ system (143). The MALT is a highly compartmentalized system which functions independently from the systemic immune system. Compared with systemic lymphoid tissue, the MALT is populated by functionally and

phenotypically distinct immunocytes such as B cells, T cells and accessory cell populations. Three roles have been suggested for mucosal immune system: 1) to protect mucosal surface against pathogen colonization, 2) to prevent uptake of undegraded antigens, and 3) to prevent the development of harmful immune responses.

Pulmonary vaccine delivery targets immune cells in the lungs with the goal of inducing both mucosal and systemic immunity against respiratory infectious disease (138). Antigens delivered to the lung can be taken up by antigen presenting cells (APCs) such as alveolar macrophages, dendritic cells and B lymphocytes through direct or indirect pathways and presented to CD4+ and CD8+ T cells located in the mucosal inductive sites. These activated mucosal immunocytes (both B and T cells) then leave the inductive sites, drain into the lymph, enter the systemic circulation, and home to selected mucosal sites mainly of the mucosal origin, where they differentiate into effector or memory cells (144). Of particularly note, the homing of immunocytes is constricted by the expression and affinity of 'homing receptors' on immunocytes and corresponding 'addressin' molecules on endothelial cells (144). This phenomenon has an important implication, which is, mucosal immunity induced in deep lungs can be transmitted to other mucosal surfaces such as the upper respiratory tract and nasal-associated lymphoid tissue, which will encounter respiratory pathogens such as *MTB*. Mucosal immune responses involve both innate and adapted immunity. The adaptive humoral response is mainly mediated by secretory IgA (SIgA) antibodies, whose resistance to proteases makes them well suited to mucosal secretions. Cell-mediated immunity at the mucosal surface is predominantly mediated by CD4+ and CD8+ T cells (138).

Mucosal immunity is the first line defense system against respiratory pathogens. A pre-existing mucosal immunity induced by pulmonary vaccination can mount a quick immune

response once encountering respiratory pathogens. In addition to mucosal immunity, a systemic immunity is highly favored and always important to combat the pathogens. Although *MTB* infection mainly occurs in the lungs, it can be transmitted into other organs such as liver and spleen. To combat *MTB* in these organs, immunocytes, predominantly T lymphocytes have to migrate into these organs *via* systemic circulation, which demands a systemic immunity. Pulmonary vaccination also induces systemic immunity as reviewed previously (138). From the TB standpoint of view, systemic immunity can be induced once activated APCs migrate into local lymph nodes and present TB antigens (delivered by aerosol) to T lymphocytes in the nodes. Activated T lymphocytes may circulate back into the primary infection sites or migrate into other infected organs through the systemic circulation (110).

1.1.7.2 Current status of pulmonary vaccine delivery

Studies about pulmonary vaccination of animals are described elsewhere (138). For example, a BCG aerosol has been used to immunize guinea pigs through the lungs, which suggests that lung immunization with BCG aerosol results in an improved protection against *MTB* than that achieved by subcutaneous injection (145).

Pulmonary vaccination of humans was realized in Soviet Union almost 40 years ago (146). Russian researchers found that pulmonary vaccination was as effective as subcutaneous vaccination against anthrax, brucellosis, plague, and tularemia (146, 147). Pulmonary delivery of BCG to people was conducted in USA in 1968 to compare tuberculosis pathology in human beings vs. in animals, which revealed similar pathology between humans and guinea pigs (148). Attenuated *Francisella tularensis* vaccine has been nebulized into human lungs for vaccination against virulent *F. tularensis* (149). The data

suggested that greater immunity to virulent strain challenge was achieved with pulmonary vaccination compared with parenteral administration.

So far the only successful clinical case of pulmonary vaccination is a pulmonary measles immunization. In this study, approximately 4 million Mexican children were immunized by an aerosol of measles vaccine and showed a high rate of successful protection (150). Pulmonary delivery of measles vaccines has been shown to induce greater seroconversion compared to injected vaccines (151).

1.1.8 Pulmonary vaccine delivery by aerosol technology

Vaccines intended for pulmonary delivery requires unique formulation strategies. Formulations also vary depending on the device used for aerosolization. Generally speaking, three devices have this capability, including pressurized metered-dose inhalers (pMDIs), nebulizers and dry-powder inhalers (DPIs). Very few vaccines have been delivered by pMDIs since the hydrophobic propellant used to generate aerosol is not a friendly environment for most vaccines (both live and subunit vaccine). It has been shown by Brown and his colleagues that *Streptococcus suis* bacteria delivered by pMDI lost 50-70% of its antigenicity after aerosolization (152).

Nebulizers have been most widely used for pulmonary delivery of vaccines. For instance, the measles vaccine, in one study, was successfully delivered into the lungs of Mexican school children by a Classical Mexican Device, which is an air-driven jet nebulizer (151). Vaccines such as BCG (153, 154) and attenuated rubella virus (155) have also been delivered by nebulizers. However, delivering vaccines by nebulizers has several disadvantages. First, operation of nebulizers requires special settings such as compressed air for jet nebulizers and power for ultrasonic nebulizers, which makes immunization inefficient

and time-consuming. Second, vaccines delivered by nebulizers should be in the liquid state. A liquid formulation of vaccine requires cold chain in the manufacture, shipping and storage, which ultimately increases the cost. In addition, unexpected temperature variation may cause potency loss of vaccines. Powder formulation increases the stability of vaccines and may not require the cold chain. However, reconstitution of the powder formulation may cause potency loss as shown in an example of measles vaccine (156). Reconstituted vaccine loses potency rapidly at both 25 and 37 ˚C. Third, the shear force generated during the nebulization process is a potential risk factor for vaccine potency (157). In one study, the potency of the measles vaccine was lost by 71% after the nebulizer was run continuously for 20 min (158).

Dry powder delivery has several advantages over the other two delivery methods. Vaccines prepared in the dry powder form have greater stability in comparing to liquid formulation. A cold chain for storage may not be required and there is no need for reconstitution. Dry powders are delivered by dry-powder inhalers (DPIs), acting *via* either passive or active mechanisms (142). To enhance dispersion of small particles, an excipient such as lactose is commonly used. Depending on the dosing regimen, vaccines can be packaged into either single-dose or multi-dose DPIs. If moisture contact is a problem for the stability of vaccines, dry powder vaccines can be sealed into a foil blister which protects the powder from exposure to high humidity or other potential risks such as sunlight.

1.1.9 Dry-powder vaccine formulation

The rapid distribution, ease of operation and acceptance by the general public will most likely result in DPIs in mass immunization campaigns for many vaccines such as tuberculosis and measles vaccines (142). Therefore, dry-powder vaccine formulations will be reviewed here.

1.1.9.1 Antigens: the active ingredient of a dry-powder formulation

Antigens are the critical component of a dry-powder vaccine formulation, which determines the immunogenicity. These include attenuated virus or bacterial strains, proteins purified from pathogen cultures, recombinant proteins purified from the heterologous expression system, and DNA encoding antigens from corresponding pathogens. The sequence or conformational information residing in antigens leads to the activation of B and T lymphocytes which eventually differentiate into the memory immunocytes.

1.1.9.2 Adjuvants: the active excipient of a dry-powder formulation

Adjuvants are needed for many vaccines especially for DNA and subunit vaccines because purified DNA and proteins are frequently poor immunogens (159, 160). Adjuvants can help elicit high and long-lasting immune responses with limited amount of antigens. Th1/Th2 immune responses can also be modulated by adjuvants to suit specific requirement of certain vaccines (161). As an example, Th1 immune responses have been suggested to play a pivotal role in TB control. With the use of a carefully chosen adjuvant, a favorable Th1 immune response may be induced.

Different mechanisms have been implicated in adjuvancy such as depot effect, immunomodulation, and effective presentation of antigens to the immune system (141). Aluminum, oils, and emulsions are classical examples of the depot effect, which creates a depot (usually by injections) at the site of administration to attract immunocytes such as dendritic cells and macrophages. Alum, i.e. potassium aluminum sulfate, is the only FDA (Food and Drug Administration) approved adjuvant for human use (141). Although causing no severe side effects, alum suffers from a profound limitation since it is known to be deficient in inducing mucosal IgA responses (one advantage of mucosal vaccination such as

pulmonary vaccination) (141). Therefore, alum may not be an ideal adjuvant for a vaccine formulation intended for pulmonary delivery.

Adjuvants also act by modulating cytokine networks and the function of immunocytes. Lipopolysaccharide (LPS), CpG motif, monophosphoryl lipid A (MPL), cholera toxoid (CT) and muramyl dipeptide (MDP) are in this category (138). Among them, MDP is the smallest component of mycobacterial cell wall which can induce the production of a series of cytokines such as IL-1α, IL-1β, and IL-6 (138). In addition, MDP is a water-soluble molecule which is completely miscible with antigens. Therefore, this molecule is a promising adjuvant for TB vaccine development. Adjuvants in this category, in general, induce stronger immune response compared to those acting on depot effect such as alum. However, none of these molecules have been approved for human use so far due to potential safety problems. This is because unexpected perturbation of the immune networks by these molecules may outweigh the potentially beneficial immunomodulation effect. In-depth studies of these compounds in both pre-clinical and clinical trials will eventually advance our standing of these molecules with respect to both adjuvancy and side effects.

Adjuvants in the third category can effectively present antigens to the immune system. Biodegradable polymers, liposomes, microparticles and nanoparticles are representative adjuvants in this class (138). Antigens encapsulated in these adjuvants are easily taken up by the antigen presenting cells leading to efficient antigen presentation. In addition, these adjuvants also serve as delivery vehicles for pulmonary vaccines and their roles will be discussed later.

1.1.9.3 Particulate systems

Attenuated live viruses or bacteria are nano- to micro-sized particles by themselves,

which may not require a particular particulate system in the vaccine formulation. With respect to formulating subunit or DNA vaccines, particulate systems have been a common theme employed in various studies. Proteins and DNA are small in size, which are not suitable for aerosol delivery into the lungs unless they are formulated into the particulate system to facilitate dispersion. In addition, without the assistance of the particulate system, proteins and DNA have very limited potential to be taken up by the target cell populations, making the induction of immune responses unlikely. Formulating antigens into particulate systems have several advantages: 1) to protect the stability of formulated antigens, 2) to improve the aerosol dispersion and lung deposition of antigens, 3) to facilitate antigen uptake by target cells, and 4) to control the release of antigens from the particulate system. Depending on the targeted cells and intended use, either microparticulate system or nanoparticulate system can be employed to make vaccine formulations (138).

Microparticulate systems have a characteristic size in the micron-size range with the target cell population of mainly macrophages (alveolar macrophages for lung immunization) and possibly dendritic cells (138, 141). This system includes liposomes, lipid-based and biodegradable polymer-based microparticles. Liposomes are widely used delivery vehicles which can be manufactured into both nano- and mirco-particles (162, 163). They are mainly composed of amphipathic lipids (either positively or negatively charged), and cholesterol mixtures at certain molar ratio. Protein and DNA antigens can be encapsulated into liposomes by different methods such as sonication, extrusion, spray-drying and lyophilization followed by milling (162, 164). Liquid liposome formulation may cause stability problem during storage or administration (e.g. nebulization) (165-167). Dry powder liposome formulations may circumvent this problem and can be delivered by dry-powder inhalers.

After being delivered into the lungs, liposomes target alveolar macrophages as demonstrated by the study of de Haan and his colleagues (168). In addition to liposomes, lipid-based microparticles have also been studied as carriers for pulmonary vaccine delivery (138). These microparticles are usually manufactured by spray-drying or solvent evaporation methods with greater stability and encapsulation efficiency compared to liquid liposome formulations. The cellular uptake of lipid particles by antigen presenting cells (APCs) can be regulated by modifying the surface properties. For example, IgG incorporated into the lipid microparticles facilitated antigen uptake *via* Fc receptor-dependent endocytosis (169).

In addition to lipids, biodegradable polymers are frequently used to prepare microparticles because of their biocompatibility and well-controlled release profile of encapsulated antigens. Polylactide-co-glycolide (PLGA) is a classical and model polymer, which is synthesized by means of co-polymerization of two monomers, the lactic acid and glycolic acid (170). The degradation products of PLGA are these two monomers, which under physiological conditions are byproducts of various metabolic pathways in the body. Therefore, PLGA shows very minimal systemic toxicity when used as the delivery vehicles, although it may cause trouble in lactose intolerant people. Controlled release of encapsulated drug or vaccine is another advantage of a PLGA based device (171, 172). The release is partly determined by the bulk erosion of this co-polymer, whose degradation is mainly mediated by the degradation of the ester bonds in the presence of water. The degradation of PLGA can be controlled by varying the ratio of two monomers where the higher the content of the glycolic acid, the shorter the time required for degradation. Owing to many unique advantages of PLGA, it has been studied as the delivery vehicle for TB subunit vaccine. For example, Kirby and his colleagues used PLGA microspheres to deliver a recombinant TB

antigen Ag85B-ESAT-6 (173). They manufactured PLGA particles within the desired sub-10 μm range by the double emulsion method. A sustained antigen release from these microspheres was observed. Immunization of mice with this formulation resulted in a cell-mediated immune response and specific antibody production. In another study, a recombinant TB antigen Ag85B was encapsulated into respirable PLGA microspheres by the emulsion/spray-drying method (125). This formulation induced significantly higher MHC II immune response specific to Ag85B in an *in vitro* antigen presentation assay. Other applications of PLGA in vaccine delivery are described elsewhere (174-176).

Nanoparticulate-based dry powder pulmonary vaccines are also under active investigation (141). Lipids and biodegradable polymers have been used in this system as well. The fundamental difference between nanoparticles and microparticles lies in their size difference and the resulting difference in target cell populations. It is generally believed that particles of a few hundred nanometers are favorably taken up by dendritic cells (DCs) either directly or indirectly *via* epithelia microfold cell (M-cell) relaying, although uptake by macrophages also occurs. The small size of nanoparticles makes them difficult to aerosolize due to strong particle-particle interactions. Also, once inhaled nanoparticles have a higher chance of being exhaled compared to microparticles. In order to make pulmonary delivery with nanoparticles a viable approach, porous nanoparticle-aggregate particles (PNAPs) of a few microns were developed, which are dried hollow particles of low density (177-180). PNAPs have good aerosolization properties to penetrate to the deep lung. The excipient matrix of the PNAPs is dissolved by the lung lining fluids, releasing antigen associated nanoparticles for uptake by immune-competent cells. Antigen associated nanoparticles are typically prepared by surface adsorption, encapsulation or covalent attachment methods

(181). These antigen-containing nanoparticles can then be formulated into PNAPs *via* spray-drying either by spraying pure nanoparticles or in the presence of excipients such as L-leucine (141). Upon careful control of the drying rate, where the rate of drying is faster than the diffusion of the nanoparticles, PNAPs are produced with the majority of nanoparticles gathering and eventually coalescing at the evaporation surface (141).

Few studies of pulmonary vaccine delivery using nanoparticulate system have been conducted. Nevertheless, there are some reports on pulmonary DNA vaccine delivery with such system. Nanoparticles (225nm) composed of PLGA and polyethyleneimine (PEI, a cationic polymer) with loaded DNA were readily internalized by the human airway submucosal epithelial cells (Calu-3) *in vitro* after 6 h (182). This is a poof-of-concept study demonstrating that nanoparticles can transfer DNA encoding antigenic information into cultured cells, which may be mimicked *in vivo* by DNA transfer into the lung epithelial M-cells. Benita and colleagues reported that pulmonary immunization of mice with 350-nm chitosan-DNA (encoding eight HLA-A*0201-restricted T-cell epitomes from *MTB*) nanoparticles induced increased levels of IFN-γ secretion compared to pulmonary delivery of plasmid in solution (183). In addition, the chitosan-DNA nanoparticles could induce the maturation of dendritic cells while chitosan solution alone could not.

1.1.9.4 Dispersion of vaccines with carrier excipient

To be efficiently delivered into the lungs, vaccine particles should have an aerodynamic diameter in the range between 1 and 5 μm (184). Depending on the nature of a vaccine formulation, excipients that facilitate powder dispersion may or may not be required. In the case of poor dispersion, certain excipient is included to improve vaccine aerosolization.

Lactose is the only excipient approved for this use in the USA. It is milled, sieved or

spray-dried into approximately 100 μm particles, which provide a large surface for small particle adhesion. Once blended with other formulation components, small vaccine particles will adsorb onto the surface of carrier lactose particles. This effectively reduces the self aggregation of small particles. Another reason to include this sugar into the formulation is to help accurate dosing of small quantity of active pharmaceutical ingredient. Lactose fines are found to improve the dispersion possibly by occupying the active sites on the surface of large carrier lactose particles or by the deaggregation mechanism and, therefore, may be included in the dry-powder formulation (185). Besides lactose, other carriers such as trehalose, mannitol, glucose and sorbitol also have the potential to be used as the carriers in DPIs (186).

1.1.10 Particle size characterization of dry powders

Particle size is one of the most important quantitative descriptors of the specific properties of dry powders. With respect to the size of a single particle, three characteristic diameters are projected area diameter (dp), equivalent volume diameter (dv) and aerodynamic diameter (da). The projected area diameter is obtained from the two-dimensional image of a particle (187). It is equal to the diameter of a circular disc with the same projected area as the particle being examined. The equivalent volume diameter represents the diameter of a sphere of the same volume as the particle. The aerodynamic diameter is proposed since both dp and dv have limited application in studying particle deposition in the respiratory tract. The da is a representative diameter of aerosol particles, which is equal to the diameter of a unit density sphere that has the same terminal setting velocity as the actual particle (188).

$$V_{TS} = \rho_0 d_a^2 g/18\eta = \rho_p d_v^2 g/18\eta\chi$$

V_{TS}: terminal settling velocity, ρ_0: unit density, ρ_p: particle density

g: the acceleration of gravity, η: air viscosity, χ: shape factor

d_a: aerodynamic diameter, d_v: equivalent volume diameter

This equation suggests that the terminal settling velocity increases proportionately to the particle size, i.e. a large particle is more likely to deposit by inertial impaction compared to a small one. Second, density has significant impact on the aerodynamic diameter. As suggested by this equation, two particles of the same volume diameter may have different aerodynamic diameters due to density difference (low-density particle has smaller aerodynamic diameter). This property has wide applications. For example, low-density particles (either hollow or porous) with large volume diameter but small aerodynamic diameter suitable for pulmonary delivery have been manufactured to circumvent the particle uptake by alveolar macrophages (189). These particles can effectively reach deep lung without being actively internalized by macrophages and, therefore, increase the systemic concentration of administrated drugs. In addition, aerodynamic diameter is also affected by particle shape. Non-spheres have a shape factor greater than unity leading to an aerodynamic diameter smaller than its equivalent volume diameter (188). Particle shape has also been utilized in aerosol delivery. For example, the needle-like particles can deliver more drugs to the deep lung at the same aerodynamic diameter to the spherical particles assuming the same density and drug loading (190). However, attention should be paid to modifying particle shape since adverse effect may be associated with the irregular particle shape such as decreased cellular uptake and irritating the lung lining cells.

Mono-dispersed spherical particles (all have the same size) can be fully described by a single diameter. In reality, most powders are composed of particles with different sizes and probably different shapes. In order to characterize the powder as a whole rather than

individual particles, various diameters, based on the statistical moment analysis, have been devised to describe the same particle population such as the count median diameter (CMD), count mean diameter, length median diameter (LMD), length mean diameter, surface median diameter (SMD), surface mean diameter, volume or mass median diameter (VMD or MMD), volume or mass mean diameter, diameter of average surface, diameter of average mass and mass median aerodynamic diameter (MMAD) (188). These descriptors are representative diameters of a particle population not of a single particle. Among these diameters, SMD, VMD, and MMAD are population averages of corresponding dp, dv and da of individual particles. There are also quantitative descriptors to describe the breadth of the particle size distribution. For a Gaussian distribution, standard deviation is such a descriptor. If the log-normal distribution is assumed for a powder, the geometric standard deviation (GSD) is a better descriptor, which in contrast to the standard deviation is a dimensionless measure (188).

$$GSD = D_{84\%} / D_{50\%} = D_{50\%} / D_{16\%} = [D_{84\%} / D_{16\%}]^{1/2}$$

$D_{84\%}$: diameter at the cumulative percentile of 84%

$D_{50\%}$: diameter at the cumulative percentile of 50%

$D_{16\%}$: diameter at the cumulative percentile of 16%

An alternative descriptor irrespective of the nature of particle size distribution is the span, which is commonly reported where laser diffraction technique is used to measure the volume median diameter (VMD) of a powder. VMD and span are frequently used to characterize the geometric size and distribution of a powder (191).

$$Span = (D_{90\%} - D_{10\%}) / D_{50\%}$$

$D_{90\%}$: diameter at the cumulative percentile of 90%

$D_{50\%}$: diameter at the cumulative percentile of 50%

$D_{10\%}$: diameter at the cumulative percentile of 10%

In contrast, MMAD and GSD are widely used to characterize the aerodynamic size and distribution of a powder (191). Their values can be derived by examining the aerodynamic particle size distribution profiles, which are determined by cascade impaction (192). Cascade impactor, which operates on the basis of inertial impaction, is used to perform such experiment (188, 193). This device consists of a series of stages with decreased orifice size at each succeeding stage. Collection surface is below each stage, which serves to obstruct the path of airflow. Particles are drawn into the cascade impactor *via* the conveying air produced by a vacuum pump. Particles are accelerated increasingly from the top to the bottom since the orifice size decreases at each successive stage. Therefore, big particles with large inertia and stopping distance tend to deposit on the upper stages of an impactor while small particles can align their motion to that of the airstream and travel through next stages. This allows particles to be separated on different stages based on their aerodynamic diameters (figure 1.1a). Subsequent chemical or gravimetrical analysis reveals the mass deposition on each stage, which after certain transformation is plotted against the cut-off particle size of each stage on the log-probability paper (figure 1.1b). Mass median aerodynamic diameter (MMAD) and geometric standard deviation (GSD) can be derived from such distribution.

1.1.11 Particle size comparator to evaluate batch-to-batch reproducibility of inhalation products

The key issue in powder technology is the batch-to-batch reproducibility. For mono-dispersed powder, reproducibility can be ensured by manufacturing different batches of particles with the same size. A simple t-test can tell whether reproducibility is achieved. For

poly-dispersed powder, reproducibility should be evaluated based on the whole particle size distribution rather than the median diameter. Aerodynamic particle size distribution (APSD), measured by cascade impaction, is an *in vitro* aerodynamic characterization of the inhalation products such as nebulizers, metered-dose inhalers and dry-powder inhalers. This distribution has significant impact on drug deposition *in vivo*. A change of APSD may shift drug deposition from the deep lung to the upper respiratory tract or even to the mouth and throat, which may eventually affect the site of action. Therefore, batch-to-batch reproducibility should be routinely examined to ensure the quality of an inhalation product. In the second scenario, if drug manufacturers plan to develop a generic version of an inhalation product, an APSD profile sufficiently similar to that of the original product should be shown. In other words, establishing equivalence is the key in this case.

To evaluate the batch-to-batch reproducibility or to determine equivalence, a particle size comparator should be available. The Product Quality Research Institute (PQRI) in collaboration with the Food and Drug Administration (FDA) has developed a comparator based on the chi-square ratio statistics (194-196). Due to the poor performance of the proposed comparator, it was not recommended for APSD profile comparison with detailed explanations in a 2007 report (195). However, their research did point out the desired feature of a potentially useful size comparator. This includes: 1) the capability to deal with the multivariate measurement; 2) the capability to resolve the covariance associated with the mass deposition; 3) having sufficient power to detect the difference; and 4) a combination statistical test may be needed.

1.2 Problem statement

Tuberculosis (TB) is the second leading infectious cause of mortality in the world.

Bacillus Calmette-Guérin (BCG) is the only vaccine currently marketed for TB. However, the prophylactic use of BCG has demonstrated varying levels of efficacy in distinct populations and different field trials. In addition, the efficacy of BCG wanes in 10 to 15 years and boosting BCG vaccinated individuals with a second dose of BCG does not confer additional protection. Therefore, there is an urgent need to develop more potent TB vaccines. A TB subunit vaccine represents a promising candidate either on its own or as a booster for BCG in the heterologous prime-boost vaccination strategy. However, most antigens selected for existing TB subunit vaccines have been recombinant antigens purified from inclusion bodies. Antigens purified this way may adopt different conformations than their native counterparts. Therefore, it is highly favored to purify antigens in their soluble forms standing the best chance to maintain native conformation. For multiple-antigen vaccination strategy, it remains unknown whether antigen fusion or a blend of multiple antigens is better for vaccine development. So far, many TB vaccines under development were delivered *via* the parenteral routes. There has been less research investigating alternative delivery systems and administration routes for TB vaccines. Pulmonary delivery of TB vaccine may be a promising route of administration since the lung is the primary site of *MTB* infection and lung immunization may induce beneficial mucosal immunity. Microparticulate system, among various delivery systems, is especially suitable for pulmonary vaccine delivery because it facilitates both vaccine deposition into the lungs and antigen uptake by antigen presenting cells in the lungs. However, a successful formulation of antigens into the microparticulate system remains a difficult task with respect to both microparticle engineering and activation of immune response. In addition, it remains challenging to determine equivalence or evaluate batch-to-batch reproducibility of inhalation products since

there is no generally accepted particle size comparator available at the moment.

1.3 Hypotheses and specific aims

1.3.1 Research goals

The first goal is to compare the *in vitro* immune response of newly designed respirable TB subunit vaccines based on Ag85B/TB10.4 and their different combinations (antigen blend vs. antigen fusion) in order to make a recommendation of the best antigen/antigen combination for future animal protection study. The second goal is to develop a particle size comparator to evaluate the batch-to-batch reproducibility of inhalation products with an ultimate goal to use it as a quality evaluation tool for making highly reproducible TB subunit vaccines for lung delivery and immunization.

1.3.2 Hypotheses

The following hypotheses will be tested in this research.

- H1: Milligram quantities of soluble recombinant antigens can be obtained by rational design of the expression constructs.
- H2: PLGA-rAg microparticles can be manufactured with a target size by optimizing spray-drying parameters.
- H3: PLGA-rAg microparticles can induce stronger and prolonged immune response *in vitro* compared to antigen solutions.
- H4: Particle size comparator constructed on the basis of orthogonal partial least square analysis has a better performance than that developed on the basis of chi-square ratio statistics.

1.3.3 Specific aims

Aim I: Recombinant antigen design, expression, purification, and characterization.

(a) In order to obtain soluble TB10.4 in milligram quantities, this protein was fused to the C-terminal of thioredoxin (Trx) in a modified pET32-b vector resulting in a fusion protein Trx-TB10.4. It was expressed in *E. coli* and purified by nickel-affinity chromatography. A method was developed to obtain free TB10.4 from the fusion protein Trx-TB10.4 by protease treatment followed by a combination of chromatographic steps.

(b) Rationally design an expression construct that can express a recombinant fusion of Ag85B and TB10.4 with the following properties: 1) improved solubility and 2) milligram quantities. Molecular engineering was employed to make the construct. Protein purification was performed by fast protein liquid chromatography (FPLC). In addition, inclusion body was resolubilized followed by *in vitro* protein refolding to purify mis-folded protein.

(c) The purity of the recombinant proteins was determined by SDS-PAGE. The pH-dependent stability of recombinant proteins was studied by dynamic light scattering (DLS) at various pH. The secondary structure and thermo-stability of proteins was probed by circular dichroism.

Aim II: Manufacture and characterization of respirable PLGA-rAg microparticles.

(a) PLGA-rAg microparticles were manufactured by primary emulsion/spray-drying method. The spray-drying parameters were systematically optimized by a half-factorial design in order to achieve a target particle size of approximately 3 μm and a yield greater than 15%.

(b) PLGA-rAg microparticles were characterized with respect to: 1) morphology by SEM, 2) thermal property by DSC, 3) surface property by IGC, 4) geometric size distribution by laser diffraction, 5) aerodynamic size distribution by cascade impaction, 6) antigen integrity by SDS-PAGE, 7) flow property and 8) release profile.

Aim III: Study of *in vitro* immune responses induced by PLGA-rAg microparticles.

(a) Ag85B-specific MHC II immune response was studied with an *in vitro* antigen presentation assay by employing two cell lines with THP-1 as the antigen presenting cell and DB-1 as the CD4+ T cell hybridoma specifically recognizing an MHC II epitope within Ag85B. Different PLGA-rAg formulations were compared based on the amount of IL-2 secretion. Six-day antigen presentation assay was used to compare the response kinetics of particle formulations to that of solution formulations.

(b) TB10.4-specific MHC I immune response was studied with an *in vitro* antigen presentation assay by employing two cell lines with Raw264.7 as the antigen presenting cell and YB8 as the CD8+ T cell hybridoma specifically recognizing a MHC I epitope within TB10.4.

Aim IV: Development of a particle size comparator to evaluate batch-to-batch reproducibility of inhalation products.

(a) Monte Carlo simulation to recover 55 realistic scenarios of aerodynamic particle size distribution profiles proposed by the Product Quality Research Institute (PQRI).

(b) An algorithm was developed to compare particle size distribution profiles based on orthogonal partial least square analysis.

(c) Different data pretreatment methods were studied with respect to a better comparator performance.

(d) The performance of the particle size comparator was evaluated and compared with the original comparator proposed by the PQRI based on the chi-square ratio statistics.

1.4 Summary

In this dissertation, soluble recombinant antigens, Ag85B, TB10.4 and TB10.4-Ag85B,

were obtained in specific aim I with high solubility and yield by rational design of the expression constructs. They were characterized with respect to their pH-dependent stability and thermal property. The accomplishment of aim I provided antigens for the next stage of formulation development. Recombinant antigens were subsequently encapsulated into PLGA microparticles with a target size suitable for pulmonary delivery. The manufacturing parameters were systematically optimized and prepared TB subunit vaccines were characterized with respect to several physicochemical properties. In specific aim II, a deep understanding of particle manufacture, particle physicochemical properties and particle-antigen interaction was developed. The efficacy of respirable TB subunit vaccines was tested by *in vitro* antigen presentation assays in specific aim III, which offered invaluable information about the nature of induced immune responses. In the last specific aim, a particle size comparator based on orthogonal partial least square analysis was developed with a better performance to evaluate the batch-to-batch reproducibility of inhalation products. Detailed results are discussed in the following chapters.

Table 1.1 Summary of new-generation tuberculosis vaccines

Vaccine	Description	Development stage	Researchers
Modified BCG			
BCG::RD1	BCG Pasteur with reintroduced of RD-1 locus	Ongoing pre-clinical studies	S. Cole
rBCG30	BCG Tice overexpressing Ag85B	Phase I trial completed	M. Horwitz, D. Hoft, T. Littlejohn
rBCG-Aeras403	BCG Dannish with endosome escape and overexpression of Ag85A, Ag85B and TB10.4	Ongoing pre-clinical studies; Phase I clinical trial planned	R. Sun, D. Hone, M. Stone, J. Sadoff
rBCG Δ Ure:Chly^{+}	BCG Pasteur with endosome escape	Phase I clinical trial planned	S. Kaufmann
Modified *MTB*			
M.tuberculosis PhoP	Mtb MT103 strain with deleted *phoP* gene	Ongoing pre-clinical studies	B. Martin, B. Gicquel
M.tuberculosis mc^{2}6020	Mtb H37Rv with deletion of the *lysA* and the *panCD* locus	Phase I clinical trial planned	W. Jacobs
M.tuberculosis mc^{2}6030	Mtb H37Rv with deletion of the *panCD* and RD-1 locus	Phase I clinical trial planned	W. Jacobs
Viral-vectored and naked DNA vaccines			
Aeras 402 (Ad35.TB-S)	Non-replicating Ad35 expressing Ag85A, Ag85B and TB10.4	Phase I clinical trial planned	Aeras, Crucell
Rv3407 DNA	Plasmid encoding *Rv3407* gene	Ongoing preclinical studies	H. Mollenkopf, L. Grode, J. Mattow
Subunit vaccines			
Mtb72F	Recombinant fusion protein of Mtb39 and Mtb32	Phase I clinical trial completed	Y. Skeiky, S. Reed
Hybrid-1 (Ag85B-ESAT6)	Recombinant fusion protein of Ag85B and ESAT6	Phase I clinical trial completed	P. Andersen

BCG: Bacillus Calmette-Guérin, *MTB*: *Mycobacterium tuberculosis*, RD1: region deleted 1

Table 1.2 Expression of four proteins belonging to the ESAT6 family in different mycobacterium strains.

Strain	Expression of proteins in different strains			
	TB10.4	TB10.3	CFP10	ESAT6
M. tuberculosis H37Rv	+	+	+	+
M. bovis	+	+	+	+
BCG Danish	+	+	-	-

+: protein expressed in bacteria
-: no expression in bacteria

Figure 1.1 Particle size characterization of micafungin aerosol by Andersen cascade impactor. a, mass deposition of micafungin at each site of the cascade impactor; b, log-probability plot of micafungin particle size distribution.

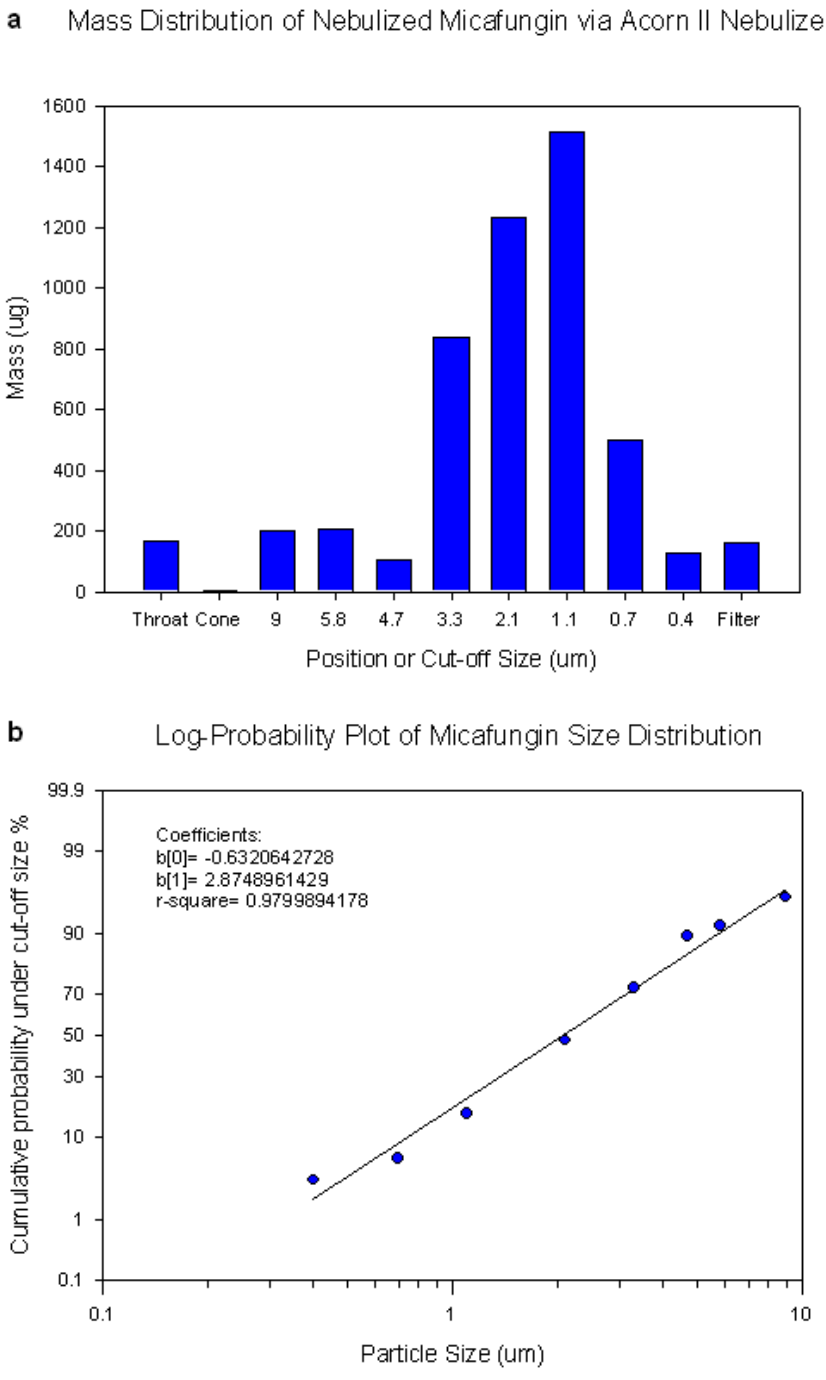

CHAPTER 2: RECOMBINANT ANTIGEN DESIGN, EXPRESSION, PURIFICATION, AND CHARACTERIZATION

In this chapter, the study focused on antigen design, expression, purification and characterization. Ag85B was previously purified as a soluble recombinant antigen (125). The effort in this study was to make the second antigen TB10.4 and the fusion antigen of Ag85B and TB10.4 soluble as well. This is because a fair comparison of antigens requires them prepared from the same source. The soluble recombinant form was chosen in this study. A so-called "pro-protein" approach was used to improve the solubility of TB10.4 and fusion antigens, where they were fused to the C-terminal of thioredoxin (Trx). The solubility of Trx-TB10.4 was dramatically improved. Compared to Trx-Ag85B-TB10.4, the solubility of Trx-TB10.4-Ag85B was increased by at least ten fold. Free TB10.4 and TB10.4-Ag85B were obtained by treating Trx-TB10.4 and Trx-TB10.4-Ag85B respectively with the TEV protease to remove the N-terminal thioredoxin. Soluble TB10.4 and TB10.4-Ag85B were subsequently purified to homogeneity with milligram quantity by a combination of chromatographic steps. A partial success was also achieved to purify TB10.4-Ag85B from the inclusion body. Circular dichroism (CD) was performed to study the secondary structure of the purified recombinant antigens. TB10.4 showed a reversible structure change. TB10.4-Ag85B purified from the soluble fraction showed similar thermal behavior as Ag85B with a characteristic melting temperature of approximately 75˚C whereas TB10.4-Ag85B purified from the inclusion body showed a completely different CD spectra and thermal behavior. In summary, the solubility and yield of TB10.4 and TB10.4-Ag85B was greatly improved by

rational design of the expression constructs. In addition, soluble Ag85B was also purified to homogeneity with well characterized secondary structure and thermal behavior.

2.1 Introduction

Ag85 complex (Ag85A, B and C) is the most abundant protein secreted by *MTB* (131), which attracts considerable interests for TB vaccine development. Ag85B has been shown to be among the most potent antigen species yet identified, which induces both humoral and cell-mediated immune responses in *MTB*-infected patients (197, 198). Ag85B encapsulated in poly lactide-co-glycolide (PLGA) induced significant amount of IL-2 production in an *in vitro* antigen presentation assay (125). Together with ESAT-6, a TB subunit vaccine comprised of these two antigens induced high levels of protective immunity in mice and reached the level of BCG-induced protection (199). An rBCG vaccine expressing Ag85B (rBCG30) induced greater protective immunity against aerosol challenge with *MTB* than conventional BCG in a highly susceptible guinea model (14). TB10.4 is a protein belonging to the ESAT-6 protein family comprising ESAT-6, CFP-10, TB10.4, and TB10.3 (122, 200). TB10.4 is strongly recognized by BCG-vaccinated donors and was even more strongly recognized in TB patients in comparing to ESAT-6 (201). Substitution TB10.4 for ESAT-6 allows the use of ESAT-6 as a diagnostic marker to distinguish *MTB* infected individuals from healthy BCG vaccinated individuals since ESAT-6 is only expressed in *MTB* but not in BCG (19). Therefore, a recombinant fusion of Ag85B and TB10.4 (Ag85B-TB10.4) was designed in Andersen's group, which has been shown to provide strong protection against *MTB* comparable to BCG (19).

Although possible to purify native antigens from the *MTB* cultures, it is much easier and safer to express them in *E. coli* as recombinant antigens (202). Moreover, molecular

engineering can be employed to redesign antigens of interest and combine the advantages of different antigens (110). A similar strategy has been used to produce recombinant antigens for other vaccines such as anthrax vaccine (203) and influenza vaccine (204). In terms of protein purification, it is generally preferred to obtain recombinant antigens from the soluble fraction of *E. coli* culture. However, most antigens currently explored for TB subunit vaccine development were frequently purified from the inclusion body (IB) as reported by several research groups (19, 201, 205, 206). The reason for IB formation is due to the tendency of incorrect folding and aggregation when proteins are over-expressed in the heterologous expression system such as *E. coli* (207, 208).

Thioredoxin is a 12 KD protein involved in several cellular functions such as sulfate metabolism, reduction of protein disulfides and as a cofactor for T7 DNA polymerase (209). It has a characteristic tertiary structure termed thioredoxin fold, which renders this protein highly stable and soluble (210, 211). When fused N-terminally to other proteins, thioredoxin remarkably increased the solubility of the fusion proteins, for example, mammalian cytokines and growth factors (212). Another advantage is that thioredoxin is localized on the cytoplasmic face of the adhesion zones between the outer and inner cell membranes (213). It can be exploited for rapid purification given that this property is retained by the fusion protein (212).

Circular dichroism (CD) has been widely used to study protein secondary structure and tertiary structure. Near-UV CD (250-350 nm) provides information on protein tertiary structure, although the signal is orders of magnitude below the far-UV CD (190-250 nm). Therefore, near-UV CD mainly serves as a quality control tool to compare proteins prepared by different methods or from different lots. With far-UV CD, protein secondary structures

can be investigated because different secondary structures have distinct CD spectra in this region. Deconvolution can be employed to analyze the complex CD spectra by dissecting out each contribution component, i.e. the secondary structure. In addition, CD can be used to study protein thermal stability by following the signal at the peak absorption wavelength as a function of temperature change. Compared to NMR or X-ray, CD offers less structural information of proteins; however, it is a fast and non-destructive technique which can be used on a routine basis to study protein stability and structure (214).

In this chapter, solubility enhancement by N-terminal thioredoxin fusion was utilized in several recombinant antigens such as TB10.4, Ag85B-TB10.4, and TB10.4-Ag85B. In order to study the effect of construct design on antigen folding, the solubility and yield of Trx-TB10.4-Ag85B was compared to that of Trx-Ag85B-TB10.4. A conformation comparison was made between TB10.4-Ag85B purified from the inclusion body and its soluble counterpart by circular dichroism (CD). CD was also used to study antigen thermal stability.

2.2 Materials and Methods

Constructs design

Four constructs were designed as shown in figure 2.1a-d. a: Trx-TB10.4. TB10.4 was amplified from the H37Rv genome by the following primers 5'-ATGGATCCATGTCGCAAATCATGTACAACTAC-3' (F) and 5'-GTAGAATTCC TAGCCGCCCCATTTGGCGGCTTCGGCCGTGT-3' (R). The PCR product was digested with BamH I and EcoR I and ligated into a customized pET32b vector, in which a TEV protease cleavage site was introduced between the $(His)_6$-tag and the multiple cloning sites. b: His-Ag85B-TB10.4. His-Ag85B was encoded in the pRSET-B vector (courtesy of Dr.

Douglas Kernodle, Vanderbilt University). TB10.4 was amplified from the H37Rv genome by the following primers 5'-ATGCATGGCGCCGGCATGTCGCAAATCATGTACAACT ACC-3' (F) and 5'-GTAGAATTCCTAGCCGCCCCATTTGGCGGCTTCGGCCGTGT-3' (R). The PCR product was digested with *Nar I* and *EcoR I* and ligated in frame with His-Ag85B to generate the fusion molecule His-Ag85B-TB10.4. c: Trx-Ag85B-TB10.4. Both 5'-TAAGGATCCTTCTCCCGTCCGGGTCTGCCGGTC-3' (F) and 5'-ATAGAATTCCT AGCCGCCCCATTTGGCGGCTTC-3' (R) were used to amplify Ag85B-TB10.4 by using His-Ag85B-TB10.4 as the template. The PCR product was then introduced into the customized pET32b vector between *BamH I* and *EcoR I* restriction sites. d: Trx-TB10.4-Ag85B. TB10.4 was amplified by 5'-ATCGGATCCATGTCGCAAATCATGTACAAC-3' (F) and 5'-GCCGCCCCATTTGGCGGCTTC-3' (R). Ag85B was amplified by 5'-^{P}TTCTCCCGTCCGGGTCTGCCGGTC-3' (F, with 5' phosphate) and 5'-ATAGAATTCTCAGCCGGCGCCTAACGAACT-3' (R). The two PCR fragments were ligated by T4 DNA ligase and re-amplified to obtain the fusion protein. The PCR product was then inserted into the customized pET32b vector between *BamH I* and *EcoR I* restriction sites.

Expression of recombinant antigens

Recombinant Ag85B and Trx-TB10.4 were expressed in *E. coli BL21 (DE3)* strain (Stratagene). Typically, 1L Luria-Bertani (LB) broth with 50 μg/ml carbenicillin was inoculated with 20 ml of an overnight culture of *E. coli* and grown at 37˚C until the OD600 reached 0.6–0.8. The culture was induced by addition of 100 μM isopropyl-β-thiogalactopyranoside (IPTG) and grown at 18˚C overnight. Recombinant His-Ag85B-TB10.4, Trx-Ag85B-TB10.4 and Trx-TB10.4-Ag85B were expressed in *E. coli Origami B*

strain (Novagen) either with or without a plasmid expressing chaperon GroEL /GroES. 50 μg/ml carbenicillin, 12.5 μg/ml tetracycline, 15 μg/ml kanamycin and 20 μg/ml chloramphenicol were supplemented into the medium. L-arabinose (1mg/ml) and IPTG (100 μM) were used to induce chaperon and antigen expression respectively at 18˚C overnight.

Antigen purification from the soluble fraction

E.coli cells were pelleted, washed twice with phosphate buffered saline (PBS), re-suspended in PBS containing 1mM phenylmethylsulphonyl fluoride (PMSF) and then probe-sonicated 3 times. The resulting preparation was centrifuged at 15,000 rpm for 30 min. The soluble fraction of the recombinant antigens resides in the supernatant while inclusion body remains in the pellet. To purify soluble His-Ag85B, the supernatant was passed through a nickel column (Ni Sepharose^{TM} 6 Fast Flow, Amersham Biosciences, Piscataway, NJ). The eluted proteins were further purified by a Superdex 75 column (Amersham Biosciences, Piscataway, NJ) with 20 mM 3-(N-morpholino)propanesulfonic acid (MOPS), 0.4 M sodium chloride, pH 7.0 as the eluting buffer at a flow rate of 1ml/min. Soluble Trx-TB10.4, Trx-Ag85B-TB10.4 and Trx-TB10.4-Ag85B were purified on a nickel column first. Eluted proteins were dialyzed against Tris-HCl buffer (pH 7.4) to eliminate imidazole. Dialyzed proteins were treated with TEV protease (His-tagged) at a ratio of 25:1 (w/w) overnight at 4˚C. The reaction mixture was spiked with 10 mM imidazole before loading onto the nickel column. Protein unbound to the nickel column was collected and the same procedure was repeated two more times (figure 2.2a). Proteins were concentrated to 5ml and further purified on a Superdex 75 column (for TB10.4) or Superdex 200 column (for TB10.4-Ag85B) eluted with 20 mM MOPS, 0.4 M sodium chloride, pH 7.0 as the eluting buffer at a flow rate of 1ml/min.

Antigen purification from the inclusion body

To purify antigen from the inclusion body, the pellet from 1L culture was first washed with PBS three times. 30 ml of Tris-HCl buffer (pH 7.4) containing 8M urea was then added to resolubilize the inclusion body at 4˚C for 4hr followed by centrifugation at 15, 000 rpm for 1hr. The supernatant was passed through a 0.2 μm filter to eliminate any insoluble matters. 1ml urea-resolubilized protein was then added dropwise into a beaker containing 50 ml Tris-HCl (pH 7.4) buffer with gentle mixing on ice. The diluted protein was passed through a 0.2 μm filter immediately after the dilution. Antigen in the filtrate was then purified by a combination of nickel-affinity and size-exclusion chromatography as described above.

SDS-PAGE, native-PAGE, image analysis and antigen concentration determination

A precast 12% SDS-PAGE gel (Biorad, Hercules, CA) was used to determine the purity of the recombinant antigens. A precast 10% Tris-glycine native gel (Biorad, Hercules, CA) was used for native-PAGE. The gel was stained with Coomassie blue. The intensity of the bands in the gel was analyzed in ImageJ (http://rsbweb.nih.gov/ij/). The antigen concentration was determined by BCA^{TM} protein assay kit (Thermo Scientific, Rockford, IL).

Effect of buffer pH on antigen stability

Citrate-phosphate buffer covering the range from pH 3 to pH 8 was prepared to study antigen stability at different pH. Antigen stock in MOPS buffer (20mM, pH7.0) was diluted 20 times into the citric-phosphate buffer with the corresponding pH. This dilution ensures that the pH of the citric-phosphate buffer was not changed significantly by the introduction of MOPS buffer. The diluted antigen solution has a concentration between 0.05mg/ml and 0.1mg/ml. The samples were left at room temperature for an appropriate time period as shown in figure 2.4. The size and distribution of antigen aggregates was measured by photon

correlation spectrometry (PCS) employing the particle sizer (NICOMP particle sizing systems, Autodilute^{PAT} Model 370, Santa Babra, CA) in the NICOMP mode and repeated three times.

Multiple sequence alignment, protein structure simulation and pI prediction

Sequence alignment of ESAT-6 family members TB10.4, TB10.3, ESAT-6 and CFP-10 was carried out in ClustalW (http://align.genome.jp/). The 3D coordinates for Ag85B (PDB accession #: 1F0N) were downloaded from protein database bank (PDB) and reconstructed in PyMOL (http://pymol.sourceforge.net/). Since there is no crystal structure available for TB10.4, SWISS-MODEL (http://swissmodel.expasy.org/) was used to simulate the structure of TB10.4 based on sequence homology. The first approach mode identified CFP-10/ESAT-6 (PDB accession #: 1wa8) as the template for simulation. Simulated structure of TB10.4 was constructed in PyMOL. ProtParam (http://www.expasy.ch/cgi-bin/protparam) was used to predict the isoelectric points (pI) of the proteins listed in table 2.1.

Circular dichroism (CD) to study antigen secondary structure and thermal stability

Applied Photophysics Pistar-180 circular dichroism was used for this study. Buffer exchange was first performed to keep antigens in the CD compatible buffer (10mM potassium phosphate buffer, pH 7.4). The final antigen concentration for CD study ranges from 0.2 to 0.3 mg/ml. A full scan from 260 nm to 185 nm was first taken on each antigen at 20˚C. The wavelength corresponding to the peak was selected to follow with temperature ramping from 20˚C to 94˚C (1˚C/min). The selected wavelength was 220 nm for TB10.4, 216 nm for Ag85B and 218 nm for TB10.4-Ag85B. A full CD spectrum was also taken at 94˚C and then antigen samples were cooled to 20˚C, at which a full CD spectrum was recorded again. Blank spectrum (buffer only) was subtracted from all antigen CD spectrums. Best fit

based on residual analysis was selected for curve fitting.

2.3 Results

2.3.1 Production of soluble Trx-TB10.4 and TB10.4

Expression of His-TB10.4 (encoded in pRSET-B vector) led to the exclusive formation of inclusion body in *E. coli*. However, fusion of thioredoxin to the N-terminal of TB10.4 dramatically increased the solubility of Trx-TB10.4 (figure 2.1a) in comparing to His-TB10.4. Figure 2.3a shows that the major band corresponding to Trx-TB10.4 (29KD, lane 1) was cleaved into two fragments corresponding to the thioredoxin and TB10.4 respectively. Surprisingly, TB10.4 released from the enzymatic (TEV protease) cleavage was remarkably soluble and could be purified to homogeneity by a combination of chromatography (figure 2.2a and 2.2c). The sharp peak in figure 2.2c represents TB10.4 while the small preceding peak may represent protein impurities or large aggregate of TB10.4. Figure 2.3b shows that TB10.4 can be purified to homogeneity (lanes 3 and 4).

2.3.2 TB10.4 exists as an oligomer

As shown in figure 2.2b, the Superdex 75 column was first calibrated with the protein standards. TB10.4 was eluted from the same column corresponding to a molecular weight of 27KD. This apparent molecular weight is slightly greater than the calculated molecular weight of a TB10.4 dimer (22.6KD). To further characterize this protein, TB10.4 was run on a native gel with Ag85B and thioredoxin for comparison (figure 2.3c). Both Ag85B (34KD) and thioredoxin (19KD) exist as monomer based on their elution volume from the Superdex 75 column. Figure 2.3c clearly shows that TB10.4 migrates faster than Ag85B yet slower than thioredoxin, which together with the chromatographic data suggest that TB10.4 exists as an oligomer.

2.3.3 Effect of pH on Trx-TB10.4 and TB10.4 stability

As listed in table 2.1, all proteins studied are predicted to have the isoelectric point (pI) in a narrow acidic range (from 4.82 to 5.24). For Trx-TB10.4, significant protein aggregation was observed at pH 4 and pH 5; while no detectable aggregation was found at lower pH (< 4) or higher pH (> 5) monitored by photon correlation spectroscopy (figure 2.4a). The aggregation of Trx-TB10.4 starts immediately after diluting protein stock into appropriate buffer (pH 4 or 5). The aggregates may sustain in suspension for a couple of hours but precipitate out eventually. The aggregation of TB10.4 occurs at a lower pH range than that of Trx-TB10.4 as shown in figure 2.4b. This difference between the two proteins may be explained by the presence of thioredoxin in Trx-TB10.4, which is predicted to increase the pI of the fusion protein as shown in table 2.1.

2.3.4 Production of soluble Trx-TB10.4-Ag85B and TB10.4-Ag85B

Initial expression of His-Ag85B-TB10.4 (figure 2.1b) led to exclusive formation of inclusion body. Since the solubility of the recombinant antigen is a major concern, the fusion molecules were redesigned. In light of the success of Trx-TB10.4, two new molecules were constructed as shown in figure 2.1c (Trx-Ag85B-TB10.4) and figure 2.1d (Trx-TB10.4-Ag85B). Figure 2.5a shows that the solubility of Trx-TB10.4-Ag85B was dramatically increased in comparing to Trx-Ag85B-TB10.4 (> 10 fold increase analyzed in ImageJ). However, the solubility of Trx-Ag85B-TB10.4 is only slightly better than that of His-Ag85B-TB10.4. In order to obtain free TB10.4-Ag85B, the fusion protein Trx-TB10.4-Ag85B was treated with TEV protease. The reaction mixture was loaded onto a nickel column and this procedure was repeated three times as shown in figure 2.5b and 2.6a. Fraction that was not trapped on the nickel column was further purified on a Superdex 200 column as shown in

figure 2.6b. In this way, soluble TB10.4-Ag85B could be purified to homogeneity (figure 2.5c).

2.3.5 Increasing the yield of Trx-TB10.4-Ag85B by co-expression of chaperon proteins

Compared to Trx-TB10.4, the yield of Trx-TB10.4-Ag85B was relatively low (table 2.1). This may be explained by: 1) the latter protein being nearly twice the size of the former one, which consumes more energy to synthesize; 2) the greater tendency for Trx-TB10.4-Ag85B to form inclusion body. Since the first explanation is an intrinsic property of the fusion protein, the improvement was focused on the second possibility. Chaperon proteins GroEL/GroES were co-expressed with Trx-TB10.4-Ag85B, which increased the yield by at least 40% (figure 2.7). However, such improvement was minimal for Trx-Ag85B-TB10.4 (figure 2.7).

2.3.6 Purification of Trx-TB10.4-Ag85B and TB10.4-Ag85B from the inclusion body

Although thioredoxin fusion improves the folding of Trx-TB10.4-Ag85B significantly, a large quantity of mis-folded proteins was still found in the inclusion body (lane 3, figure 2.8). An effort was made to purify this protein from the inclusion body. The sharp peak in figure 2.8 represents Trx-TB10.4-Ag85B from the inclusion body, which was almost purified to homogeneity as demonstrated by SDS-PAGE (figure 2.8, lane 4). Trx-TB10.4-Ag85B purified from the inclusion body was also cleavable by TEV protease, evidenced by the appearance of two new polypeptides corresponding to TB10.4-Ag85B and thioredoxin respectively (figure 2.8, lane 5). Further purification of TB10.4-Ag85B was performed with the same procedure as described previously.

2.3.7 Study antigen secondary structure and thermal stability by circular dichroism

Figure 2.9a shows the tertiary structure of Ag85B which is composed of alpha-helixes,

beta-sheets and linking loops. Based on sequence homology between TB10.4 and three other ESAT-6 family members (figure 2.9c), the structure of TB10.4 was simulated and constructed as shown in figure 2.9b. Significantly different from Ag85B, the structure of TB10.4 is dominated by alpha-helixes by prediction.

The CD spectrum of TB10.4 at 20˚C (figure 2.10a, blue trace) again indicates that this antigen adopts an alpha-helix conformation. The results of thermal stability study suggest that TB10.4 lost its secondary structure gradually with temperature increase (figure 2.10aa). The CD spectrum recorded at 94˚C (figure 2.10a, yellow trace) indicates a dramatic loss of secondary structure at high temperature. Surprisingly, TB10.4 almost fully regains its secondary structure when cooled to 20˚C, suggesting a reversible structure change (figure 2.10a, pink and black traces in comparing to the blue trace).

Remarkably, in contrast to TB10.4, Ag85B shows a clear melting temperature (Tm) at 73.7˚C (figure 2.10bb). Moreover, Ag85B was not able to fully recover its secondary structure when cooled to 20˚C (figure 2.10b, green and light blue traces in comparing to the red trace), suggesting an irreversible structure change of this antigen.

The CD spectrum of soluble TB10.4-Ag85B (figure 2.10c) mimics that of Ag85B (figure 2.10b) but differs significantly from that of TB10.4 (figure 2.10a). The spectrum also suggests an irreversible structure change for soluble TB10.4-Ag85B (figure 2.10c, green and light blue traces in comparing to the red trace). A Tm of 75.1˚C was observed for soluble TB10.4-Ag85B (figure 2.10cc). In contrast, TB10.4-Ag85B purified from the inclusion body showed a reversible structure change (figure 2.10d, green trace in comparing to the red trace). Moreover, no Tm was observed for this protein (figure 2.10dd). These data considered together suggest that TB10.4-Ag85B purified from the inclusion body with the current

method does not regain the conformation adopted by its soluble counterpart.

2.4 Discussion

Protein overexpression in *E. coli* frequently led to the formation of inclusion body (207, 208). High concentration of denaturant was always used to resolubilize the inclusion body followed by protein renaturation (215). Although there are some rules to follow, successful protein renaturation is case dependent, which requires an extensive screen of buffers (216). With respect to mass production of recombinant proteins, obtaining protein from the inclusion body has several drawbacks (215). First, the use of a large amount of denaturant increases the cost of production. Second, removal of denaturant requires additional quality control. Third, it is difficult to know whether renatured proteins fully regain their conformation and function especially for proteins that have no enzymatic activities. Despite these disadvantages, recombinant TB antigens such as Ag85B (206), TB10.4 (201), Ag85B-ESAT-6 (205) and Ag85B-TB10.4 (19) were frequently purified from inclusion bodies and formulated into TB vaccines without comparing their conformations to that of corresponding native antigens or soluble counterparts.

A comparison of this nature may be necessary since antigen obtained from the inclusion body may adopt a significantly different conformation (depending on renaturation) compared to its soluble counterpart or native antigens and may also mount different immune responses (217). For instance, it was reported that although T cells stimulated by differently folded prion protein (PrP) recognized similar immunodominant epitopes, the cytokine profiles in response to different conformers were significantly different (217). In addition, the humoral response induced by one conformer led to the production of predominantly IgG1 isotype antibody; however, IgG2b was significantly produced with the other conformer

immunization (217). This study indicates that both humoral and cell-mediated responses to these differently folded conformers of the same protein are quite different. This may also hold true for TB antigen induced immune response. Therefore, it is highly favored to purify recombinant antigens from the soluble fraction, standing the best chance to fold correctly.

One possibility for inclusion body formation is that protein disulfide bonds are mismatched (215). However, this is not the case for TB10.4 since there is no cysteine residue in its primary sequence. Another explanation could be that recombinant proteins are treated as exogenous when expressed in *E. coli*, whose folding machinery may not be suited to certain exogenous proteins (212). Not surprisingly, the N-terminal fusion of thioredoxin greatly improved the solubility of Trx-TB10.4 possibly because thioredoxin is an endogenous bacteria protein and its first appearance after translation can prime the bacterial folding machinery (212). It is also possible that overexpression of thioredoxin or its fusions can alter the redox environment of *E. coli* cytoplasm creating a different folding environment (212). However, fusion of thioredoxin to the N-terminal of Ag85B-TB10.4 only slightly increased the solubility of Trx-Ag85B-TB10.4 in comparing to His-Ag85B-TB10.4. In contrast, the solubility of Trx-TB10.4-Ag85B was increased at least ten fold in comparison to Trx-Ag85B-TB10.4. These observations can be explained by two possibilities. First, the order of the fusion protein may be involved in solubility enhancement. As suggested by the terminal structure of Ag85B (figure 2.9a), seven residues were out of the secondary structure at the N-terminal while only three such residues exist at the C-terminal. TB10.4, however, has the same number of such residues at each terminal (figure 2.9b). These residues may serve as flexible linkers for its fusion partner. Therefore, recombinant antigen designed in the Trx-TB10.4-Ag85B direction may have a longer flexible linker in comparing to Trx-Ag85B-

TB10.4 between the two fusion moieties. Shorter linker in the later design may hamper the folding of the fusion antigen. Second, the solubilization effect of thioredoxin on TB10.4 could be greatly diluted or compromised by the longer spacer Ag85B (285 AAs) in the Trx-Ag85B-TB10.4 design.

The structure of TB10.4 lends some insights into its oligomerization. This structure may result in an extensive exposure of hydrophobic residues to the aqueous environment and thus increasing Gibbs free energy. Protein oligomerization may reduce the exposure of hydrophobic residues and thus minimizing Gibbs free energy and maximizing entropy (218). Oligomerization was also reported for CFP-10 and ESAT-6 (formation of a heterodimer), another two members in ESAT-6 family (200).

For some proteins, aggregation occurs near the isoelectric point (pI) since their surface charges are neutralized at this pH. Trx-TB10.4 and TB10.4 belong to this class of protein. It should be noticed that further decrease of pH to 3 does not lead to detectable Trx-TB10.4 aggregation, which can be explained by the fact that proteins are recharged below pI and ionic exclusion may outweigh hydrophobic interaction. However, it is still unknown whether Trx-TB10.4 possesses the same conformation at this low pH as in physiological conditions. Ag85B which has a predicted pI of 5.24, on the other hand, does not aggregate at the testing pH range. There are two possible explanations for this observation. First, the globular structure of Ag85B renders this protein highly resistant to pH change. Second, the actual pI for Ag85B may be significantly different from the predicted. The pI prediction by ProtParam is based on protein primary sequence, which does not take the tertiary structure into account. Some amino acids contributing to pI may hide inside the core of Ag85B and have limited or no access to the aqueous environment.

Circular dichroism (CD) is a useful tool to study protein secondary structure (174). Ag85B and soluble TB10.4-Ag85B have similar CD spectrum and similar pattern of thermal stability. The structural characteristics for these two proteins are 1) the presence of a clear melting temperature; 2) irreversible structure change. It should be noted that the slope of the sigmoidal fit is steeper for soluble TB10.4-Ag85B than for Ag85B, which could be explained by the contribution of TB10.4 in the fusion protein. Soluble TB10.4 and TB10.4-Ag85B purified from the inclusion body, on the contrary, underwent a reversible structure change while lacking a clear melting temperature. Protein structure may explain the different behaviors in the CD experiments. Ag85B, which has a globular structure, is resistant to the temperature increase to a certain extent. At the melting temperature, the intramolecular forces are not strong enough to hold the tertiary structure thus a dramatic loss of CD signal occurs. Since the loss of conformation is so dramatic and fast, Ag85B may not be able to recover all intramolecular interactions correctly when cooled. In contrast, structure loss of TB10.4 took place gradually all the way with temperature increase. This may explain the reversible structure change when TB10.4 was cooled. Although soluble, TB10.4-Ag85B purified from the inclusion body does not regain the confirmation adopted by its counterpart purified from the soluble fraction. It may adopt an intermediate conformation. Since the main purpose of this study is to purify large quantities of soluble antigens, no further effort was made to optimize the renaturation condition for TB10.4-Ag85B. This could be an interesting topic for the future study.

Only partial success was achieved to purify TB10.4-Ag85B from inclusion bodies, in other words, we were only able to resolubilize TB10.4-Ag85B from its insoluble aggregates and maintain its solubility after denaturant removal whereas the conformation of TB10.4-

Ag85B was not recovered. Initial trial to renature this protein at high protein concentration failed possibly because protein refolding is a first order reaction and protein aggregation is at least a second order reaction (219). Therefore, aggregation is favored over refolding at high protein concentrations. A rapid dilution procedure was then used to decrease the protein concentration by slowly diluting concentrated TB10.4-Ag85B into buffers with constant stirring. This procedure led to a partial success with soluble yet incorrectly folded TB10.4-Ag85B as evidenced by CD differentiation. There are two explanations for this result. First, rapid dilution procedure caused a shock-decrease of the denaturant concentration used for resolubilization and, therefore, TB10.4-Ag85B may not have enough time to fold correctly but otherwise became a soluble molten globule or even less ordered structure. Second, the renaturation buffer used in our experiment is not optimal. Renaturation buffer is always protein dependent, which requires conditions such as redox state and pH empirically optimized for each protein. However, no reagent was added into our renaturation buffer to control the redox conditions.

Based on our understanding of protein aggregation and research experience in protein refolding, we can envision how to achieve a full success of refolding TB10.4-Ag85B into its native conformation in the future. Factors we may consider include protein concentration, rate of denaturant removal (on-column refolding rather than dialysis), buffer pH and redox conditions, renaturation excipients such as dithiothreitol (DTT) and L-arginine, as well as temperature, and pressure (219, 220).

2.5 Summary

In this chapter, soluble antigens, Ag85B, TB10.4 and TB10.4-Ag85B, were expressed in *E. coli* and purified to homogeneity in large quantities. In addition, TB10.4-Ag85B is a

complete new fusion molecule designed in our lab representing a novel antigen candidate for TB subunit vaccine. Rational design of the expression constructs dramatically increased the solubility and yield of recombinant antigens leading to mass production of these antigens feasible. Circular dichroism experiments showed a significant conformation difference between TB10.4-Ag85B purified from the inclusion body and its soluble counterpart. The pH and thermal stability data provide invaluable information that will guide further formulation development based on these antigens.

Table 2.1 Characterization of recombinant antigens

Protein	AAs	MW (KD)	pI[a]	Solubility	Yield (mg/L)
Ag85B	318	34	5.24	S[b]	5
His-TB10.4	129	14	5.23	IB[c]	N/A
Trx-TB10.4	269	29	5.16	S	14
TB10.4	105	11.3	4.82	S	4
Trx-Ag85B-TB10.4	554	60	5.05	WS[d]+IB	N/A
Trx-TB10.4-Ag85B	554	60	5.05	S+IB	2.5
TB10.4-Ag85B	390	42	4.85	S	1
His-Ag85B-TB10.4	414	45	5.02	IB	N/A

a: isoelectric point (predicted by ProtParam, see materials and methods)
b: soluble; c: inclusion body; d: weekly soluble

Figure 2.1 Construct design for recombinant antigens. a, Trx-TB10.4 in customized pET32b vector; b, His-Ag85B-TB10.4 in pRSET-B vector; c, Trx-Ag85B-TB10.4 in customized pET32b vector; d, Trx -TB10.4-Ag85B in customized pET32b vector.

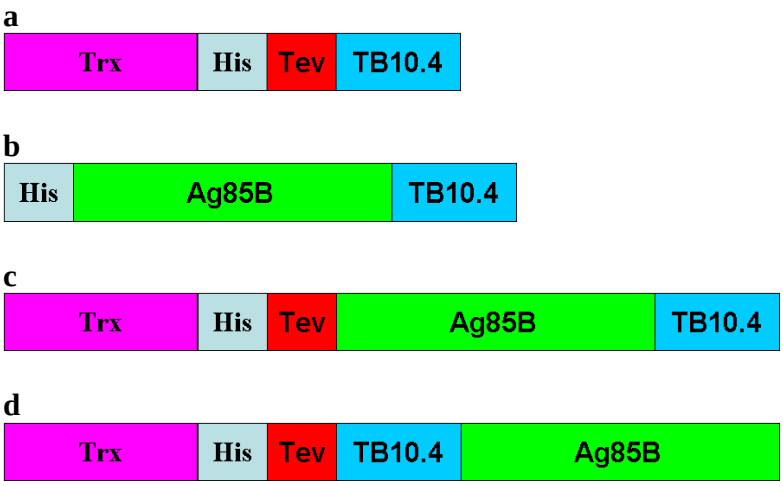

Figure 2.2 Purification of TB10.4 by nickel-affinity and size-exclusion chromatography. a, chromatogram of TB10.4 purified by nickel-affinity column; b, calibration of Superdex 75 column with protein standards (cytochrome c: 12.4KD; carbonic anhydrase: 29KD; bovine serum albumin: 66KD; β-amylase: 200KD). The log-transformation of protein molecular weight was linearly correlated with the elution volume (inset, upper left corner); c, chromatogram of TB10.4 further purified by Superdex 75 column.

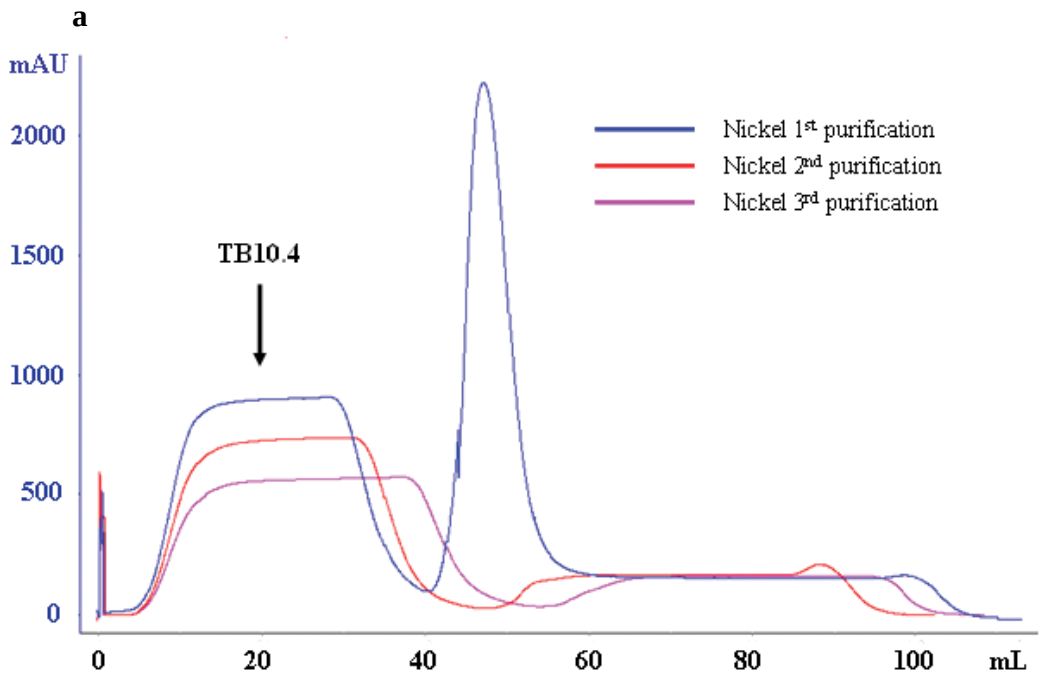

b

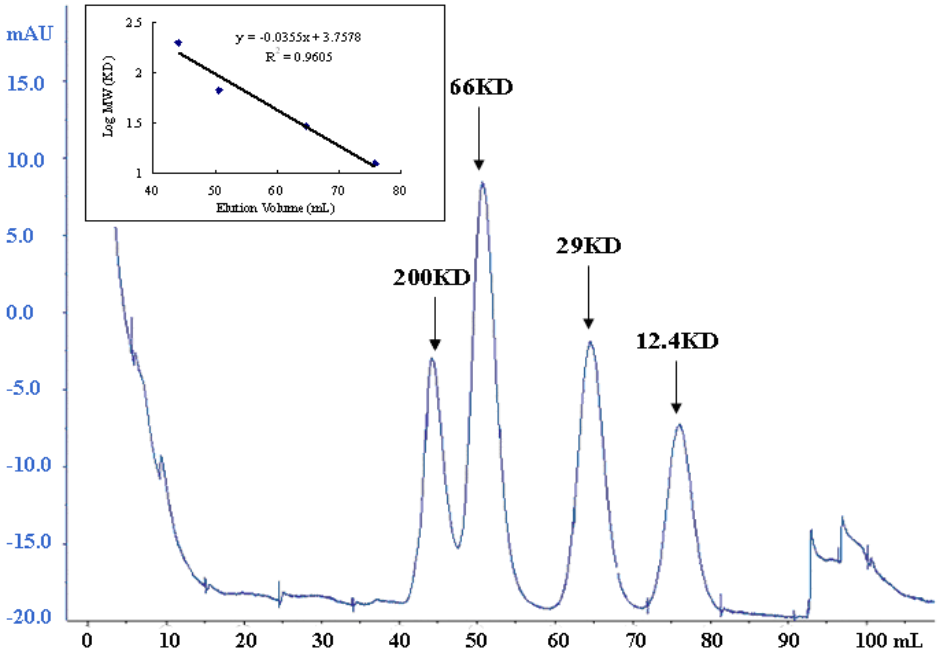
mAU
15.0
10.0
5.0
0.0
-5.0
-10.0
-15.0
-20.0
0
10
20
30
40
50
60
70
80
90
100 mL
66KD
200KD
29KD
12.4KD
y = -0.0355x + 3.7578
R² = 0.9605
Log MW (KD)
Elution Volume (mL)

c

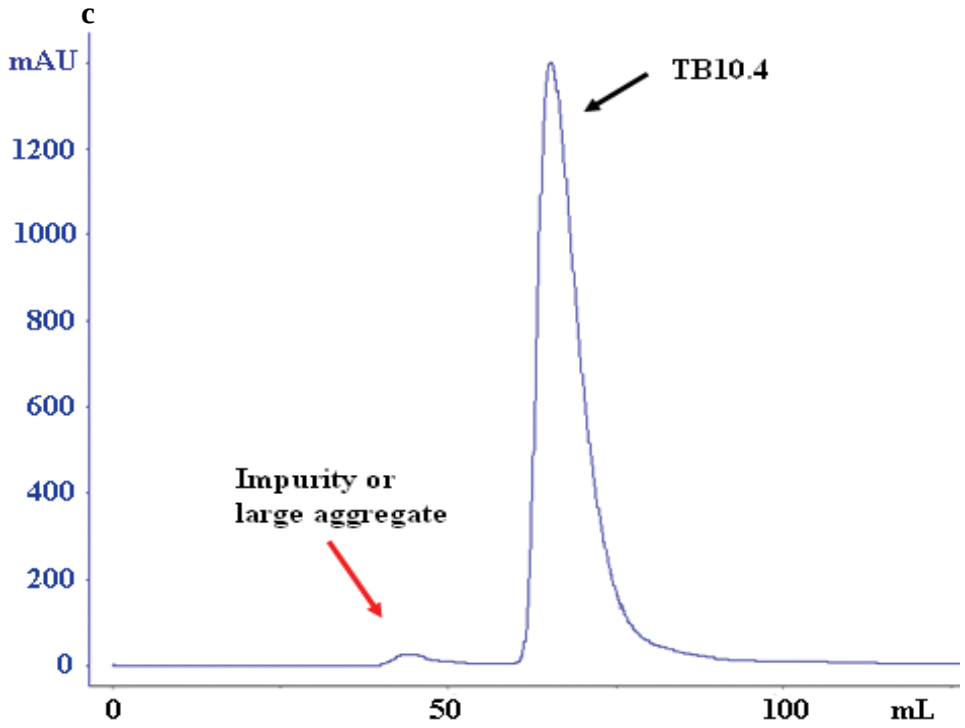
mAU
1200
1000
800
600
400
200
0
0
50
100
mL
TB10.4
Impurity or
large aggregate

Figure 2.3 SDS-PAGE and native-PAGE analysis of recombinant antigens. a, SDS-PAGE analysis of Trx-TB10.4 and its digestion products. lane 1: Trx-TB10.4; lane 2: Trx-TB10.4 was treated with TEV protease and then passed through the nickel column. The flow-through was collected; lane 3: proteins bound to the column were eluted and collected; lane 4: duplicate of lane 2; lane 5: duplicate of lane 3; b, SDS-PAGE analysis of purified antigens. lane 1: Ag85B; lane 2: Trx-TB10.4; lane 3 and 4: TB10.4; c, native-PAGE analysis of purified antigens. lane 1: Ag85B; lane 2 and 3: TB10.4; lane 4: thioredoxin.

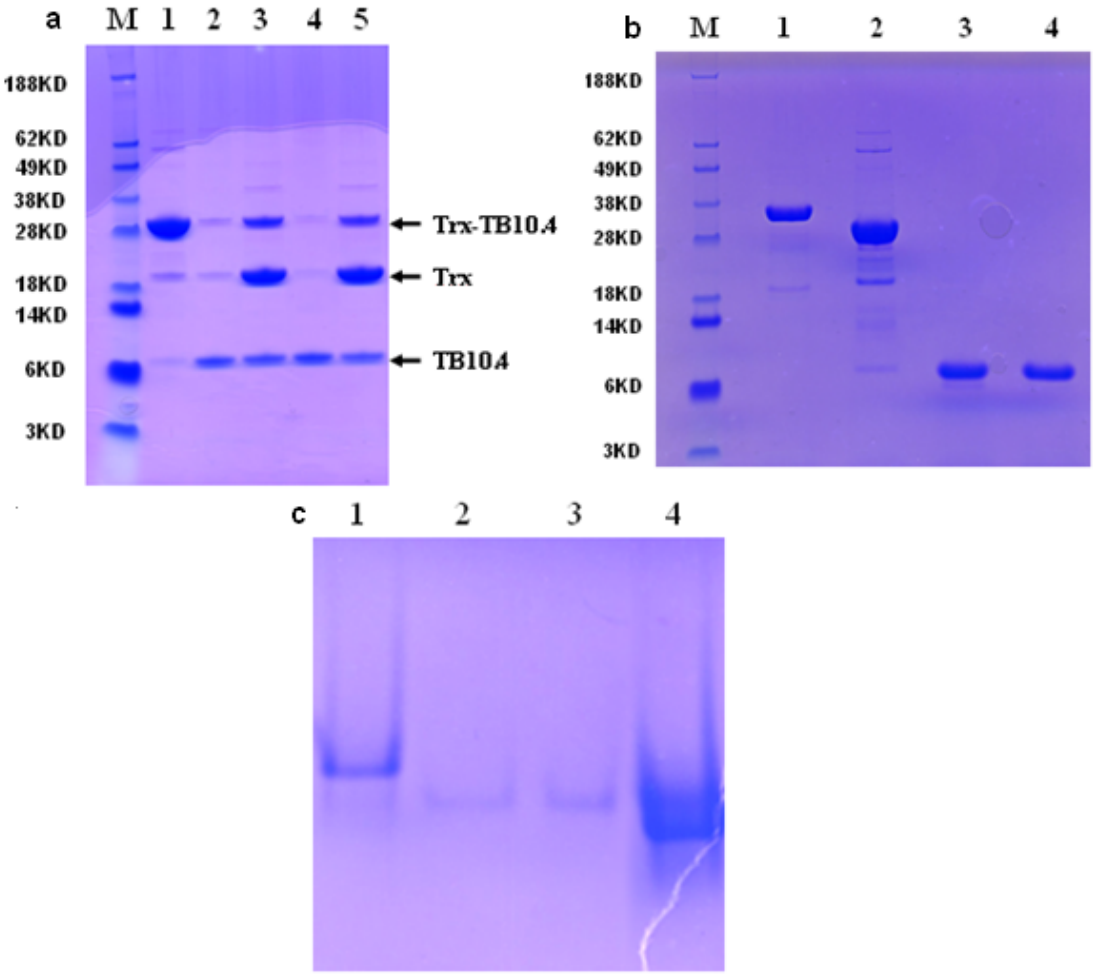

Figure 2.4 Effect of buffer pH on antigen stability (n=3, mean ± SD). a, buffer pH on Trx-TB10.4 stability; b, buffer pH on TB10.4 stability. For PCS (photon correlation spectrometry) intensity greater than 300, the size and distribution could be accurately calculated and labeled in the figure. For overnight incubation, the protein aggregates precipitate out from the solution and no PCS intensity was recorded.

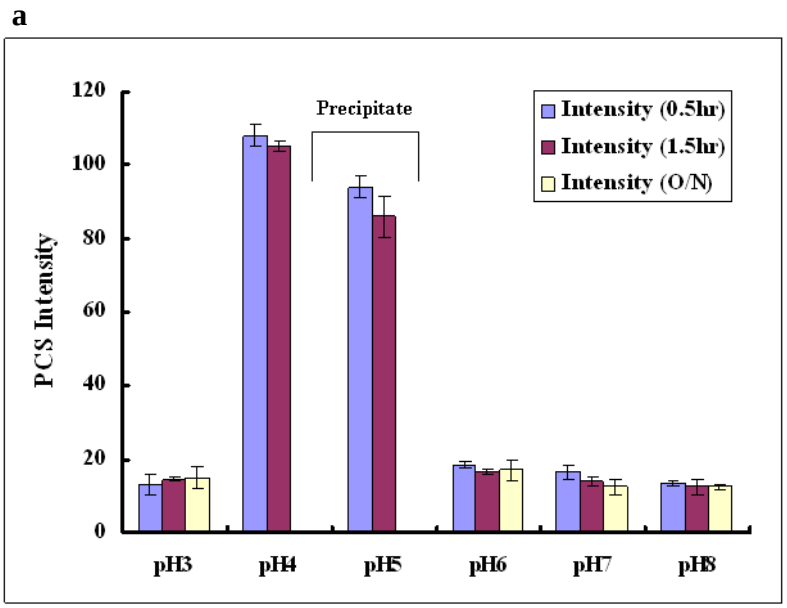

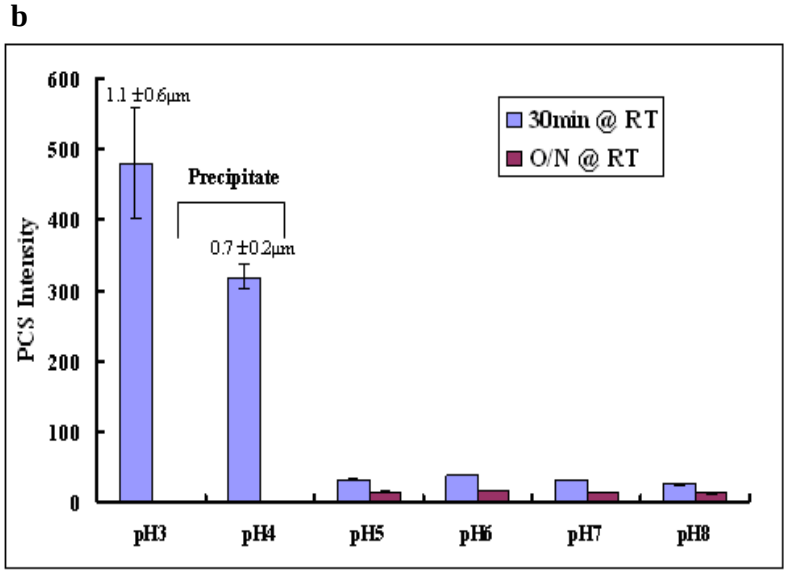

Figure 2.5 SDS-PAGE analysis of recombinant fusion antigens. a, SDS-PAGE analysis of nickel column purified antigens. lane 1: Trx-Ag85B-TB10.4 (indicated by asterisk); lane 2: Trx-TB10.4-Ag85B (indicated by asterisk); b, TB10.4-Ag85B released by TEV protease treatment was analyzed by SDS-PAGE. lane 1: Trx-TB10.4-Ag85B was treated with TEV protease overnight; lane 2: eluant of first pass through nickel column; lane 3: eluant of second pass through nickel column; lane 4: eluant of third pass through nickel column; lane 5: 10 times concentrate of the third eluant. c, TB10.4-Ag85B was further purified by GPC200 column. lane 1: 1 μg TB10.4-Ag85B; lane 2: 3 μg TB10.4-Ag85B; lane 3: 3 μg TB10.4-Ag85B prior to GPC200 purification.

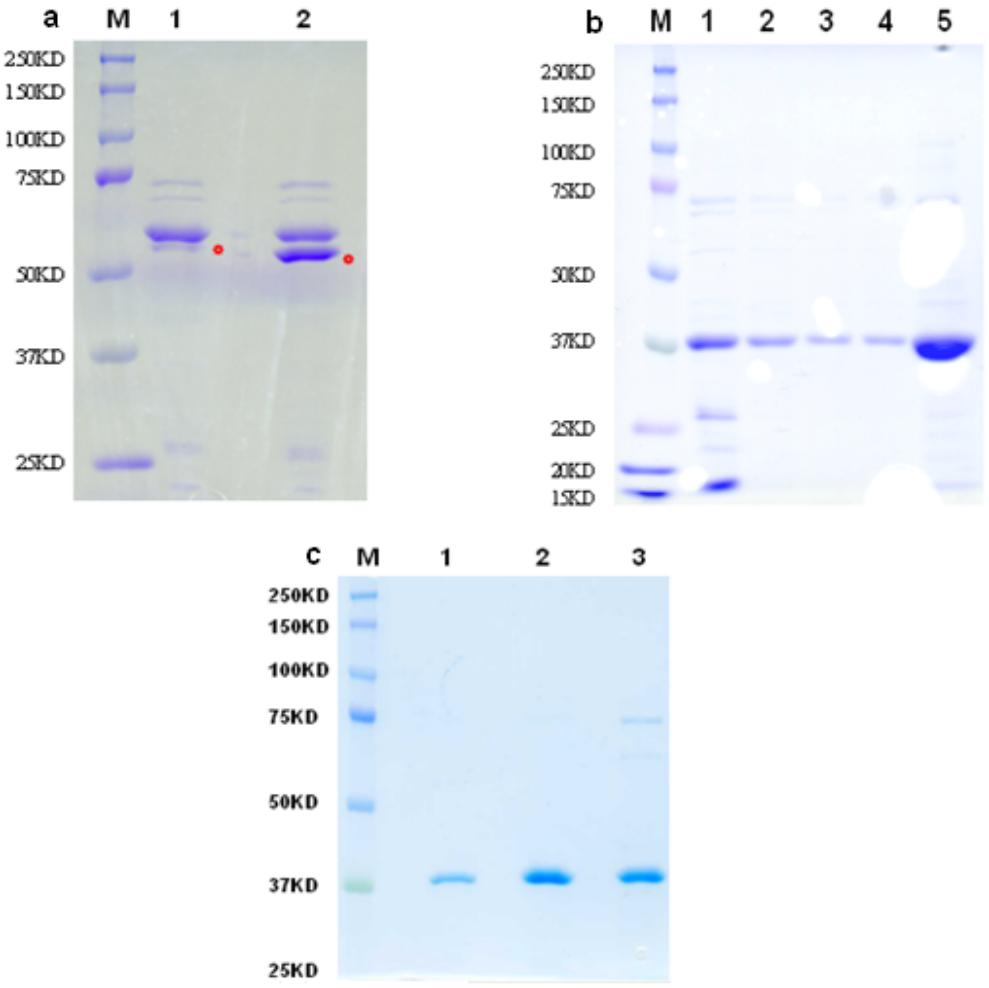

Figure 2.6 Purification of TB10.4-Ag85B by nickel-affinity and size-exclusion chromatography. a, chromatogram of TB10.4-Ag85B purified by nickel-affinity column; b, chromatogram of TB10.4-Ag85B further purified by Superdex 200 column.

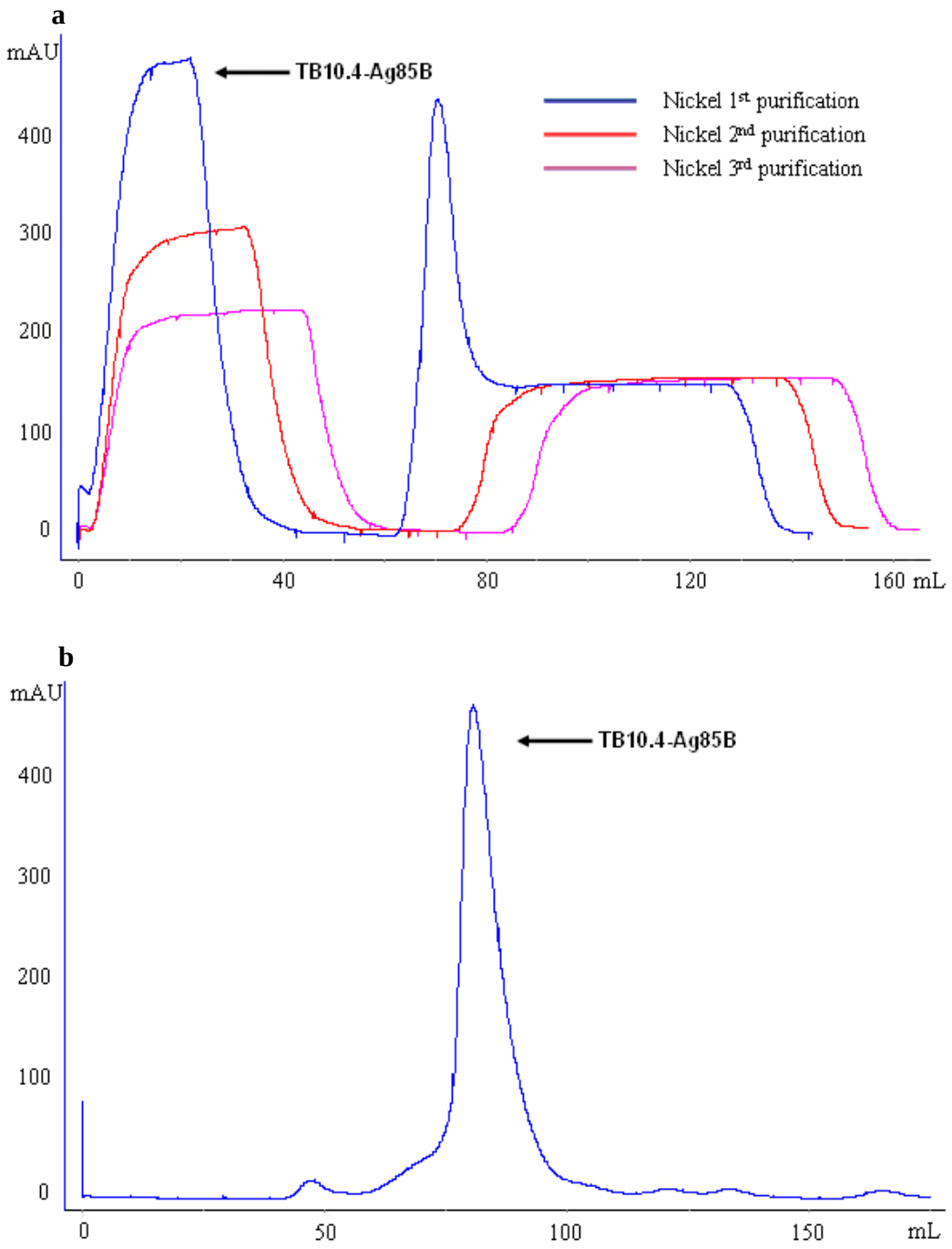

Figure 2.7 Comparison of the yield of two recombinant antigens with or without the co-expression of chaperons. Chromatograms were shown of antigens purified by nickel-affinity chromatography.

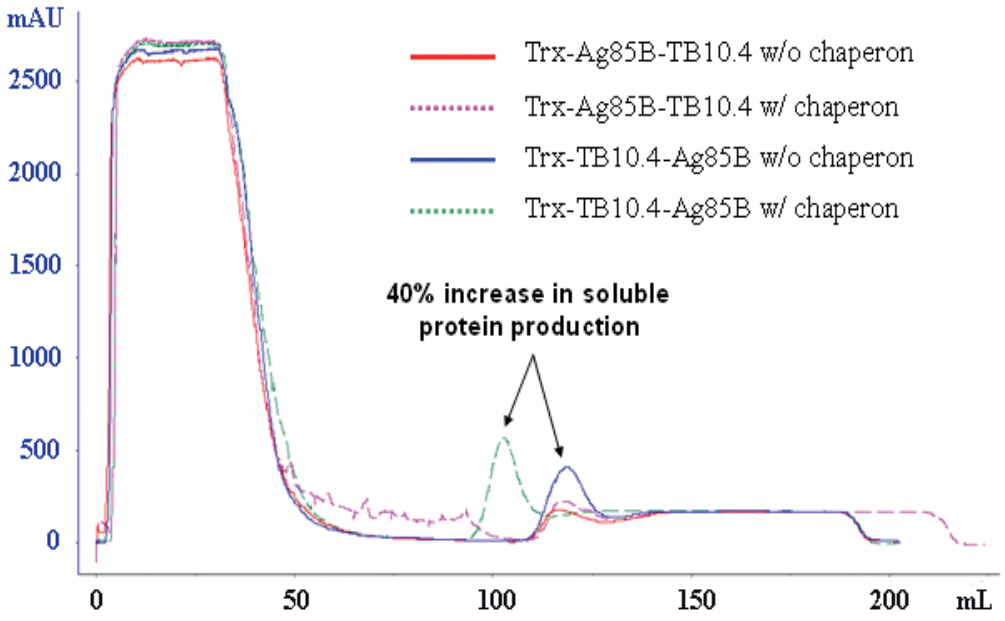

Figure 2.8 Purification of Trx-TB10.4-Ag85B and TB10.4-Ag85B from the inclusion body. Inset (upper left corner). lane 1, soluble Trx-TB10.4-Ag85B was treated with TEV protease; lane 2, same as lane 1 but different loading; lane 3, urea resolubilized Trx-TB10.4-Ag85B; lane 4, Trx-TB10.4-Ag85B in lane 3 was purified by nickel column; lane 5, purified Trx-TB10.4-Ag85B in lane 4 was cleaved by TEV protease into two fragments.

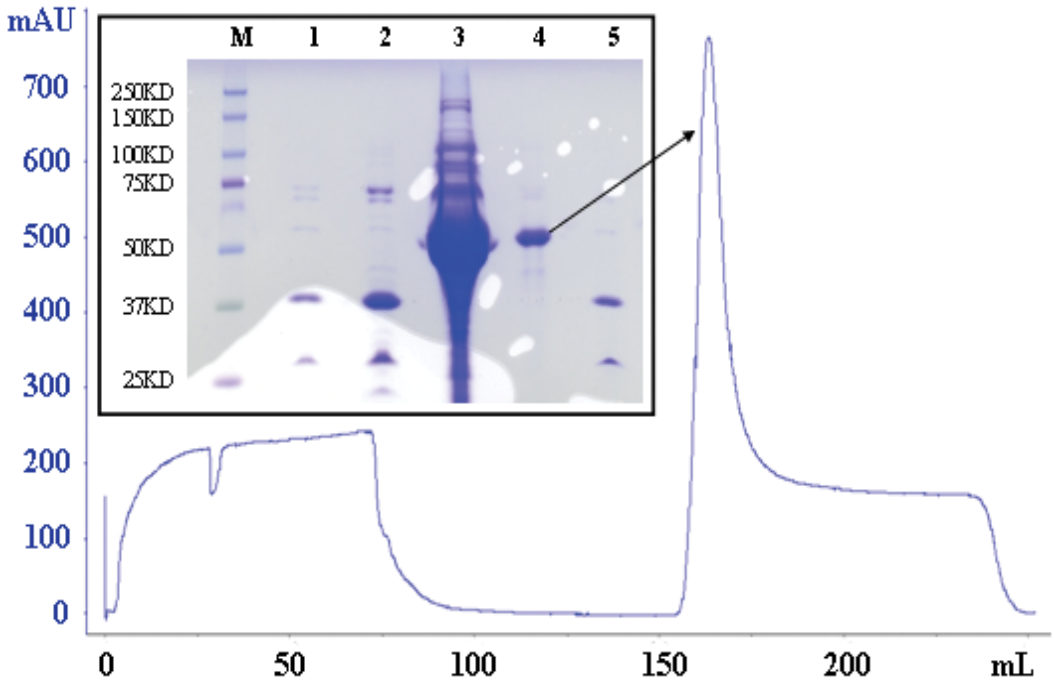

Figure 2.9 Structures of Ag85B and TB10.4. a, structure of Ag85B (PDB accession #: 1F0N); b, structure of TB10.4 (simulated); c, multiple sequence alignment of ESAT-6 protein family members TB10.4, TB10.3, ESAT-6 and CFP-10.

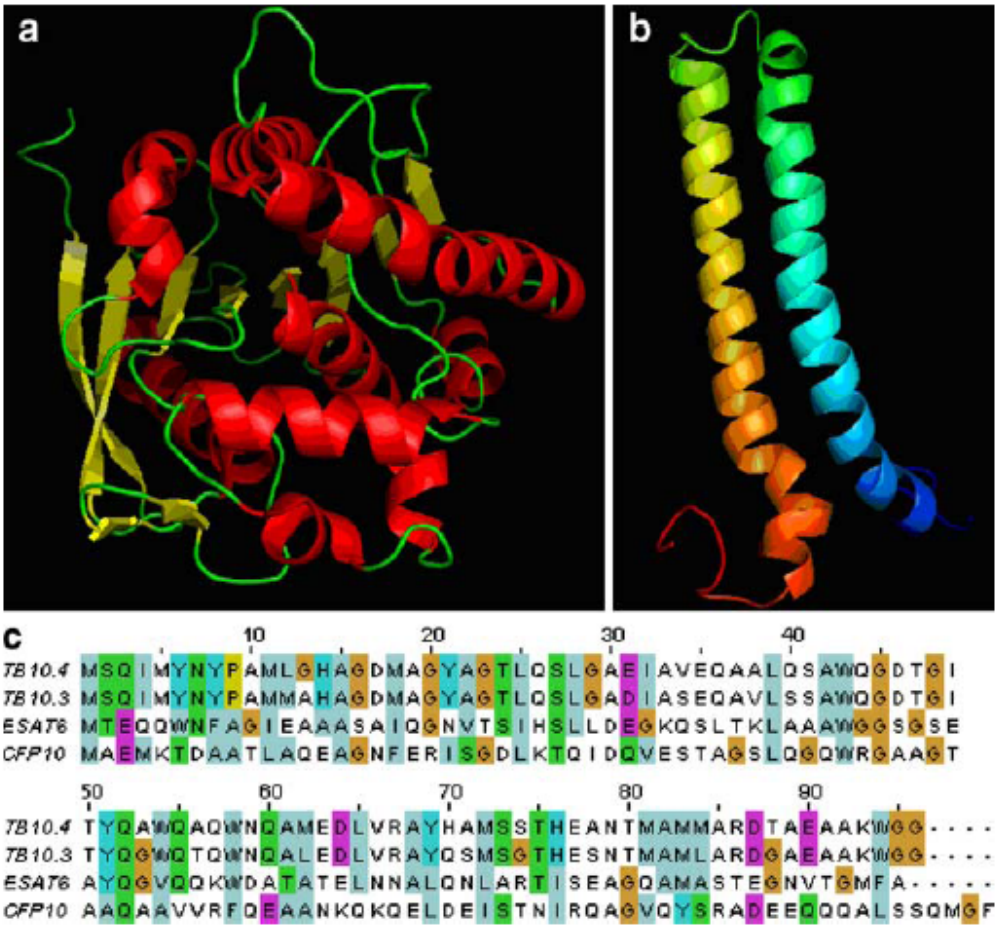

Figure 2.10 Study antigen secondary structure and thermal stability by circular dichroism (CD). a, CD spectrum of TB10.4; aa, thermal stability study of TB10.4; b, CD spectrum of Ag85B; bb, thermal stability study of Ag85B; c, CD spectrum of soluble TB10.4-Ag85B; cc, thermal stability study of soluble TB10.4-Ag85B; d, CD spectrum of TB10.4-Ag85B purified from the inclusion body; dd, thermal stability study of TB10.4-Ag85B purified from inclusion body.

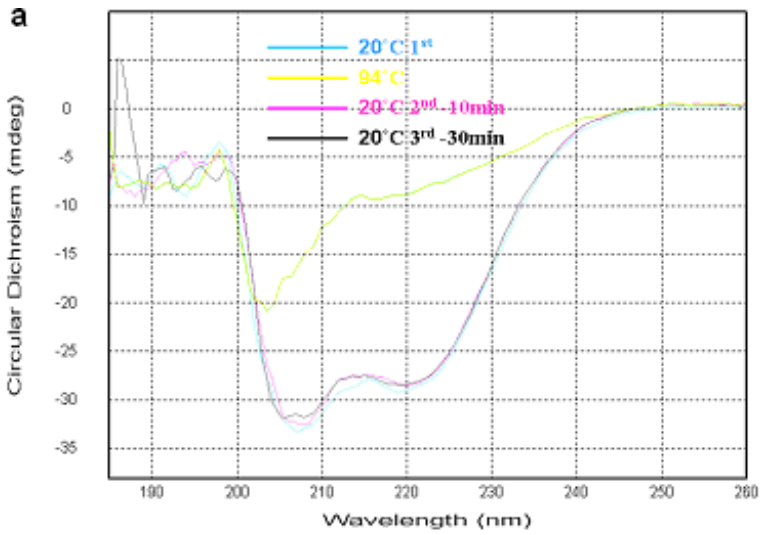

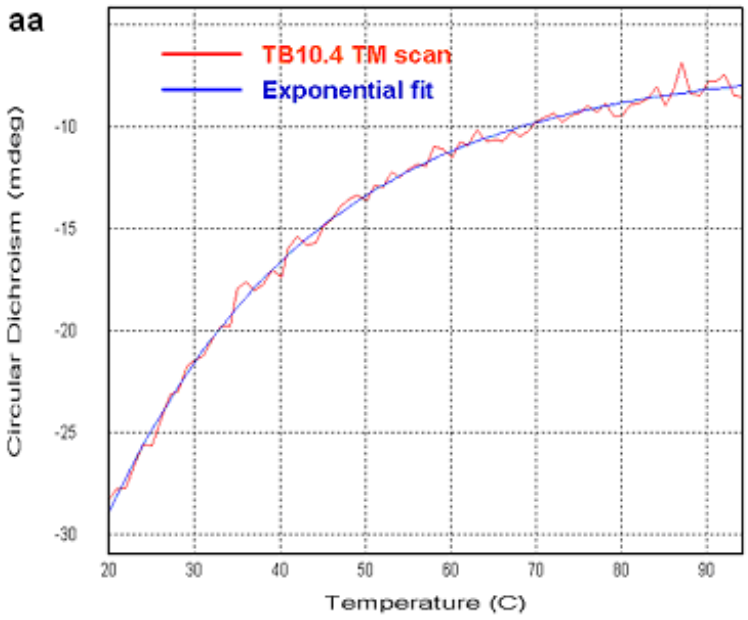

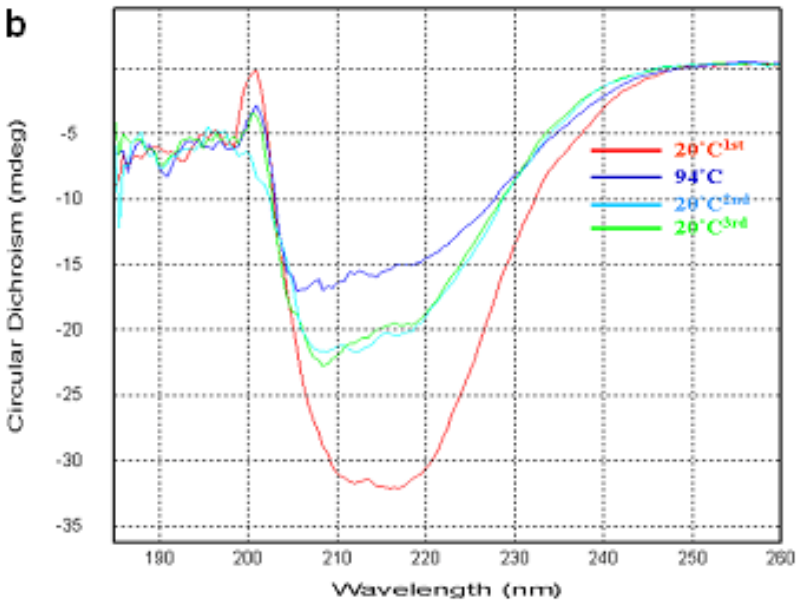
b
Circular Dichroism (mdeg)
-5
-10
-15
-20
-25
-30
-35
180
200
210
220
230
240
250
260
Wavelength (nm)
20°C1st
94°C
20°C2nd
20°C3rd

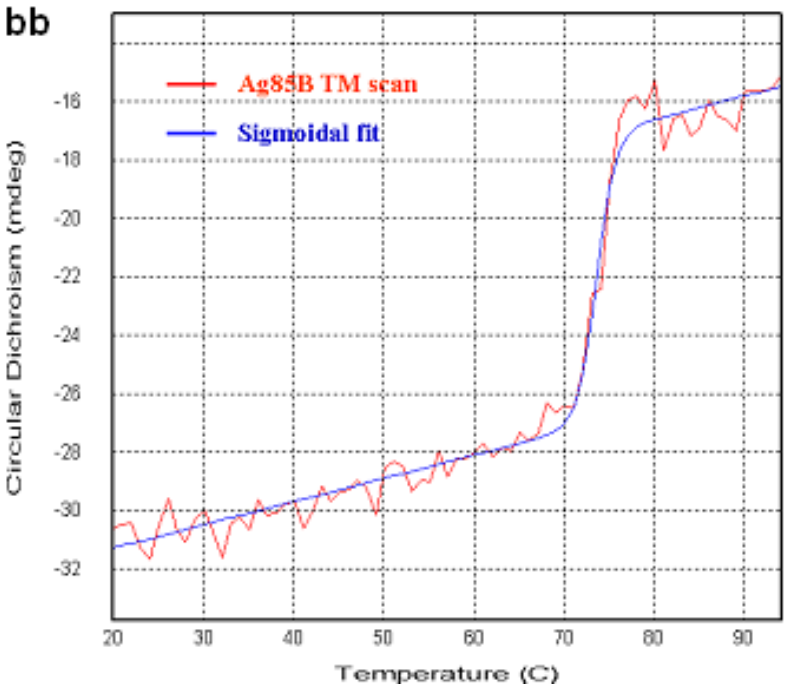
bb
Circular Dichroism (mdeg)
-16
-18
-20
-22
-24
-26
-28
-30
-32
20
30
40
50
60
70
80
90
Temperature (C)
Ag85B TM scan
Sigmoidal fit

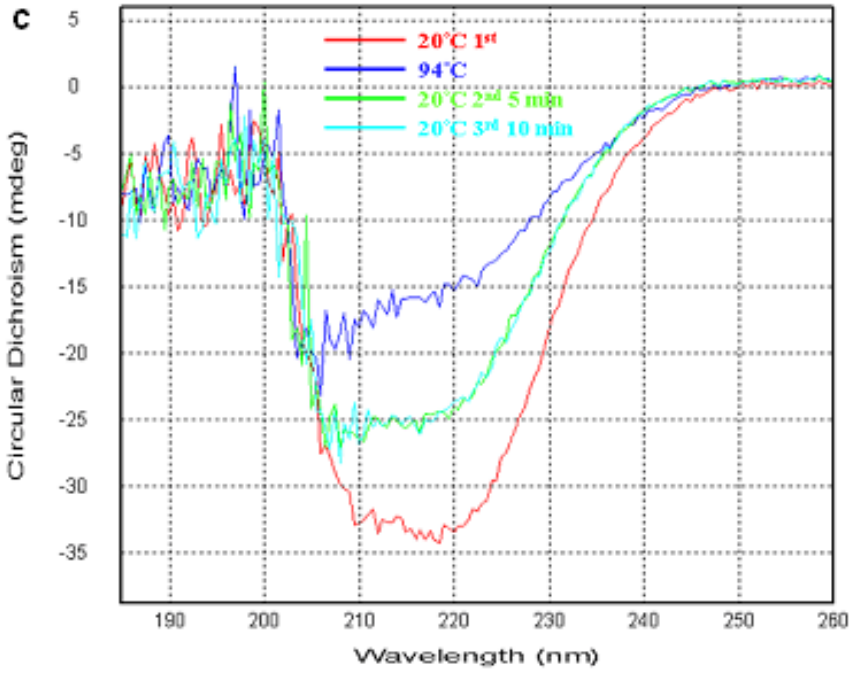
c
20°C 1st
94°C
20°C 2nd 5 min
20°C 3rd 10 min
Circular Dichroism (mdeg)
Wavelength (nm)

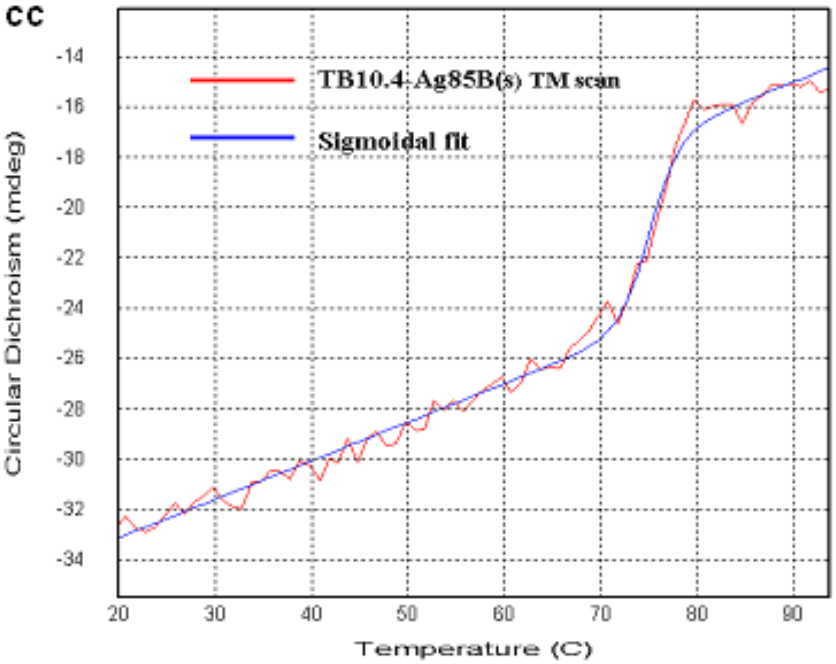
cc
TB10.4 Ag85B(s) TM scan
Sigmoidal fit
Circular Dichroism (mdeg)
Temperature (C)

d

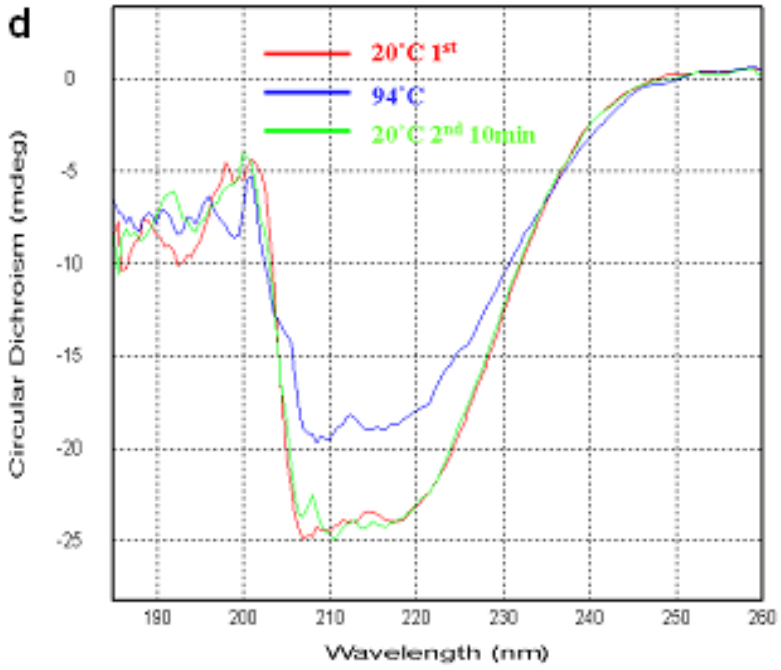
20°C 1st
94°C
20°C 2nd 10min
Circular Dichroism (mdeg)
0
-5
-10
-15
-20
-25
190
200
210
220
230
240
250
260
Wavelength (nm)

dd

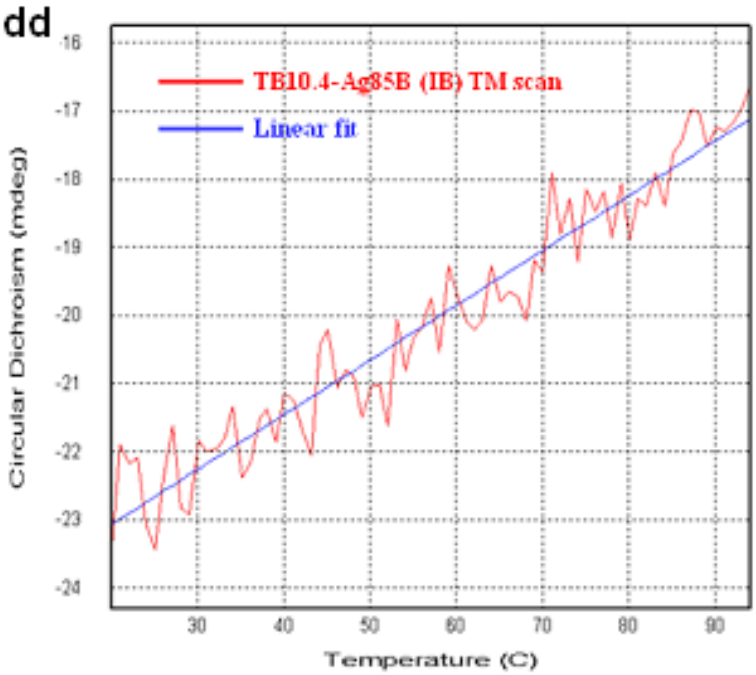
TE10.4-Ag85B (IB) TM scan
Linear fit
Circular Dichroism (mdeg)
-16
-17
-18
-19
-20
-21
-22
-23
-24
30
40
50
60
70
80
90
Temperature (C)

CHAPTER 3: MANUFACTURE AND CHARACTERIZATION OF RESPIRABLE PLGA-rAg MICROPARTICLES

In the last chapter, recombinant antigens were designed, expressed, purified and characterized. These antigens include Ag85B, TB10.4, and TB10.4-Ag85B. In this chapter we will discuss how to make vaccine formulations by encapsulating antigens into PLGA microparticles (PLGA-rAg). PLGA was selected as the delivery vehicle for several reasons: 1) PLGA has well documented safety profile; 2) the release from PLGA can be controlled by varying the ratio of two building monomers; 3) the density of PLGA particles is low which is particularly suitable for pulmonary delivery. PLGA-rAg microparticles were manufactured by emulsion/spray-drying method. Since the particle size is primarily determined by spray drying, this process was optimized systematically with a half-factorial design. The condition that gave rise to the target particle size and yield was chosen to prepare subunit vaccine formulations. In addition to antigens, an adjuvant muramyl dipeptide (MDP) was also included in the formulation. There are a total of six formulations made under the optimized condition including: PLGA (blank particles), PLGA-MDP (adjuvant included), PLGA-MDP-Ag85B, PLGA-MDP-TB10.4, PLGA-MDP-TB10.4+Ag85B (blend), and PLGA-MDP-TB10.4-Ag85B (fusion). The first two formulations serve as the control while the rest are subunit vaccine formulations. These formulations were characterized in terms of particle size, aerodynamic size and distribution, flow properties, surface charge, energy and morphology, thermal behavior, antigen integrity, and release profiles. Such characterizations provide a comprehensive understanding of the physicochemical properties of the manufactured

microparticles. In this chapter, optimization of the spray-drying parameters will be discussed first followed by a detailed physicochemical characterization of the prepared formulations.

3.1 Introduction

Poly (lactide-co-glycolide) (PLGA) is a copolymer that has been used in a number of FDA approved therapeutic devices due to its biodegradability and biocompatibility (221). For example, Lupron Depot® is a commercially available drug delivery device using PLGA for the treatment of advanced prostate cancer (222, 223). In addition, there have been numerous reports employing PLGA to encapsulate insulin for improved pharmacokinetics and pharmacodynamics as well as reduced dosing frequency (224-226). PLGA has also been employed to manufacture tuberculosis subunit vaccine by several research groups. For example, Lu *et al* reported that PLGA microspheres containing recombinant Ag85B could induce significant interleukin-2 secretion *in vitro* (125). Kirby *et al* reported that Ag85B-ESAT6 encapsulated in PLGA microspheres induced a cell-mediated immune response and raised specific antibodies after immunization of the mice (173).

For the purpose of pulmonary delivery of vaccines, recombinant antigens should be encapsulated into PLGA particles with an aerodynamic size range from 1 to 5 μm (138). This requires the selection of the right microencapsulation technique, which in turn depends on the active ingredients, the nature of polymer and the intended use. In general, five rules should be considered in terms of choosing the microencapsulation method: 1) the biological activity and physicochemical stability of the active ingredients should not be adversely affected by the encapsulation procedure; 2) the size of manufactured microparticles should meet the requirement; 3) the yield of microparticles with the required particle size range should be acceptable; 4) the microparticles should have good flow properties with little aggregation or

adherence; 5) the microencapsulation procedure should have a good scalability. There are three common methods widely used to manufacture microparticles including emulsion/solvent evaporation (227), phase separation (228) and spray drying (229).

Two successive steps are involved in the emulsion/solvent evaporation method. The first step is emulsion, which can be a single emulsion or double emulsion. Single emulsion involves only one emulsion procedure such as oil-in-water (o/w) or oil-in-oil (o/o) emulsion. Polymers are usually not water soluble and, therefore, dissolved in a water immiscible solvent (usually a volatile organic solvent). Active ingredients depending on their solubility in the organic solvent can either dissolve or disperse as particles in the polymer solution (228). This mixture is then emulsified into a large quantity of a second phase such as water in o/w emulsion or oil in o/o emulsion in the presence of an emulsifier. In contrast to the single emulsion, double emulsion involves two emulsion processes, for instance, water-in-oil-in-water (w/o/w) double emulsion and oil-in-water-in-oil (o/w/o) double emulsion. The w/o/w double emulsion is well suited to encapsulate water-soluble substances such as hydrophilic drugs and peptides/proteins into PLGA microparticles (173). Water-soluble substances are first dissolved in a small volume of aqueous buffer, which is then emulsified into a large volume of oil phase containing dissolved PLGA. The primary emulsion is then transferred to an aqueous solution for the preparation of the second emulsion either by homogenization or sonication. Oil-in-water emulsifier is always used to make the second emulsion, for instance, poly (vinyl alcohol) (PVA) is selected for the purpose of preparing PLGA microspheres (173). Solvent evaporation is the second step of the emulsion/solvent evaporation method, which hardens the oil droplets leading to the formation of microparticles (228, 230). This is usually done by evaporating the volatile organic solvent at reduced pressure with constant

stirring but can also be done at ambient conditions. The solidified microparticles are then washed and collected by filtration, centrifugation, or sieving. After lyophilization or drying at appropriate conditions, these particles are ready for use or storage. A number of drugs have been encapsulated into PLGA microparticles by the emulsion/solvent evaporation method (231-233). However, a few disadvantages are associated with this method. First, the encapsulation efficiency is relative low for hydrophilic drugs which tend to diffuse into the water phase during the second emulsion process. Second, the residual organic solvent is difficult to remove completely by sole evaporation. Third, this method is difficult to scale up due to various factors that are involved.

Phase separation is another method to manufacture microparticles. This method relies on decreasing the solubility of polymer in its solvent by adding an organic nonsolvent (228). Two phases are formed during this process with the polymer containing coacervate phase and the other phase depleted in polymer. Similar to the emulsion/solvent evaporation method, hydrophilic drugs are first dissolved in an aqueous buffer followed by emulsifying into the polymer solution to create the primary w/o emulsion. However, evaporation is not used to harden the particles. Rather, an organic nonsolvent is added into the emulsion with stirring to extract the solvent out of the polymer solution. This leads to the phase separation of the polymer, which then forms soft coacervate droplets that entrap the active ingredients. The coacervates are hardened by transferring to a large volume of organic nonsolvent for further extraction and separation (228). The hardened microparticles can be collected by similar ways as described in the first method. Phase separation method is less used then the solvent evaporation method for several reasons: 1) it requires a large quantity of organic solvent; 2) particles prepared by this method have poor flow characteristics due to particle

agglomeration; 3) it is a non-equilibrium system and, therefore, the formulation and process variables have a very significant impact on the characteristics of the final microparticles (228).

The third method to prepare PLGA microparticles is spray drying (229). Compared to the other two methods, spray drying has its unique advantages such as convenience, delicate controlling system, reproducibility and scalability. Encapsulation of hydrophobic drugs is relatively easy. They can be co-dissolved with PLGA in the organic solvent. In this way drugs are dissolved (homogeneously distributed) in the matrix of PLGA microparticles after spray drying. For hydrophilic drugs/proteins which are immiscible with the solvent, they can be either dispersed as solid particles in the polymer solution or first dissolved in an aqueous buffer followed by emulsifying into the polymer solution. The resulting preparation is then spray dried to yield the desired microparticles. One concern with this method is that hydrophilic drugs/proteins may not be homogeneously distributed in the matrix of PLGA microparticles but rather exist as a separate phase, i.e. fine drug particles dispersed in the large polymer particles (172). It is possible to circumvent this problem by dissolving PLGA in a water miscible organic solvent such as acetone which is then mixed with an aqueous solution of hydrophilic drugs/proteins. This approach assumes that mixing two solutions does not cause precipitation of either the polymer or the drugs from the system. The size of spray-dried particles can be controlled to some extent by the polymer concentration, drug loading and the nature of solvent but to large extent by the spray-drying process (191, 229). Solutions fed into the spray drier are dispersed by the atomization gas to create fine droplets, which are then dried in the drying chamber with heated air flow. The temperature of the drying air is well controlled to provide enough heat transfer to evaporate water and the organic solvent but

pose no risk to the encapsulated drugs. With solvent removal, PLGA particles get hardened and are subsequently removed from the air stream by the centrifugal forces generated in the cyclone. The yield is relatively low at bench-size production but can be very high once scaled up. Both the size and yield are controlled by spray-drying parameters, which should be optimized for the desired features.

Particle characterization is an integrative part of the powder technology (234, 235). Particle size is one of the most important characters of a powder. The geometric size and distribution can be measured by a laser diffraction particle sizer, which works on the principle that large particles diffract light to a small angle while small particles diffract light to a large angle. Geometric size is important in terms of particle uptake by target cells. The aerodynamic particle size and distribution can be obtained with a cascade impactor based on the Stokes' law. This size determines the lung deposition of delivered aerosol particles. In addition to size, particle size distribution is also an important index with a narrow size distribution highly desired. Particle morphology can be examined by a scanning electron microscope. The surface structure of particles has great impact on particle aggregation and flow properties, which will ultimately affect particle delivery and deposition. To characterize the thermal behavior of a powder, differential scanning calorimetry (DSC) is typically used by measuring the difference of heat flow. Useful thermodynamic parameters such as the glass transition temperature and the change of heat capacity can be obtained by DSC.

In this chapter, the spray-drying parameters were first systematically optimized in terms of both particle size and yield by employing the concept of Quality-by-Design (QbD). Under optimized conditions, TB subunit vaccines were prepared by encapsulating different recombinant TB antigens/antigen combinations into PLGA microparticles in the presence of

an adjuvant muramyl dipeptide. Manufactured particles were extensively characterized in terms of particle size, surface energy, charge and morphology, thermal property, antigen integrity and release profiles.

3.2 Materials and Methods

Preparation of recombinant antigens

Recombinant antigens Ag85B, TB10.4 and TB10.4-Ag85B were expressed in *E. coli* and purified by a combination of nickel-affinity and size-exclusion chromatography as described in the second chapter. The homogeneity of purified antigens was determined by SDS-PAGE under reducing conditions.

Microparticle preparation

Poly (lactide-co-glycolide) (PLGA, lactic/glycolic ratio 75:25, MW 84.7 kDa, intrinsic viscosity 0.68 dL/g in $CHCl_3$) was purchased from Durect (Lactel® Absorbable Polymers, Pelham, AL, USA). Muramyl dipeptide (MDP) was purchased from Sigma (St. Louis, MO, USA). Dichloromethane (DCM) was purchased from Burdick & Jackson (HPLC grade, Muskegon, MI, USA). To optimize spray-drying condition, PLGA (700 mg) was dissolved in 200 ml DCM (0.35%, w/v). MDP (adjuvant, 3.5 mg) and bovine serum albumin (BSA, 1mg) were dissolved in 2.4 ml phosphate buffered saline (PBS, pH7.4). The aqueous and organic phases were probe sonicated for three 10s periods on an ice bath immediately prior to spray drying. The emulsion was spray-dried through a 0.7-mm diameter nozzle of a Buchi mini spray-dryer (B-191, Buchi, Flawil, Switzerland) according to the half-factorial design (table 3.1) constructed in the statistical software Design-Expert®. Particles were collected from the jar and cyclone wall of the spray dryer. These particles were labeled as PLGA-MDP-BSA. To prepare subunit vaccines for *in vitro* antigen presentation assay, recombinant TB antigens

rather than BSA were encapsulated into PLGA microparticles with the same procedure as described above except that they were manufactured under optimized spray-drying condition. These formulations include PLGA, PLGA-MDP, PLGA-MDP-TB10.4, PLGA-MDP-Ag85B, PLGA-MDP-TB10.4+Ag85B and PLGA-MDP-TB10.4-Ag85B. The loading of MDP in all these formulations is 0.5%. The loading of Ag85B in PLGA-MDP-Ag85B and PLGA-MDP-TB10.4+Ag85B is 0.14%. The loading of TB10.4 in PLGA-MDP-TB10.4 and PLGA-MDP-TB10.4+Ag85B is 0.048%. The loading of TB10.4-Ag85B in PLGA-MDP-TB10.4-Ag85B is 0.188%, which corresponds to 0.14% Ag85B and 0.048% TB10.4.

Characterization of PLGA microparticles

Encapsulation efficiency: 50mg of PLGA-rAg microparticles were dissolved in 5ml of DMSO and 25 ml of 0.05 M NaOH solution containing 0.5% (w/v) SDS (sodium dodecyl sulfate) were added and incubated at room temperature for 1 h. The concentration of antigens was determined by the BCA method. The encapsulation efficiency is the ratio of calculated antigen amount to that of theoretical amount.

Projected area diameter and particle morphology: microparticles were first suspended in water and then dispersed onto the surface of the stub, which was subsequently dried in a desiccator. Stubs were coated with gold-palladium alloy using a sputter coater (Polaron 5200, Structure Probe Incorporated Supplies, West Chester, PA, USA) and then examined under the scanning electron microscope (Hitachi S-4700).

Volume median diameter (VMD, $D_{v,\ 50}$): a small amount of each PLGA-rAg formulation was first suspended in the PBS buffer supplemented with 0.1% Tween 80 by bath sonication for 1 min. Approximately 1 ml of the suspension was added into the sample cell which had a volume of 15 ml PBS buffer under constant stirring. The ideal suspension

concentration was achieved at a laser obscuration of 0.15 to 0.25. $D_{v,10}$, $D_{v,50}$, $D_{v,90}$ and the span were measured by the laser diffraction particle sizer (Malvern 2600, Worcestershire, UK).

Mass median aerodynamic diameter (MMAD): MMAD was measured by an eight stage non-viable Andersen cascade impactor (Andersen, Smyrna, GA) operated at a flow rate of 60 L/min. The plates of the cascade impactor were coated with 1% silicon oil dissolved in hexane in order to reduce particle bouncing. Sodium fluorescein (1% w/w) was incorporated into PLGA-MDP-BSA microparticles during preparation. The particles were discharged from a dry powder inhaler device (Inhalator®, Boehringer Ingelheim, Germany) and sampled into the cascade impactor. Mass deposition at each stage, the sampling inlet (throat) and preseparator was calculated based on the fluorescein content assayed by UV spectrophotometry at 490nm.

Bulk and tapped density: approximately 1g PLGA-MDP-BSA microparticles were placed in a graduated cylinder. The mass/volume before tapping was calculated as bulk density. The tapped density was obtained following about 100 taps which allowed the powder volume to plateau. Carr's compressibility index (CCI) was calculated as (tapped density-bulk density)/tapped density. Hausner ratio was calculated as tapped density/bulk density.

Static angle of response: static angle of response was measured by pouring PLGA-MDP-BSA microparticles through a glass funnel onto a flat collection surface until the angle of response did not change with the addition of powder. The angle to the horizontal surface was measured. Greater than 1g of microparticles was needed for this experiment.

Thermal analyses: thermal analyses were carried out with differential scanning

calorimetry (Perkin Elmer DSC 6, Wellesley, MA). Known quantities of PLGA-rAg microparticles were sealed in an aluminum pan. An empty pan was used as the reference. Different temperature ramping rates were used from 10˚C/min to 40˚C/min for each sample. Three experiments were performed to check the reproducibility.

Zeta potential: PLGA-rAg microparticles were suspended in the PBS buffer at a concentration of approximately 0.2 mg/ml. This suspension was then transferred into a sampling cuvette and thermostated at 37˚C for 2 min before the start of measurement. Zeta potential was measured by a Malvern Zetasizer (NanoZS, Malvern Instruments Inc., Worcestershire, UK).

Surface free energy: surface free energy of PLGA-MDP-BSA microparticles was studied by inverse gas chromatography (IGC). IGC experiments were performed with a Hewlett-Packard 5890 Series II GC with flame ionization detector as described previously (236). A series of alkanes (C6-C10) were used as probes. Dry N_2 was used as the carrier gas with a flow rate of 30 mL/min. Oven temperature was controlled at 25 ˚C. PLGA microparticles were packed into the deactivated glass columns and then plugged with silanated glass wool at each end of the column. After installation, packed columns were allowed to equilibrate at 25 ˚C for 2 h before making injections. Injections were made by using a 1 μL-Hamilton syringe and infinite dilution was ensured by the detector response.

SDS-PAGE analysis of antigen integrity

To study the effect of spray drying on antigen integrity, 5 mg PLGA-rAg microparticles encapsulating different antigens were weighed after two-month storage. 300 μL SDS sampling buffer with dithiothreitol (DTT) as the reducing agent was added into microparticles and extracted for 30 min at room temperature. The mixture was then boiled

for 5 min at 95 ˚C to denature the protein followed by centrifugation at 12, 000g for 10 min. 5 μg soluble antigens were also boiled for 5 min at 95 ˚C after mixing with SDS sampling buffer containing DTT. 20μL samples from each preparation were loaded into a 12% SDS-PAGE gel (Biorad, Hercules, CA). Proteins were visualized by Coomassie Blue staining.

PLGA microparticle release profile

PLGA microparticles encapsulating BSA (90 mg) were put into 5 ml PBS (0.1% Tween 80) solution. The tubes were placed in a shaker bath at 37˚C running at 60 strokes/min. A volume of 0.6 ml suspension was removed at selected intervals and centrifuged for 10 min at 8, 000 g. 0.5 ml of supernatant was removed and stored. The rest of the sample and 0.5 ml fresh medium were added back into the dissolution vial. Bicinchoninic acid assay was used to determine BSA concentration and MDP was quantified by HPLC. HPLC conditions for MDP were: C18 reversed phase column (4.6×25 mm), mobile phase: 95% phosphate buffer (25 mM, pH 3.0) and 5% methanol at a flow rate of 1 ml/min and UV wavelength of 200 nm.

Statistical analysis

Multivariate statistical analysis was performed in Design-Expert® software to optimize the spray-drying conditions.

3.3 Results

3.3.1 Half-factorial design for optimization of spray-drying parameters

Spray-drying method was employed to produce poly (lactide-co-glycolide) (PLGA) microparticles. Variables playing pivotal roles in the spray-drying process include atomization pressure, spray flow, aspirator flow, inlet temperature and pump feeding rate. In order to dissect out the contribution of each variable and their interactions with respect to

achieving favorable particle properties, a half-factorial design (2^{5-1}) was constructed in Design-Expert® as shown in table 3.1 (16 design points plus 4 midpoints to check reproducibility), where five process variables and four response variables were listed with corresponding set and measured values. Among the four response variables, volume median diameter (VMD) and the yield were used to optimize the spray-drying parameters simultaneously. The optimization criteria were as follows: a) a VMD around 3μm (greater macrophage uptake), b) a yield greater than 15% (cost saving), c) a single mode of size distribution and a span less than 1 (uniformity) and d) mass median aerodynamic diameter (MMAD) between 1 and 5μm (aerosol delivery to the lung). Among these, MMAD was not an independent variable since it was determined by VMD, particle density, aggregation states and dispersion.

3.3.2 Analysis of spray-drying parameters with respect to size and yield respectively

Process variables were first analyzed with respect to size (VMD) since this is the most important factor determining particle aerosolization and macrophage uptake. The half-normal plot in figure 3.1a suggests that spray flow (B), inlet temperature (C), aspirator flow (D) and the interaction between spray flow and inlet temperature (BC) are main contributors in determining particle size. B and C contribute almost 75% of the overall effect; while together with D and BC, they contribute almost 85% of the overall effect based on statistical analysis. Pump feeding rate and atomization pressure showed minimal effect on particle size in the test range. According to above analysis, spray flow and inlet temperature deserve most attention with respect to target particle size. As shown in figure 3.1b, VMD decreased when spray flow and inlet temperature increased. In addition, VMD was more sensitive to spray flow.

Process variables were next analyzed with respect to the yield. Figure 3.1c clearly

suggests that only spray flow (B) and aspirator flow (D) have statistically significant contributions. Spray flow accounts for 80% of the overall effect and aspirator flow accounts for 15% of the overall effect according to statistical analysis. However, it should be noticed that the effect of spray flow is negative, indicating that particle yield decreased with the increase of spray flow. None of other variables or interactions was statistically significant. Therefore, attention should be drawn to these two variables to achieve greater yield.

3.3.3 Simultaneous optimization of spray-drying parameters

Multivariate statistical analysis was employed to optimize spray-drying parameters to achieve target particle properties proposed above. A desirability function was used to make an overall assessment of the desirability of the combined response variables, particle size and yield. In the desirability plot as shown in figure 3.1d, only one parameter combination (marked by the red dot) leads to a desirability of 1 while all other combinations give rise to 0. The optimized spray-drying conditions are as follows: atomization pressure (3 bars), spray flow (700 L/hr), pump feeding rate (4 ml/min), aspirator flow (100%) and inlet temperature (55 ˚C). Although the mode and span listed in table 3.1 were not used for optimization, particles prepared under optimized condition showed a unimodal and narrow size distribution, which meet the proposed criteria for optimization. The encapsulation efficiency for different PLGA-rAg formulations is 83.2±2.5% for Ag85B, 84.8±2.4% for TB10.4, 84.4±1.8% for TB10.4+Ag85B (blend), and 82.3±2.5% for TB10.4-Ag85B (fusion).

3.3.4 Morphology analysis of spray-dried microparticles

First, 6 batches of particles with a VMD around 3μm and 1 batch with the largest VMD from the optimization experiments were selected and imaged by SEM (figure 3.2a). The projected area diameter revealed by SEM images was always smaller than VMD

obtained from the laser diffraction experiment (figure 3.2a). Spray-dried PLGA particles showed a wrinkled and irregular surface morphology for all batches except the one with a VMD of 9.58μm. PLGA-rAg microparticles (subunit vaccines) prepared for efficacy evaluation were also imaged by SEM as shown in figure 3.2b, these particle preparations all had very similar surface morphology although different proteins were encapsulated, indicating a high reproducibility of particle preparation under optimized spray-drying conditions.

3.3.5 Particle size analysis of microparticles

Particle sizes for six PLGA-rAg formulations were listed in table 3.2. All formulations have a VMD of approximately 3.0μm, $D_{v,10}$ of 2.2μm and $D_{v,90}$ of 4.4μm. Again, these data suggested a high reproducibility of particle preparation under optimized conditions. Aerodynamic diameter of PLGA microparticles was measured with PLGA-MDP-BSA. Figure 3.3a suggests that 80% of the total mass was deposited inside the impactor yet very little deposition was observed below 1.1μm. Fine particle fraction (FPF) of the emitted dose was 61.5±6.4% and FPF of the total dose was 37.0±5.5%. It should be noticed that particle size distribution deviated from the ideal log-normal distribution with a MMAD of 3.3± 0.2μm and GSD of 2.7±0.1 (figure 3.3b).

3.3.6 Flow property of microparticles

The flow characteristics of PLGA-MDP-BSA microparticles were evaluated. The bulk density of these powders is 0.071 g/ml. The tap density is 0.094 g/ml. Calculated Carr's compressibility index (CCI) is 24.5% and Hausner ratio is 1.32. It is generally accepted that the free-flowing powder has a CCI less than 20% (237) and a Hausner ratio less than 1.20 (238). Powder with a CCI greater than 30% and a Hausner ratio greater than 1.50 always

means poor flow property. Therefore, our powder showed an intermediate flow characteristic. Powder with a large static angle of response suggests poor flow property due to large cohesive forces within the powder. It is accepted that a free-flowing powder should have a static angle of response less than 40˚ (237). The measured static angle of response for PLGA-MDP-BSA microparticles is 37 ± 2˚, which is pretty close to 40˚. All these data suggest that PLGA microparticles have intermediate flow characteristics between free-flowing powder and poor-flowing powder.

3.3.7 Effect of scanning rate on the glass transition temperature of microparticles

The glass transition temperature (Tg) of microparticles was measured by DSC experiments. As shown in figure 3.4a, the Tg of PLGA microparicles increased with a faster scanning rate. A polynomial equation of the second order could better describe the change of Tg as a function of the scanning rate (figure 3.4aa). Similar phenomenon was observed for two other formulations: PLGA-MDP (figure 3.4b and bb), and PLGA-MDP-Ag85B (figure 3.4c and cc). Such a dependence of Tg on the scanning rate could be explained by the fact that polymer may not respond quickly enough to the temperature change at fast ramping rate and thus displaying a lag of glass transition. Another interesting phenomenon that deserves attention is that DSC trace scanned for the first time at 10˚C/min does not overlap with the two traces from subsequent scans at the same ramping rate (figure 3.4a). This is also true for PLGA-MDP formulation (figure 3.4b) and PLGA-MDP-Ag85B formulation (figure 3.4c). One possible explanation is that the first DSC trace may represent the thermal history of microparticles (e.g. particle preparation and storage) whereas subsequent scans more likely represent the true material thermal behaviors.

3.3.8 Thermal characterization of PLGA-rAg formulations and MDP

Since the glass transition temperature (Tg) is affected by the scanning rate and thermal history, a comparison of themograms for all six PLGA-rAg formulations was made at the same scanning rate of 10˚C/min after the second scan. Thermal analysis in figure 3.5a suggests that all formulations have very similar glass transition temperature of approximately 44 ˚C. Detailed thermodynamic parameters were calculated and listed in table 3.3, which again showed almost equivalent thermal behavior for all formulations. The DSC thermogram of MDP was shown in figure 3.5b, which suggests that MDP has a melting temperature of approximately 125˚C and decomposes above 160˚C.

3.3.9 Surface energy and charge characterization of microparticles

The dispersive surface free energy of PLGA-MDP-BSA microparticles at 25 ˚C is 31.65 mJ/m^2 based on the IGC experiment as shown in figure 3.6. Surface free energy was calculated from the slope of the linear line covering a series of non-polar probes. Tetrahydrofuran (THF) and ethyl acetate were used as the polar probes, which showed a deviation from the linear line. This could be explained by the specific interaction between non-polar probes and PLGA microparticles. Surface charges of different PLGA-rAg formulations were also measured. These particles were negatively charged with a zeta potential of approximately -25 mV for all formulations (table 3.2, last column). The negative charge may be explained by the presence of ionized carboxyl groups on the microparticle surface (239).

3.3.10 Effect of spray-drying on antigen integrity

Antigen integrity may be compromised during spray-drying because of the process temperature and atomization pressure. SDS-PAGE was performed to investigate whether

spray drying or PLGA encapsulation compromised antigen integrity. As shown in figure 3.7, antigens prior to and post processing migrated to the same position. No degradation or truncated fragments were visible on the gel. However, this experiment was performed under reducing condition and, therefore, protein aggregation or structure change was not able to be detected by this assay. Alternatively, protein aggregation could be studied by size-exclusion chromatography while secondary/tertiary structure change could be studied by circular dichroism at far-UV or near-UV regions.

3.3.11 Release profiles of microparticles

The release of BSA and MDP from PLGA microparticles was characterized in a 10-day period. As shown in figure 3.8, MDP exhibited almost complete burst release during the first half hour and no release from the subsequent sampling period. In contrast, BSA showed an initial burst release of 58% in the first half hour. Subsequent release exhibited a sustained manner with another 25% released during the first six-day period.

3.4 Discussion

The half-factorial design (2^{5-1}) reduced the number of spray-drying experiments from 2^5 to 2^4. An advantage of this particular design lies in that it is a resolution V design, which means that both main effects and two-factor interactions are not confounded with each other. Particle size is the most important particle property which affects both lung deposition and alveolar macrophage uptake (192, 240-242). Hirota *et al.* reported that the most efficient delivery of rifampicin-loaded PLGA microspheres into alveolar macrophage was achieved by the phagocytosis of 3 μm particles (240). Therefore, a volume median diameter (VMD) of 3 μm was selected as the optimization target. Statistical analysis showed that spray flow and inlet temperature were main contributors in determining particle size, by reducing droplet

size and facilitating evaporation rate respectively. Unexpectedly, atomization pressure showed minimal effect on particle size, which, however, did affect the maximal spray flow achieved at given pressure. With respect to particle yield, only spray flow and aspirator flow were significant contributors yet they exerted effects in the opposite direction. Smaller droplet was created by higher spray flow and thus collected less efficiently by the centrifugal force. Higher aspirator flow created greater centrifugal force and thus increasing the collection efficiency. Interestingly, no interaction between these two factors was observed. In addition to particle size and yield, the risk of thermal denaturation of antigens during spray drying should be considered. As described in the previous chapter, the melting temperature for Ag85B and TB10.4-Ag85B was 73.7˚C and 75.1˚C respectively. Therefore, the inlet temperature was kept as low as 55˚C to avoid potential antigen denaturation. Spray flow was maintained at high level (700L/h) for acceptable particle sizes. Maximal aspirator flow was used to compensate the low yield caused by high spray flow.

PLGA particles were frequently spheres prepared by the double emulsion-solvent evaporation method (173, 243). In contrast, particles prepared by primary emulsion/spray drying method showed irregular surface morphology, in agreement with previous report (125, 244). Such morphology may explain why particles with a VMD of 3μm had a mass median aerodynamic diameter (MMAD) of 3.3 μm. MMAD is correlated with VMD by multiplying the square root of particle density (244). Theoretically, the low density nature of PLGA particles should result in significantly smaller MMAD than VMD. However, the irregular surface morphology of PLGA particles may greatly increase the contact surface area of nearby particles, which again increased particle aggregation. These aggregates may be partly deaggregated after being discharged from the dry powder inhaler yet a complete dispersion

of particles was not achieved. This may also explain why few particles were deposited on stages with cutoff diameters less than 1.1μm (figure 3.3a), resulting in a distribution significantly deviating from an ideal log-normal distribution (figure 3.3b). Therefore, although PLGA particles prepared under optimized conditions showed narrow primary size distributions, they underwent incomplete deaggregation and existed as heterogeneous aggregates when delivered as aerosols. However, the MMAD and fine particle fraction of the aerosols were still acceptable and no excipients such as lactose were blended with PLGA particles.

Thermal analyses of PLGA particles revealed a glass transition temperature (Tg) of approximately 44˚C. This temperature had important implications for particle storage. Polymers exist in rubbery state above Tg and have increased mobility compared to the glassy state (245). Polymer annealing would likely to occur above this temperature, which may affect particle morphology, microstructure and ultimately the release kinetics of encapsulated antigens (172). In order to minimize polymer annealing, PLGA particles should be stored below the Tg. In addition, moisture contact should be avoided since water serves as a plasticizer to lower the Tg (246). Therefore, PLGA particles are recommended to store with desiccant at either room temperature or in the fridge.

Emulsifiers were not used to prepare the primary water-in-oil emulsion since they might influence phagocytosis (247-249). The high initial burst of MDP and protein from PLGA microparticles indicates that the primary emulsion was not sufficiently stable to retain the internal water phase. Therefore, it is possible that a portion of MDP and protein are associated with microparticle surfaces after spray drying *via* electrostatic and hydrophobic interactions (250). In addition, both MDP and BSA are water soluble molecules immiscible

with the PLGA polymer. Rather than dissolved in the matrix of PLGA, they were more likely to be dispersed in the matrix by occupying internal voids. Channels/pores may directly connect these voids to the particle surface, thus, leading to a high burst release before the bulk erosion of PLGA occurs (172). All these mechanisms may explain the high initial burst. Interestingly, the sustained release phase of BSA was absent for MDP. The nearly complete burst release of MDP may be partly explained by the rapid diffusion of this small molecule which has a molecular weight two orders of magnitude below BSA.

3.5 Summary

In this chapter, various recombinant antigens/antigen combinations purified from the previous chapter were encapsulated into PLGA microparticles (PLGA-rAg) by primary emulsion/spray drying method. By employing the concept of Quality-by-Design (QbD), the spray-drying parameters were successfully optimized with a half-factorial design to give the desired particle size and yield. Antigen integrity was not compromised by the formulation procedure (i.e. encapsulation, spray drying) as evidenced by the SDS-PAGE experiment. Manufactured microparticles have a mass median aerodynamic diameter around 3.3 μm suitable for pulmonary delivery and a volume median diameter of approximately 3 μm ideal for cellular uptake by alveolar macrophages. Thermal characterization suggested that these formulations should be better stored in the fridge with a desiccant present to avoid polymer plasticization. In summary, TB subunit vaccine formulations were prepared and extensively characterized with respect to their physicochemical properties. Highly reproducible PLGA-rAg microparticles (subunit vaccines) were obtained, which sets the foundation for the next stage of vaccine development, that is, *in vitro* efficacy study which will be discussed in the next chapter.

Table 3.1 Half-factorial design (2^{5-1}) to optimize the spray-drying parameters

Run	Factor 1 Atomization Bar	Factor 2 Spray Flow L/hr	Factor 3 Inlet Temp ˚ C	Factor 4 Aspirator %	Factor 5 Pump ml/min	Res1 VMD µm	Res2 Yield %	Res3 Mode	Res4 Span
1	4	700	75	100	8	2.79	27.86	1	0.76
2	3	550	65	75	6	3.87	42.32	2	0.92
3	2	400	75	100	8	6.40	66.71	3	1.80
4	2	400	55	50	8	9.58	46.57	2	1.56
5	4	700	55	50	8	4.21	5.86	2	0.95
6	2	700	75	100	4	2.98	22.14	2	1.10
7	3	550	65	75	6	3.77	39.66	2	0.88
8	4	700	75	50	4	3.26	6.43	2	0.78
9	2	700	55	50	4	5.05	1.14	2	1.03
10	2	400	75	50	4	5.74	47.00	2	1.25
11	4	400	55	50	4	7.74	46.71	1	1.33
12	4	400	75	50	8	6.28	45.14	1	1.37
13	4	400	55	100	8	8.27	69.57	2	1.54
14	3	550	65	75	6	3.75	39.32	2	0.91
15	2	700	55	100	8	3.32	24.29	2	0.98
16	2	700	75	50	8	4.27	2.86	2	0.89
17	4	400	75	100	4	5.43	49.86	2	1.36
18	2	400	55	100	4	7.19	64.57	3	1.62
19	3	550	65	75	6	3.80	40.57	2	0.90
20	4	700	55	100	4	3.06	18.71	1	0.65

Labeled in red are four experimental runs to check reproducibility

Table 3.2 Particle size and surface charge characterization of spray-dried microparticles (n=3, mean ± SD)

Formulation	$D_{v,10}$ (μm)	$D_{v,50}$ (μm)	$D_{v,90}$ (μm)	Zeta Potential (mV)
PLGA	2.36 ± 0.06	3.06 ± 0.06	4.34 ± 0.34	-26.8 ± 5.2
PLGA-MDP	2.21 ± 0.07	2.97 ± 0.08	4.53 ± 0.26	-25.7 ± 4.7
PLGA-MDP-Ag85B	2.16 ± 0.08	3.10 ± 0.10	4.26 ± 0.32	-25.2 ± 4.9
PLGA-MDP-TB10.4	2.43 ± 0.05	3.02 ± 0.09	4.45 ± 0.28	-26.1 ± 5.0
PLGA-MDP-TB10.4+Ag85B	2.27 ± 0.08	2.95 ± 0.12	4.58 ± 0.41	-24.4 ± 5.1
PLGA-MDP-TB10.4-Ag85B	2.12 ± 0.06	3.08 ± 0.07	4.31 ± 0.35	-24.6 ± 3.9

$D_{v,10}$: diameter at the cumulative percentile of 10%
$D_{v,50}$: diameter at the cumulative percentile of 50%
$D_{v,90}$: diameter at the cumulative percentile of 90%

Table 3.3 Thermal characterization of spray-dried microparticles (n=3, mean ± SD)

Formulation	Δ Cp (J/g*˚C)	Tg onset (˚C)	Tg end (˚C)	Tg (˚C)
PLGA	0.478 ± 0.014	43.6 ± 0.2	46.7 ± 0.1	44.9 ± 0.1
PLGA-MDP	0.476 ± 0.008	42.2 ± 0.1	45.9 ± 0.1	43.9 ± 0.1
PLGA-MDP-Ag85B	0.495 ± 0.010	42.6 ± 0.1	45.8 ± 0.2	44.0 ± 0.2
PLGA-MDP-TB10.4	0.451 ± 0.018	41.9 ± 0.2	45.5 ± 0.1	43.5 ± 0.1
PLGA-MDP-TB10.4+Ag85B	0.456 ± 0.011	41.6 ± 0.2	45.1 ± 0.0	43.1 ± 0.0
PLGA-MDP-TB10.4-Ag85B	0.473 ± 0.013	42.9 ± 0.3	45.6 ± 0.2	43.8 ± 0.3

Δ Cp: difference in heat capacity
Tg: glass transition temperature
Tg onset: the onset of glass transition temperature
Tg end: the end of glass transition temperature

Figure 3.1 Optimization of spray-drying parameters. a, half-normal plot with respect to particle size (VMD); b, response surface plot of particle size (VMD) as a function of spray flow and inlet temperature; c, half-normal plot with respect to particle yield; d, desirability plot with respect to the simultaneous optimization of both particle size (VMD) and yield.

a

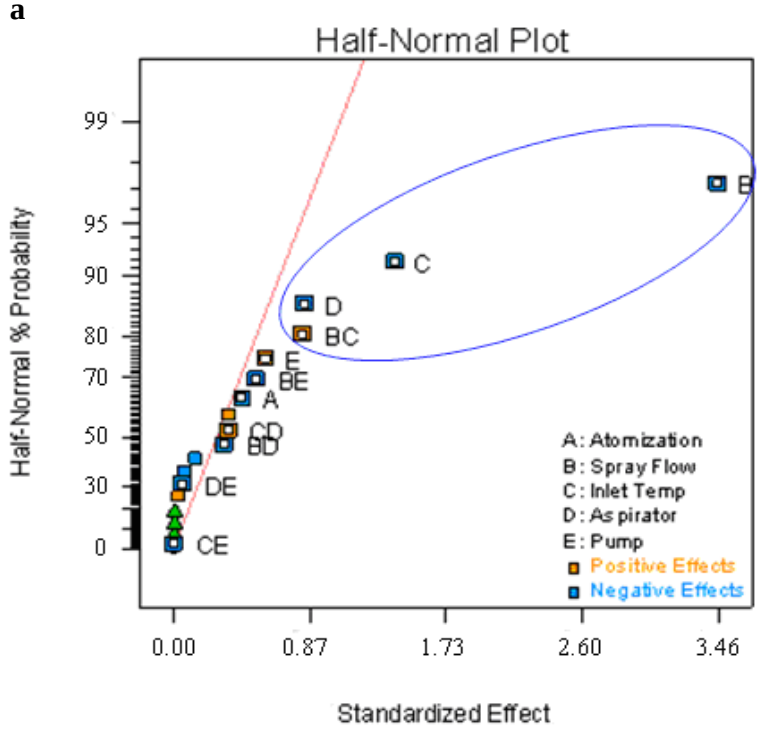

b

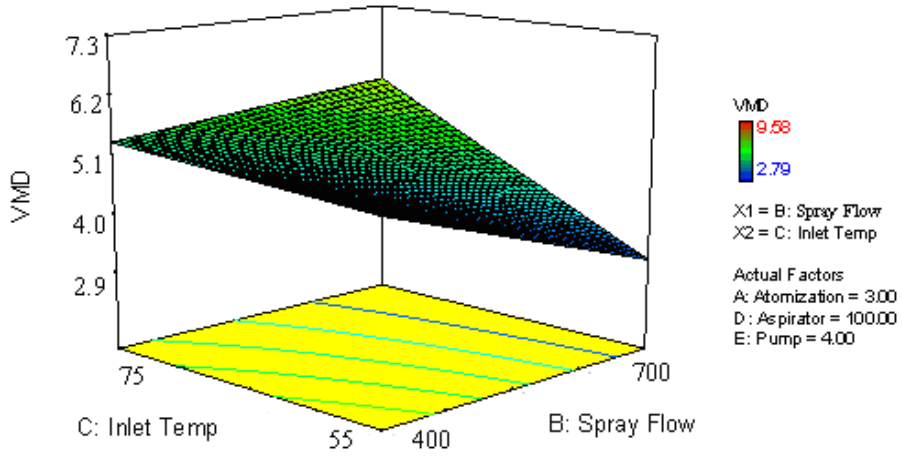

c

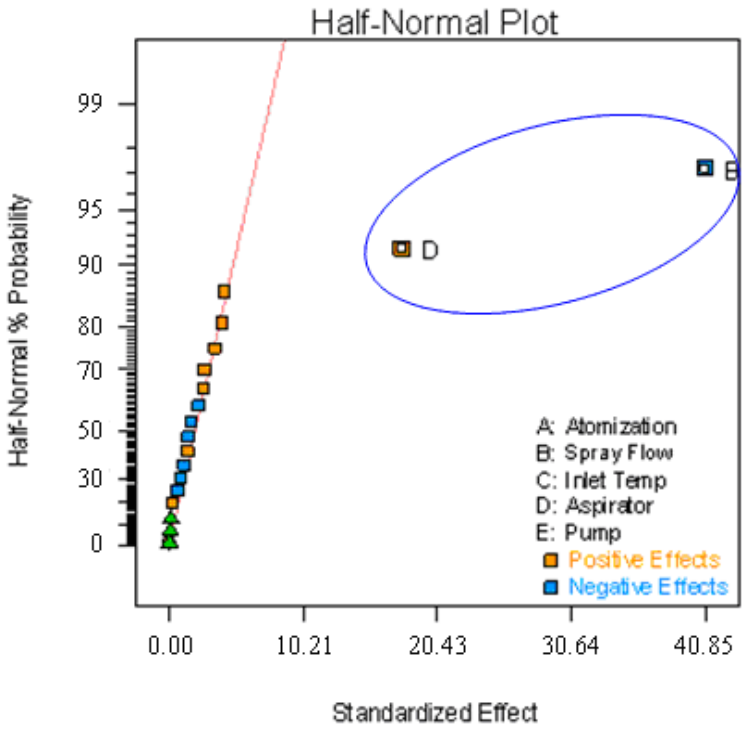
Half-Normal Plot
Half-Normal % Probability
99
95
90
80
70
50
30
0
D
A: Atomization
B: Spray Flow
C: Inlet Temp
D: Aspirator
E: Pump
Positive Effects
Negative Effects
0.00
10.21
20.43
30.64
40.85
Standardized Effect

d

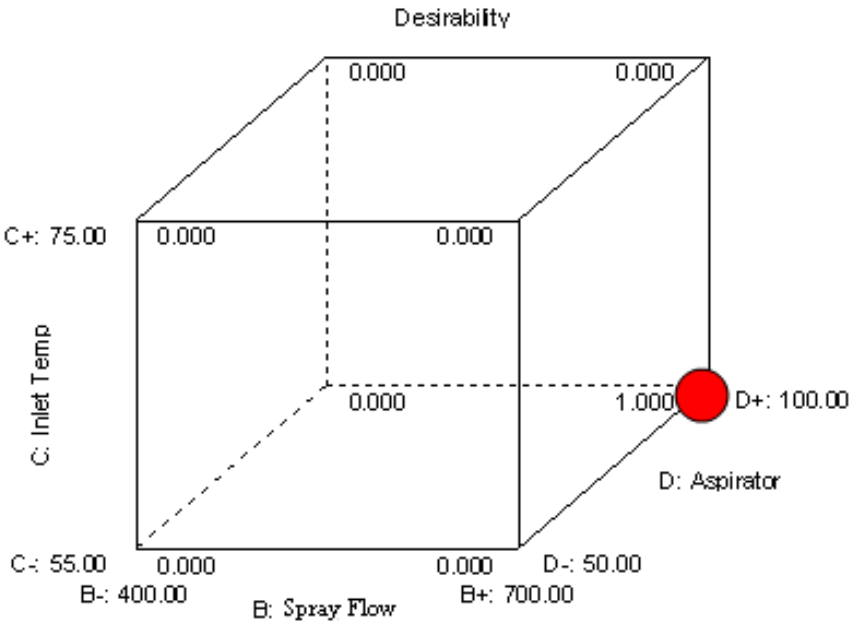
Desirability
0.000
0.000
C+: 75.00
0.000
0.000
C: Inlet Temp
0.000
1.000
D+: 100.00
D: Aspirator
C-: 55.00
0.000
0.000
D-: 50.00
B-: 400.00
B: Spray Flow
B+: 700.00

Figure 3.2 Morphology analyses of spray-dried microparticles. a, SEM images of seven batches of microparticles prepared according to the half-factorial design. Experimental run numbers labeled in figure 3.2a correspond to the run number in table 3.1; b, SEM images of six PLGA microparticle formulations with different antigens encapsulated. Particles were prepared under optimized spray-drying conditions.

a

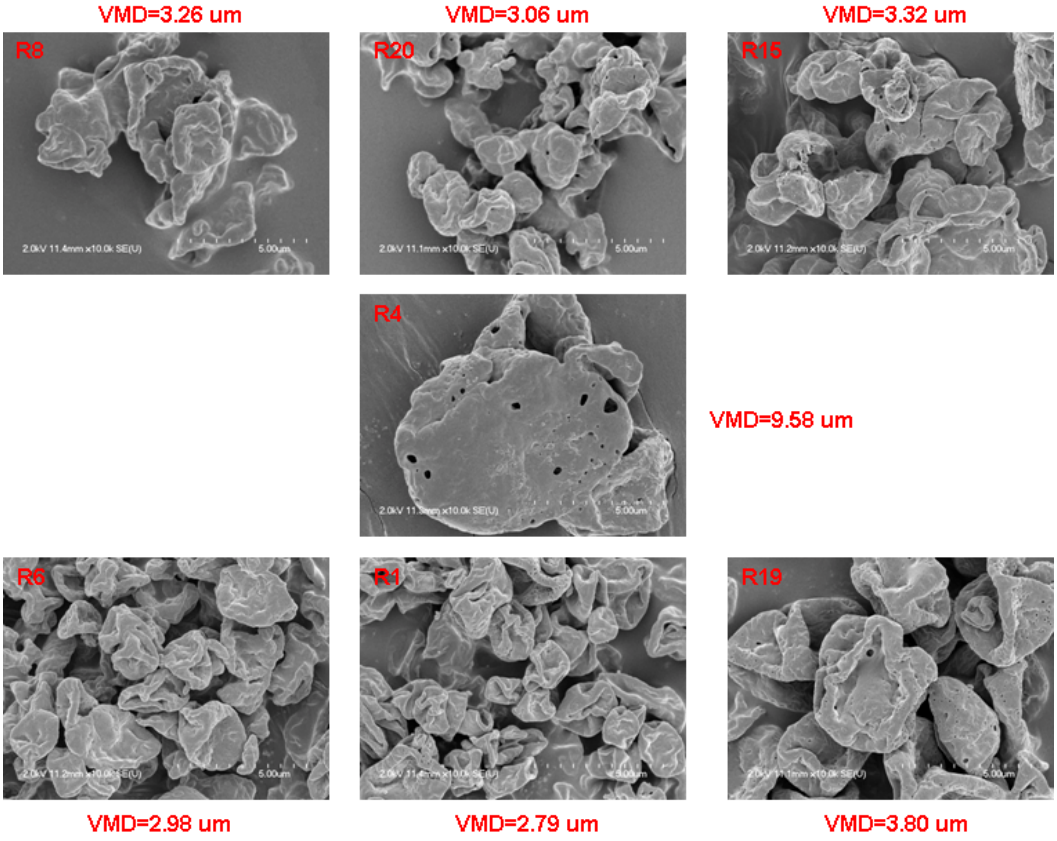

b

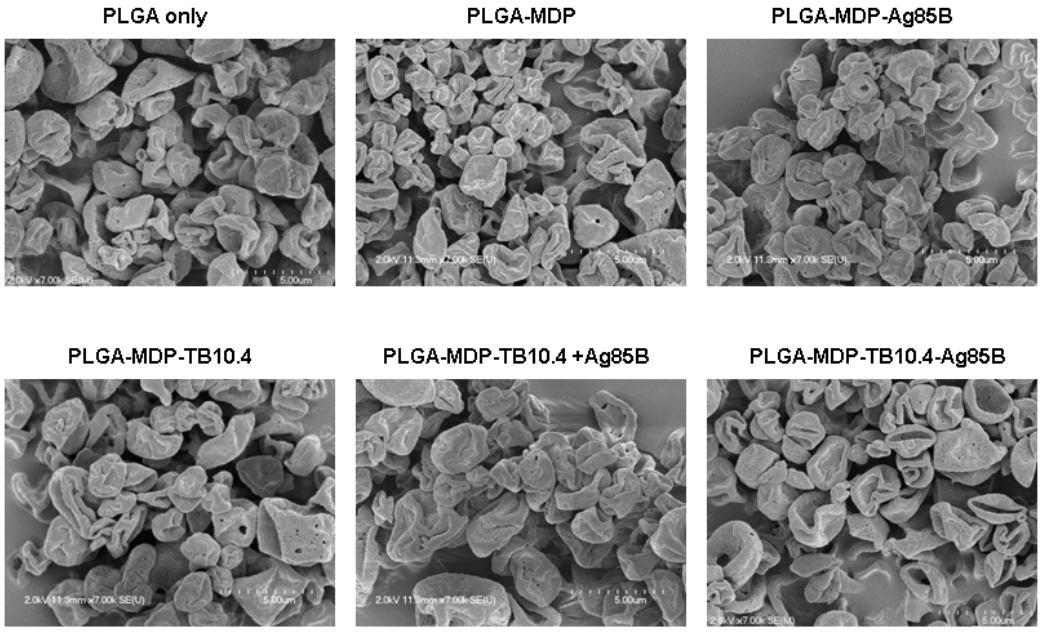
PLGA only
PLGA-MDP
PLGA-MDP-Ag85B
PLGA-MDP-TB10.4
PLGA-MDP-TB10.4 +Ag85B
PLGA-MDP-TB10.4-Ag85B

Figure 3.3 Aerodynamic particle size analysis of spray-dried microparticles prepared under optimized conditions. a, relative mass deposition measured by Andersen cascade impactor (n=3, mean ± SD); b, log-probability plot of the mass distribution shown in a.

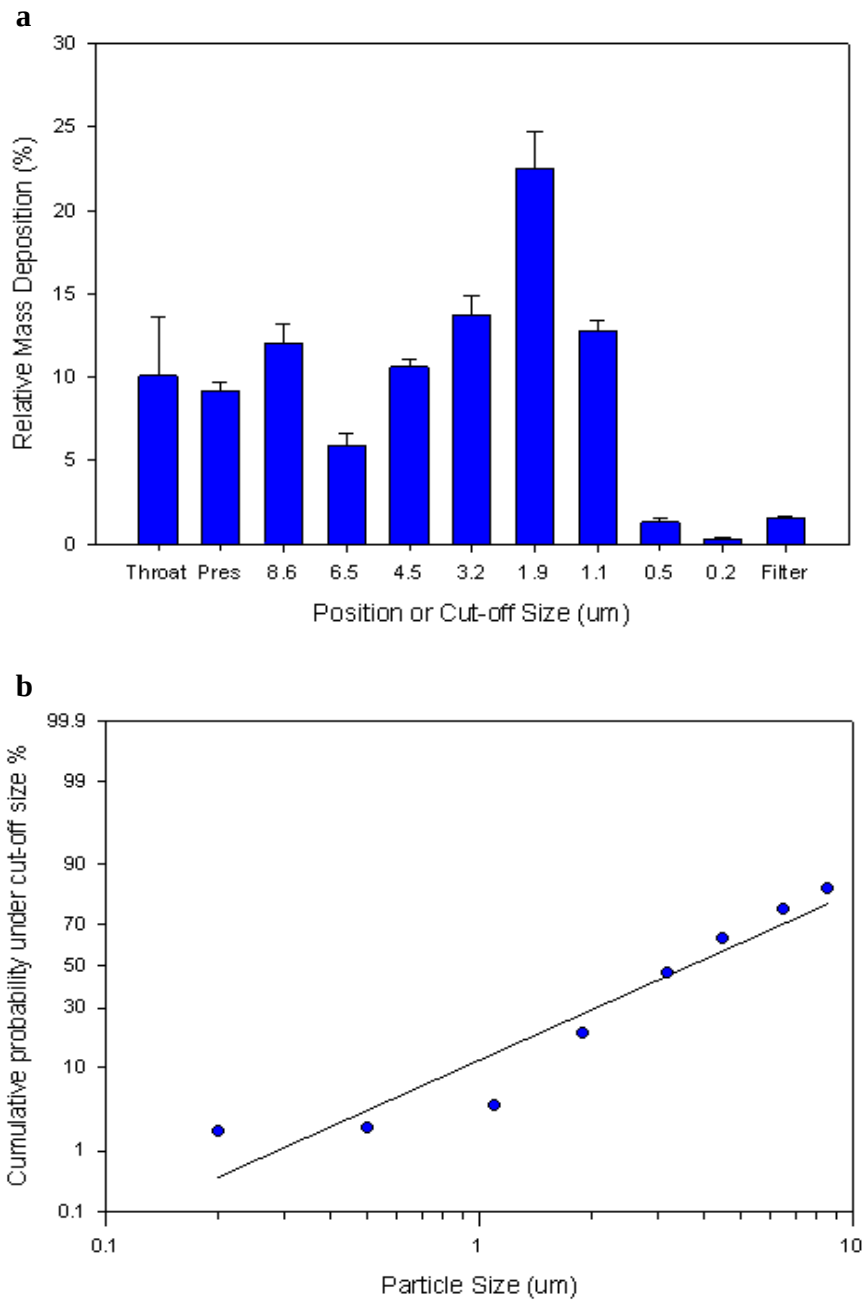

Figure 3.4 Effect of scanning rate on the glass transition temperature (Tg) of three PLGA formulations. a, DSC thermograms of PLGA recorded at different scanning rates; aa, regression analysis of Tg as a function of the scanning rate for PLGA; b, DSC thermograms of PLGA-MDP recorded at different scanning rates; bb, regression analysis of Tg as a function of the scanning rate for PLGA-MDP; c, DSC thermograms of PLGA-MDP-Ag85B recorded at different scanning rates; cc, regression analysis of Tg as a function of the scanning rate for PLGA-MDP-Ag85B.

a

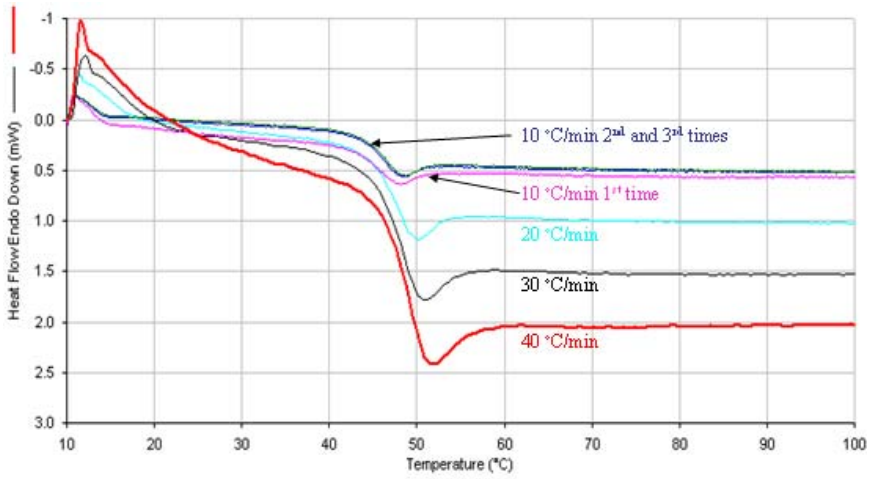

aa

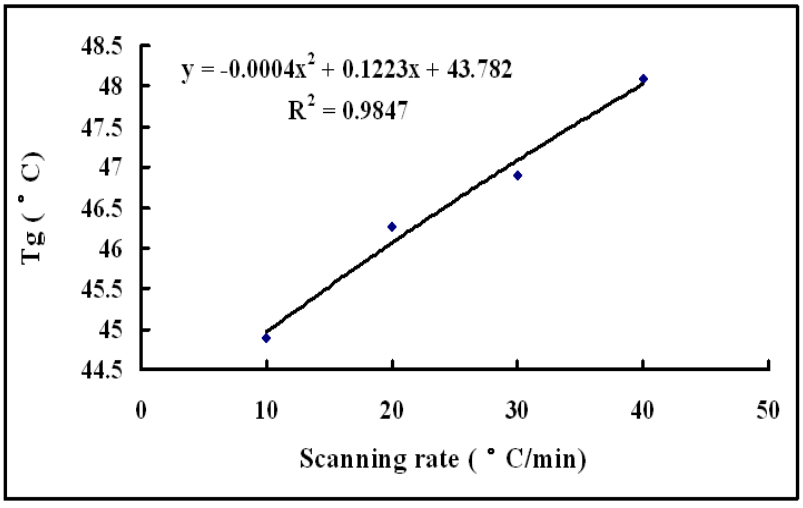

b

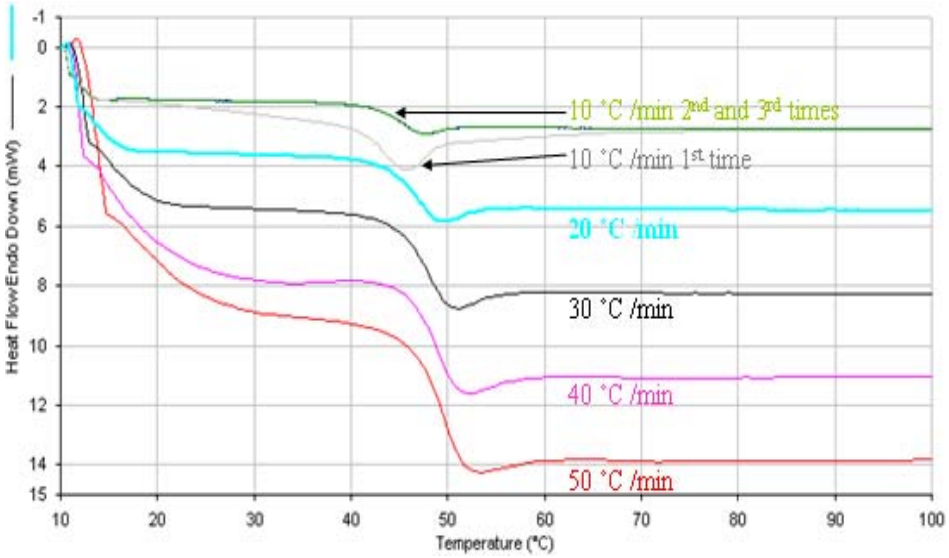
Heat Flow Endo Down (mW)
Temperature (°C)
10 °C /min 2nd and 3rd times
10 °C /min 1st time
20 °C /min
30 °C /min
40 °C /min
50 °C /min

bb

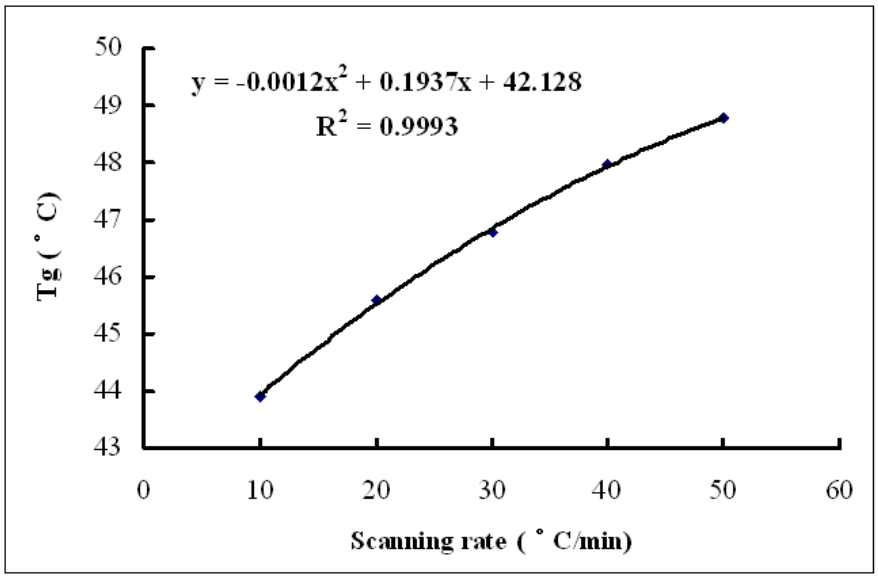
y = -0.0012x2 + 0.1937x + 42.128
R2 = 0.9993
Tg (° C)
Scanning rate (° C/min)

c

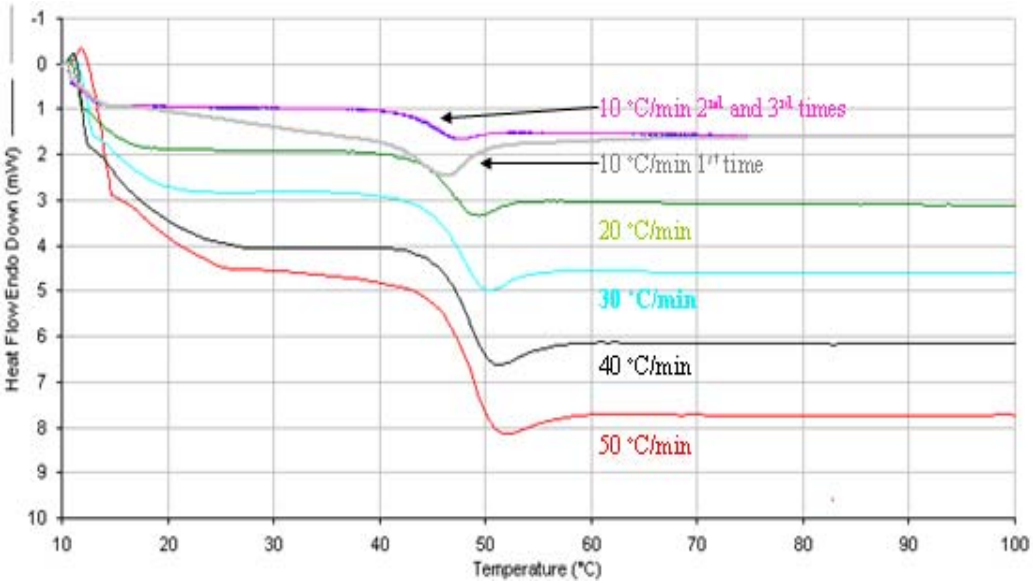
Heat Flow Endo Down (mW)
Temperature (°C)
10 °C/min 2nd and 3rd times
10 °C/min 1st time
20 °C/min
30 °C/min
40 °C/min
50 °C/min

cc

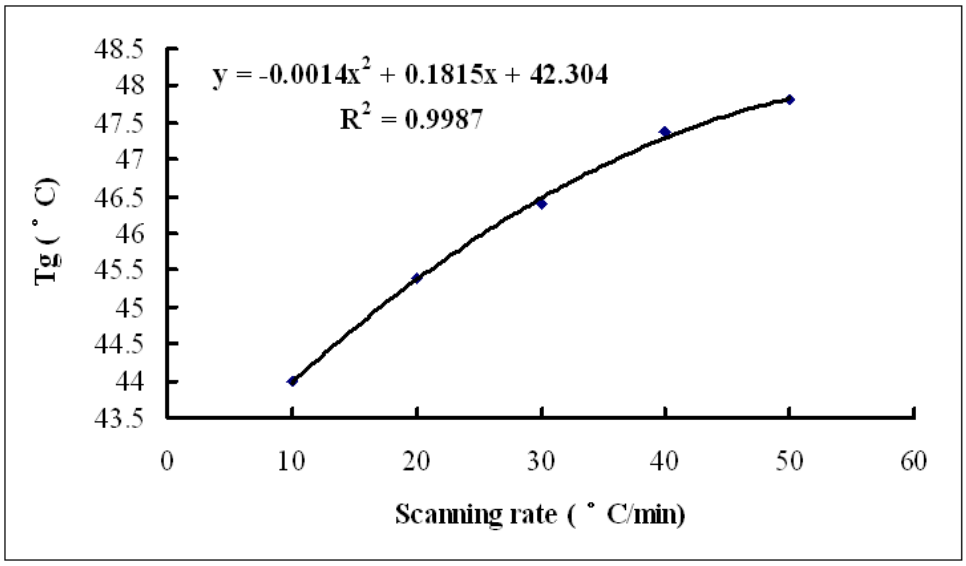
y = -0.0014x2 + 0.1815x + 42.304
R2 = 0.9987
Tg (˚ C)
Scanning rate (˚ C/min)

Figure 3.5 Thermal characterization of different PLGA-rAg formulations and MDP by DSC. a, DSC thermograms of different PLGA-rAg formulations (1: PLGA, 2: PLGA-MDP-TB10.4-Ag85B, 3: PLGA-MDP-Ag85B, 4: PLGA-MDP-TB10.4+Ag85B, 5: PLGA-MDP-TB10.4, 6: PLGA-MDP); b, DSC thermogram of MDP. The scanning rate was 10˚C/min.

a

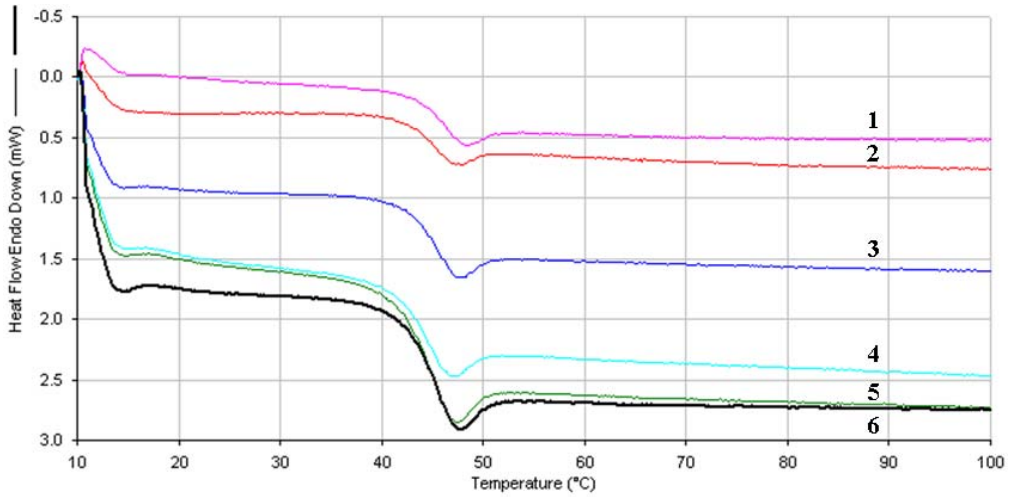

b

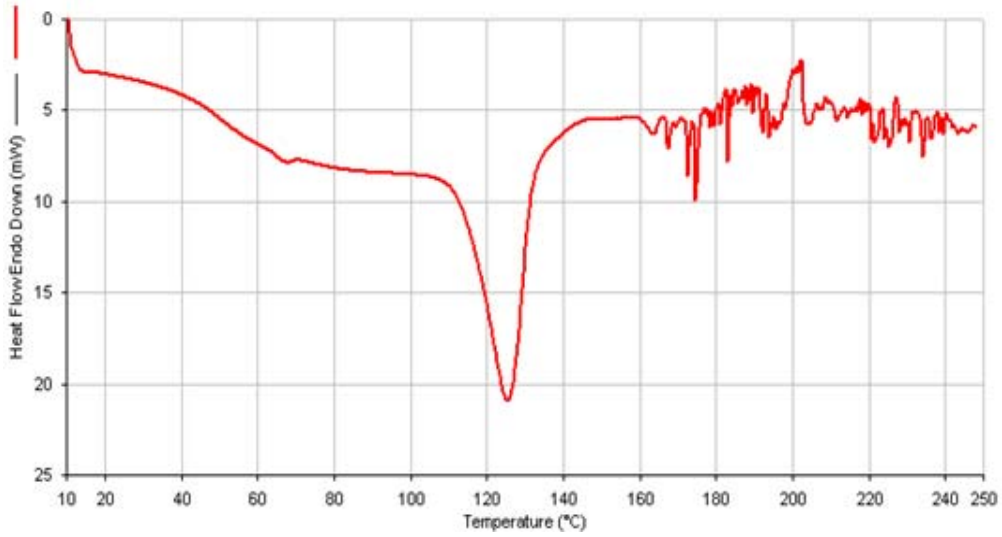

Figure 3.6 Characterization of the surface free energy of microparticles. C6: hexane, C7: heptane, C8: octane, C9: nonane, C10: decane, THF: tetrahydrofuran.

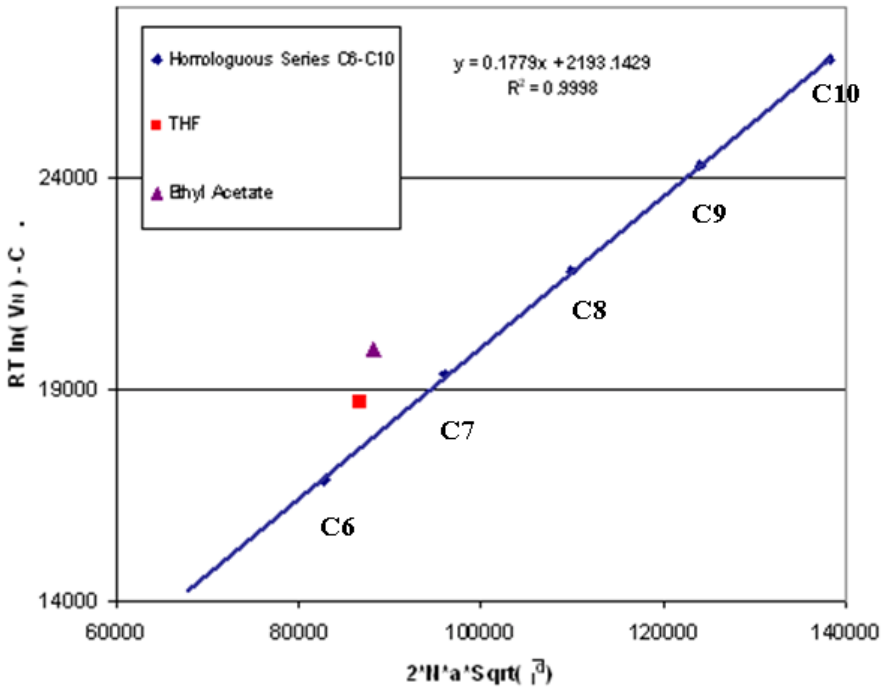

Figure 3.7 SDS-PAGE analysis of antigen integrity after spray drying (lane 1: Ag85B (s: solution), 2: Ag85B (p: powder), 3: TB10.4 (s), 4: TB10.4 (p), 5: TB10.4+Ag85B (s), 6: TB10.4+Ag85B (p), 7: TB10.4-Ag85B (s), 8: TB10.4-Ag85B (p)). Difference in band intensity was due to different loading.

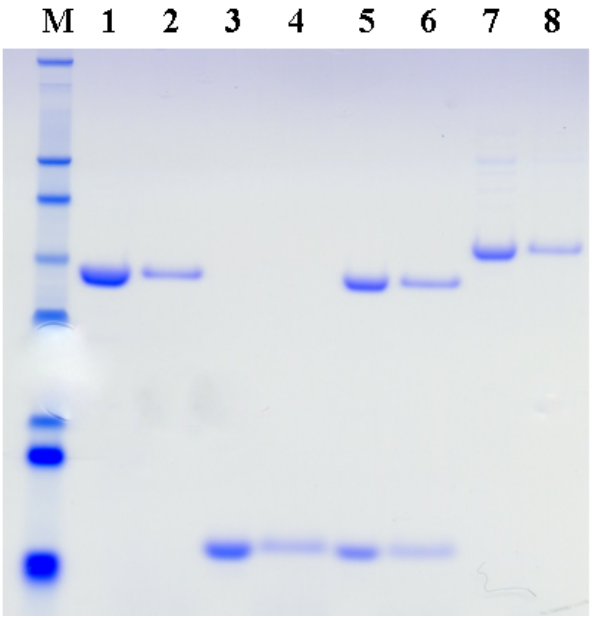

Figure 3.8 Release profile of microparticles (n=3, mean ± SD). a, MDP release profile; b, protein (BSA) release profile.

a

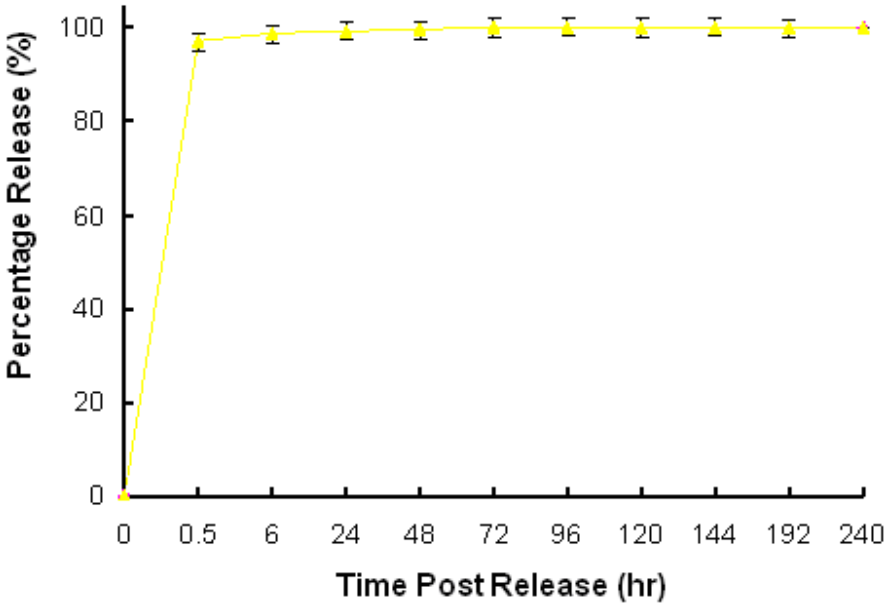

b

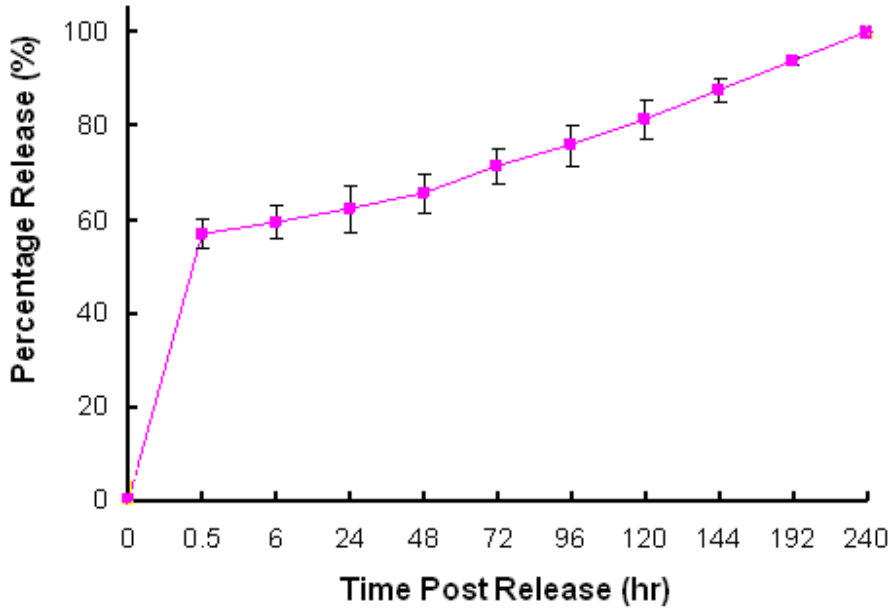

CHAPTER 4: STUDY OF *IN VITRO* IMMUNE RESPONSES INDUCED BY PLGA-rAg MICROPARTICLES

In the last chapter, various antigens and antigen combinations have been successfully encapsulated into PLGA microparticle formulations. In this chapter, we studied the *in vitro* immune responses induced by these formulations. Ag85B specific MHC II immune response was first studied to compare different formulations. The kinetic study was performed with two antigen combinations (TB10.4-Ag85B and Ag85B+TB10.4) to compare a) antigen blend vs. antigen fusion and b) particle formulation vs. solution formulation with respect to inducing Ag85B specific MHC II response. TB10.4 specific MHC I immune response was also studied in this chapter. Our data suggested that PLGA-rAg induced a predominant MHC II immune response *in vitro*. Among all formulations tested, powder formulations are much more powerful than solution formulations in terms of generating Ag85B specific MHC II response. Among powder formulations, Ag85B induced the strongest IL-2 response. A comparable IL-2 response was also induced by the antigen blend (Ag85B+TB10.4). However, this response was decreased more than 50% by the fusion antigen (TB10.4-Ag85B). Kinetic study again suggested that particle formulation induced a much stronger and prolonged Ag85B specific MHC II response compared to solution formulation. In addition, antigen blend showed continuously higher MHC II immune response than antigen fusion up to six days. The titration of TB10.4 immune response suggested a lack of sensitivity of this antigen presentation assay currently.

4.1 Introduction

Cell mediated immune (CMI) response is believed to play a key role in TB control since *Mycobacterium tuberculosis* (*MTB*) is an intracellular organism (84). CD4+ and CD8+ T cells are two major mediators of CMI. CD4+ T cells recognize epitopes presented by major histocompatibility complex (MHC) class II molecules on the surface of antigen presenting cells (APCs). After activation, CD4+ T cells secret a spectrum of cytokines to act on *MTB* infected cells. There are numerous studies to support the pivotal role of CD4+ T cells in combating tuberculosis (28). One evidence comes from the increased susceptibility of subjects tested positive for human immunodeficiency virus (HIV) to tuberculosis (251). This was correlated to the diminished CD4+ T cells in HIV positive subjects. CD8+ T cells recognize MHC I epitopes presented by APCs. Activated CD8+ T cells not only secret cytokines but also induce cytotoxic T cell killing (84). However, in contrast to CD4+ T cells, the evidence for an essential role of CD8+ T cells in tuberculosis is not very compelling. For many years, researchers in this field almost ignored this T cell subset. This is because *MTB* lives primarily within vacuoles inside the cell rather than in the cytoplasm, which makes cross-presentation of antigens to CD8+ T cells less likely to happen. Recent studies with gene-disrupted mice provided stronger data supporting the role of CD8+ T cells in TB control (85, 86, 252-254). In one study, it was concluded that classically restricted (TAP-1 dependent) CD8+ T cells contribute to *in vivo* protection against *MTB* (252). In another study, it has been shown that depletion of CD8+ T cells led to the reactivation of latent tuberculosis in a murine model (255). To develop new tuberculosis vaccines, it is widely accepted that CD4+ T cells should be targeted for vaccine design. In addition, more and more researchers believe that CD8+ T should also be considered in vaccine design (84).

In vitro antigen presentation assay serve as a surrogate assay to evaluate vaccine efficacy by employing APCs and T-hybridoma cell lines. The advantage of such assay lies in its capability to screen many different formulations in a fast and high-throughput manner without sacrificing animals. However, the limitation of this assay is two fold. First, only epitope specific response can be probed since T-hybridoma is developed against specific epitopes within antigens. Study of other epitopes requires the development of more T-hybridoma cells lines restricted to each epitope. The second limitation is associated with the degree of *in vitro-in vivo* correlation of this assay, that is, to what extent the result from the *in vitro* assay can be correlated to the *in vivo* performance of vaccines. Despite these limitations, *in vitro* antigen presentation assays have been widely used to study vaccines in their early stage of development (125).

An *in vitro* antigen presentation assay to study Ag85B specific MHC II immune response was developed in Dr. Boom's group (256). This assay employed THP-1 cell as an APC and DB-1 T hybridoma as the CD4+ T cell line restricted to an MHC II epitope within Ag85B ($Ag85B_{97-112}$) (256). THP-1 is a cell line of human origin which presents epitopes in the context of human MHC molecules. DB-1, a murine T-hybridoma, was derived from transgenic mice with human MHC genes. Therefore, DB-1 is restricted to human HLA alleles and responds to antigens presented by human APCs. Upon cell recognition, the activation of DB-1 leads to IL-2 secretion which can be easily quantified by IL-2 ELISA. This assay has been successfully employed to evaluate Ag85B specific MHC II immune response *in vitro* (125).

The second assay was developed in Dr. Majlessi's group to study TB10.4 specific MHC I immune response by employing Raw264.7 cell as the APC and YB8 cell as the CD8+

T-hybridoma restricted to an MHC I epitope within TB10.4 ($TB10.4_{20-28}$) (136). Both Raw264.7 and YB8 cells are of mice origin and have been shown to be able to recognize each other when $TB10.4_{20-28}$ epitope was loaded onto the MHC I molecule of Raw264.7 cell. The activation of YB8 cells leads to the secretion of IL-2 into medium which can be easily quantified by ELISA.

4.2 Materials and Methods

Cells and media

THP-1 cells (American Type Culture Collection) were maintained in RPMI 1640 (Invitrogen Corp., Grand Island, NY) supplemented with 10% heat-inactivated fetal bovine serum (FBS) (Hyclone, Logan, UT), 50 μM 2-mercaptoethanol, 1 mM sodium pyruvate, nonessential amino acids, 1% antibiotics/antimycotics (Invitrogen Corp., Grand Island, NY). The CD4 T-hybridoma DB1 cells (kindly provided by Dr. W. Henry Boom, Case Western Reserve University) were derived from transgenic mice with human MHC genes for HLA-DR1. They are restricted to human HLA alleles and respond to human MHC II molecules presenting $Ag85B_{97–112}$ epitope. DB-1 cells were maintained in DMEM (Invitrogen Corp., Grand Island, NY) supplemented as indicated above (complete DMEM). Raw 264.7 cells (American Type Culture Collection, ATCC) were maintained in ATCC-formulated DMEM supplemented with 10% heat-inactivated FBS and 1% antibiotics/antimycotics. The CD8 T-hybridoma YB8 cells (kindly provided by Dr. Laleh Majlessi, the Pasteur Institute) responds to mouse MHC I molecules presenting $TB10.4_{20-28}$ epitope. YB8 cells were maintained in ATCC-formulated DMEM supplemented with 10% heat-inactivated FBS and 1% antibiotics/antimycotics.

In vitro antigen presentation assay for Ag85B specific MHC II immune response

Ag85B specific MHC II immune response was evaluated by a modified CD4 T cell hybridoma recognition assay as shown in figure 4.1a. THP-1 cells were incubated in 96-well flat-bottom plates (10^5 cells/well) with 20 ng/ml of phorbol myristate acetate (PMA, Sigma, St Louis, MO) for 24 h to promote adherence. Cells were washed once with PBS and incubated with 5 ng/ml of recombinant human IFN-γ (Endogen, Woburn, MA) for 24 h to promote differentiation. The cells were washed twice with PBS prior to antigen exposure. Antigen solutions were added into THP-1 cells at a concentration of 28ng/well for Ag85B, 9.3ng/well for TB10.4, and 37.3ng/well for TB10.4-Ag85B (corresponds to 9.3ng/well TB10.4 and 28ng/well Ag85B). A blend of TB10.4 (9.3ng/well) and Ag85B (28ng/well) were also added into THP-1 cells for Ag85B+TB10.4. Antigens encapsulated in PLGA microparticles were added at corresponding same concentrations as antigen solutions. DB-1 T-hybridoma cells (10^5 cells/well) were added 6 h later after antigen exposure. The cells were co-incubated at 37˚C for 24 h and supernatants were harvested to measure the amount of IL-2 secreted by DB-1 with mouse IL-2 ELISA (Biosource, Camarillo, CA).

In vitro antigen presentation assay for TB10.4 specific MHC I immune response

TB10.4 specific MHC I immune response was evaluated by a CD8 T cell hybridoma recognition assay as shown in figure 4.1b. Raw264.7 cells were seeded in 96-well flat-bottom plates (10^5 cells/well). Cells were incubated with 2 ng/ml of recombinant mouse IFN-γ (Endogen, Woburn, MA) for 24 h to promote differentiation. The cells were washed twice with PBS prior to antigen exposure. To titrate TB10.4 specific MHC I response, the homologous MHC I peptide (GYAGTLQSL, donation of Dr. Laleh Majlessi) was added to Raw264.7 cells at series of concentrations from 0.1ng/ml to 10μg/ml. Recombinant antigen

solutions were added at 5μg/well for Ag85B, 1.67μg/well for TB10.4, 6.67μg/well for TB10.4-Ag85B (corresponds to 1.67μg/well TB10.4 and 5μg/well Ag85B). A blend of TB10.4 (1.67μg/well) and Ag85B (5μg/well) were also added into Raw264.7 cells for Ag85B+TB10.4. Antigens encapsulated in PLGA microparticles were added to Raw264.7 cells at a concentration of 28ng/well for Ag85B, 9.3ng/well for TB10.4, 28ng/well+9.3ng/well for Ag85B+TB10.4, and 37.3ng/well for TB10.4-Ag85B (corresponds to 9.3ng/well TB10.4 and 28ng/well Ag85B). YB8 T-hybridoma cells (10^5 cells/well) were added 6 h later after antigen exposure. The cells were co-incubated at 37˚C for 24 h. Supernatants were harvested to measure the amount of IL-2 secreted by YB8 by mouse IL-2 ELISA assay.

Six-day antigen presentation assay for Ag85B specific MHC II immune response

THP-1 cells (10^5 cells/well) were first stimulated with PMA and IFN-γ as described previously. THP-1 cells were then pulsed with soluble TB10.4-Ag85B (6.67μg which corresponds to 1.67μg TB10.4 and 5μg Ag85B), Ag85B+TB10.4 (5μg Ag85B+1.67μg TB10.4), PLGA-MDP-TB10.4-Ag85B (37.3ng which corresponds to 9.3ng/well TB10.4 and 28ng/well Ag85B) and PLGA-MDP-Ag85B+TB10.4 (28ng/well Ag85B and 9.3ng/well TB10.4) respectively followed by further incubation for 6 h. The cells were then washed extensively with PBS to remove the antigen solution or microparticles. DB-1 (10^5 cells/well) were added at each time point (from day 1 to 6). After 24 h co-incubation, the supernatant was harvested for mouse IL-2 ELISA assay.

Six-day antigen presentation assay for TB10.4 specific MHC I immune response

Raw264.7 cells were seeded at a concentration of 10^5 cells/well and stimulated with IFN-γ . Cells were then exposed to either soluble antigens or PLGA-rAgs at the same

concentrations as described previously. YB8 T-hybridoma cells (10^5 cells/well) were added after each interval (from day 1 to 6) and co-incubated at 37˚C for 24 h. Supernatant was harvested to measure the amount of IL-2 secreted by YB8.

Statistical analysis

ANOVA was used for statistical comparisons. The statistical significance was set at $p<0.05$.

4.3 Results

4.3.1 PLGA-rAg induced Ag85B specific MHC II immune response

The effect of different formulations in generating Ag85B specific MHC II immune response was first studied after one-day antigen exposure as shown in figure 4.2. Not surprisingly, neither control PLGA microparticles nor PLGA-MDP-TB10.4 induced any detectable IL-2 secretion due to the absence of Ag85B specific epitope in these formulations. Among powder formulations, particles encapsulating Ag85B induced the strongest IL-2 secretion. The blend of Ag85B and TB10.4 induced a comparable amount of IL-2 secretion ($p>0.05$). However, IL-2 elicited by the fusion antigen TB10.4-Ag85B was decreased by 54.8% compared to the blend of Ag85B and TB10.4 ($p<0.05$). In contrast to the powder formulation, antigen solutions at the same concentration failed to induce IL-2 secretion for all tested antigen or antigen combinations.

4.3.2 Kinetic study of PLGA-rAg induced Ag85B specific MHC II immune response

Prolonged epitope presentation may be an advantageous property for a vaccine. The ability of PLGA-MDP-TB10.4-Ag85B (fusion) and PLGA-MDP-Ag85B+TB10.4 (blend) to present epitope over time was studied (figure 4.3). In this experiment, antigen solutions were used at a concentration of 178 fold higher since they failed to induce IL-2 secretion at the

same concentration as in the particle formulation (figure 4.2). Although a much higher concentration was used, IL-2 elicited by TB10.4-Ag85B or Ag85B+TB10.4 solution was continuously lower than that induced by the particle formulation. For antigen solutions, IL-2 secretion peaked at day 2 yet decreased rapidly afterwards and only 20% of the peak IL-2 concentration was observed at day 6. Ag85B+TB10.4 induced slightly better IL-2 secretion than TB10.4-Ag85B for the first three days and there was no significant difference between them after day 3. In contrast, both PLGA-MDP-TB10.4-Ag85B and PLGA-MDP-Ag85B+TB10.4 induced a prolonged IL-2 secretion. IL-2 concentration was fairly stable in the first four days and declined afterwards. However, approximately 70% of the peak IL-2 was still observed at day 6. Moreover, particle formulation of antigen blend (Ag85B+TB10.4) induced continuously higher concentration of IL-2 than antigen fusion (TB10.4-Ag85B).

4.3.3 Study of TB10.4 specific MHC I immune response

In order to study TB10.4 specific MHC I immune response, the *in vitro* antigen presentation assay was first titrated with the homologous TB10.4 peptide (GYAGTLQSL) at various concentrations. IL-2 secretion could only be induced at two highest concentrations of TB10.4 peptide. At a peptide concentration of 10μg/ml, IL-2 secretion was 74pg/ml; at a peptide concentration of 1μg/ml, IL-2 secretion was 25.5pg/ml (figure 4.4). All lower peptide concentrations failed to induce IL-2 secretion as indicated in figure 4.4 with IL-2 concentrations below the lower limit of detection. Experiments with TB antigens suggest that neither antigen solutions nor PLGA-rAgs could induce IL-2 secretion either after one-day antigen exposure or six-day antigen exposure. A simple calculation of TB10.4 epitope concentration in PLGA-rAg microparticles indicates that such *in vitro* antigen presentation assay doesn't have enough sensitivity to detect TB10.4 specific MHC I immune response.

4.4 Discussion

Antigen solutions failed to elicit Ag85B specific IL-2 secretion at the same concentration as in the particle formulation. However, IL-2 was induced by antigen solutions at much higher concentration possibly because the cellular uptake of soluble antigens into endosomes is concentration dependent (257). Encapsulation of antigens into PLGA microparticles induced significant amount of IL-2 secretion even at very low antigen concentration. The data from figure 4.3 showed that the powder formulation of TB10.4-Ag85B or Ag85B+TB10.4 induced a stronger response even at a concentration two orders of magnitude below the solution formulation. This suggests that PLGA microparticles increased the potency of encapsulated antigens. Similar observation has been reported with other antigens. For instance, intranasal instillation of encapsulated protective antigen in the microspheres resulted in a significant increase in the percentage of activated CD4+ T cells, whereas instillation of the soluble antigen failed to do so (258). The adjuvancy of microparticles can be partly attributable to the enhanced cellular uptake of these particles by antigen presenting cells (APCs). Microparticles less than 10 μm in diameter can be effectively taken up by macrophages or dendritic cells *via* active phagocytosis (258). In contrast, soluble antigens gain access to APCs primarily *via* pinocytosis which is a process utilized by cells to take up extracellular fluid. Therefore, encapsulated antigens can be more effectively and efficiently brought into the intracellular compartment by PLGA microparticles. At least two signals are required for naïve CD4+ T cells to be activated by APCs. Signal one is delivered by APCs by presenting class II epitope to CD4+ T cells, while only specific cytokines or co-stimulatory molecules on the surface of APCs can offer signal two. In the absence of signal two, signal one fails to activate naïve T cells. This may explain

why antigen solution poorly induced IL-2 secretion even at very high concentration since soluble antigen is less likely to generate sufficient signal two required for CD4+ T cell activation. In contrast, PLGA microparticles have been shown to significantly increase the expression of co-stimulatory molecules on the surface of APCs (259).

Compared to Ag85B alone or antigen blend, there is a more than 50% decrease in IL-2 secretion induced by the fusion antigen TB10.4-Ag85B. A possible explanation for this observation is that the fusion of TB10.4 and Ag85B alters the structure of the fusion antigen and may affect the processing of Ag85B epitopes inside endosomes, which may ultimately affect Ag85B specific MHC II epitope presentation.

The kinetic study of Ag85B specific MHC II immune response illustrated another advantage of microparticle formulation, that is, prolonged epitope presentation and IL-2 secretion. This prolonged immune activation may be correlated to the sustained release of proteins from PLGA microparticles. The rapid decrease of IL-2 secretion observed with the solution formulation can be explained by the fact that soluble antigens are quickly used up after cellular uptake *via* pinocytosis. The results from this *in vitro* study also have important implications for the potential *in vivo* performance of PLGA-rAg. In order for naïve T cells to be activated, APCs bearing TB epitopes have to transit from the place where they receive the vaccine to the local lymph node and present epitopes to the T cells (28). Epitope presentation should be available once APCs reach the local lymph node. In addition, a continuous presentation for a certain period of time may be required for a successful T cell activation. Antigen given in a solution formulation may compromise the continuous epitope presentation due to rapid decrease of antigen concentration intracellularly. However, prolonged epitope presentation was promoted by the PLGA microparticle formulation, which favors the T cell

activation.

PLGA-rAg induced TB10.4 specific MHC I immune response can not be evaluated in the present study due to the lack of sensitivity of TB10.4 antigen presentation assay. Efforts in the future should address this problem by either improving assay sensitivity or increasing the loading of encapsulated antigens.

Figure 4.5 illustrated our current knowledge of MHC I and MHC II antigen presentation pathways. Soluble antigens and PLGA-rAgs are taken up by antigen presenting cells (APCs) *via* pinocytosis and phagocytosis respectively. They are processed by the MHC class II pathway in the endosome/lysosome or phagolysosome. MHC II epitope loading occurs in these cellular compartments. Epitope loaded MHC II complex is then transported onto the surface of APCs, where it recognizes DB-1 T-hybridoma and induces IL-2 secretion. In order for MHC I epitope presentation to occur, soluble antigens or PLGA-rAgs have to leave the MHC II compartment and enter into the cytoplasm, where antigens are processed by the proteasome. Transporter associated with antigen processing (TAP) assists in the translocation of processed epitopes into the lumen of endoplasmic reticulum for MHC I epitope loading. Epitope loaded MHC I complex is then transported onto the surface of APCs, where it can recognize YB8 T-hybridoma. This process is termed MHC I epitope presentation, which is the basis of TB10.4 specific *in vitro* antigen presentation assay. TB10.4 specific MHC I response was observed when two highest concentrations (10μg/ml and 1μg/ml) of homologous peptide were added to antigen presenting cells. Such epitope presentation does not require intracellular processing because the peptide (MHC I epitope) was directly loaded onto the MHC I molecule extracellularly.

4.5 Summary

The efficacy of PLGA-rAgs was evaluated by *in vitro* antigen presentation assays in this chapter. A predominant Ag85B specific MHC II immune response was observed for formulations that contain Ag85B. Powder formulation is much more potent than the solution formulation to induce Ag85B specific MHC II response. Moreover, a prolonged immune response was observed for the powder formulation. Antigen blend (Ag85B+TB10.4) showed much better Ag85B specific MHC II response than antigen fusion (TB10.4-Ag85B). With all current information, a recommendation was proposed that antigen blend in the particle formulation should better be used for multiple-antigen TB subunit vaccines.

Figure 4.1 Schematic description of two *in vitro* antigen presentation assays. a, Ag85B specific MHC II epitope presentation; b, TB10.4 specific MHC I epitope presentation.

a

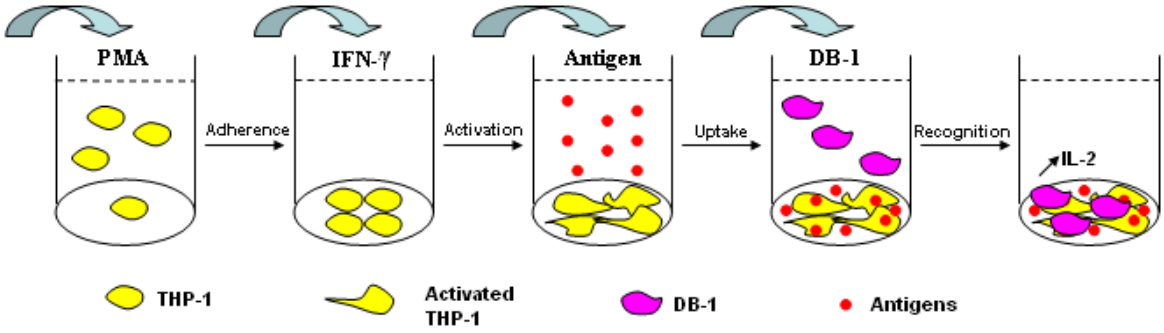

b

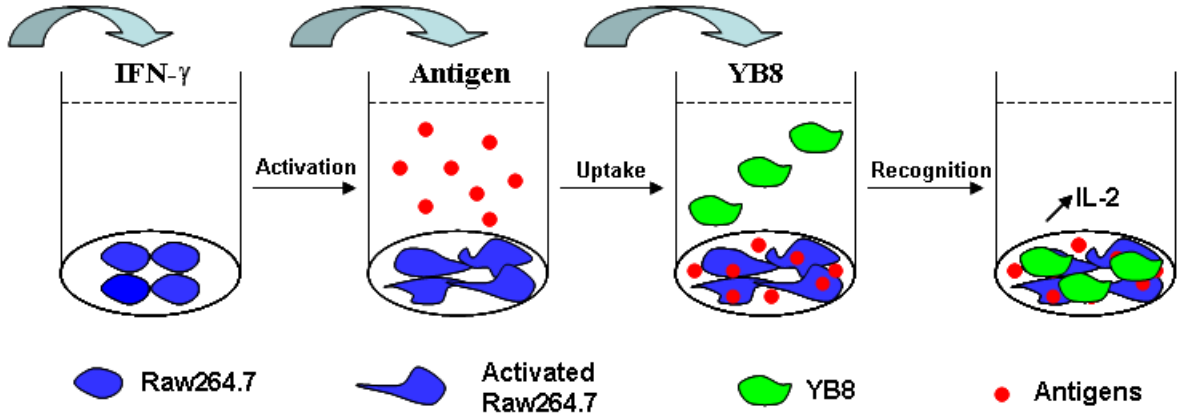

Figure 4.2 Comparison of Ag85B specific MHC II immune response induced by different formulations after 1-day antigen exposure. (Powder (black bar): antigens encapsulated in PLGA microparticles; Solution (grey bar): antigen solutions, n=3, mean ± SD, Ctrl: PLGA microparticles w/o antigen, Ag85B: PLGA-MDP-Ag85B, TB10.4: PLGA-MDP-TB10.4, A+T: PLGA-MDP-Ag85B+TB10.4, T-A: PLGA-MDP-TB10.4-Ag85B). Antigen solutions failed to induce IL-2 response and, therefore, no grey bar. Antigen concentration was the same for both powder and solution formulations (Ag85B:28ng/well, TB10.4: 9.3ng/well, TB10.4-Ag85B: 37.3ng/well).

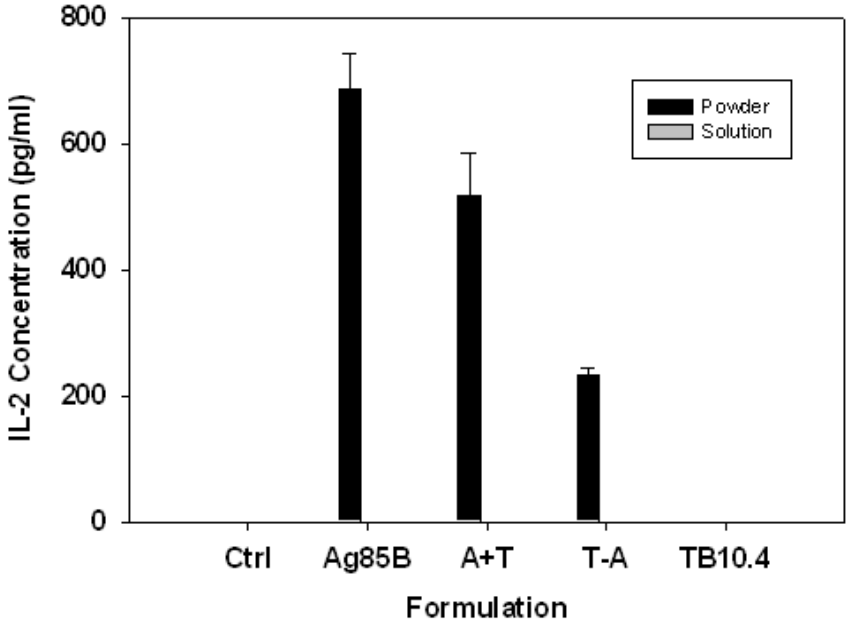

Figure 4.3 Kinetic study of Ag85B specific MHC II immune response. (Powder: TB10.4-Ag85B (37.3ng/well) or Ag85B (28ng/well) +TB10.4 (9.3ng/well) encapsulated in PLGA microparticles; Solution: TB10.4-Ag85B (6.67μg/well) or Ag85B (5.0μg/well) +TB10.4 (1.67μg/well), n=3, mean ± SD)

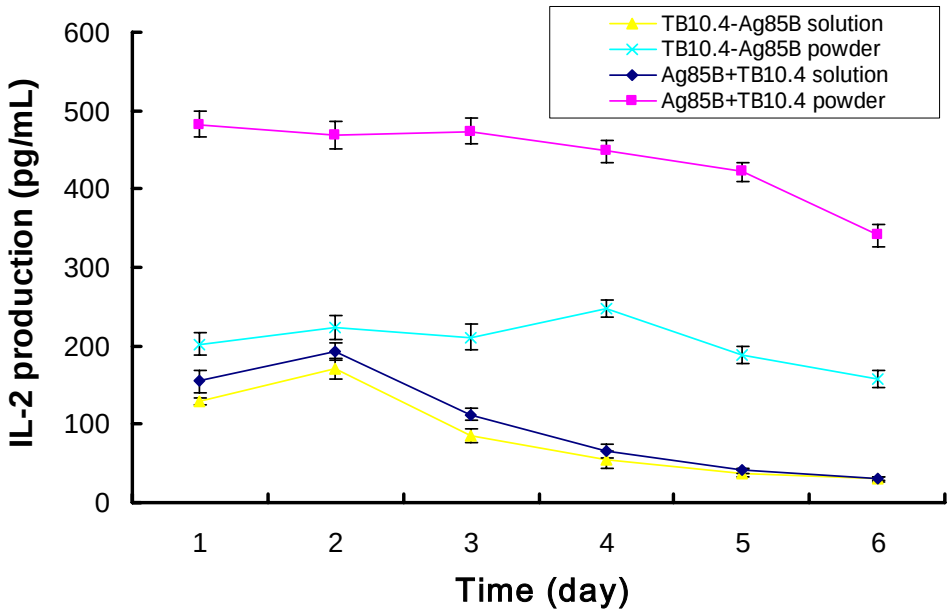

Figure 4.4 Titration of TB10.4 specific MHC I response with various concentrations of homologous TB10.4 peptide (n=3, mean ± SD). LLD: lower limit of detection.

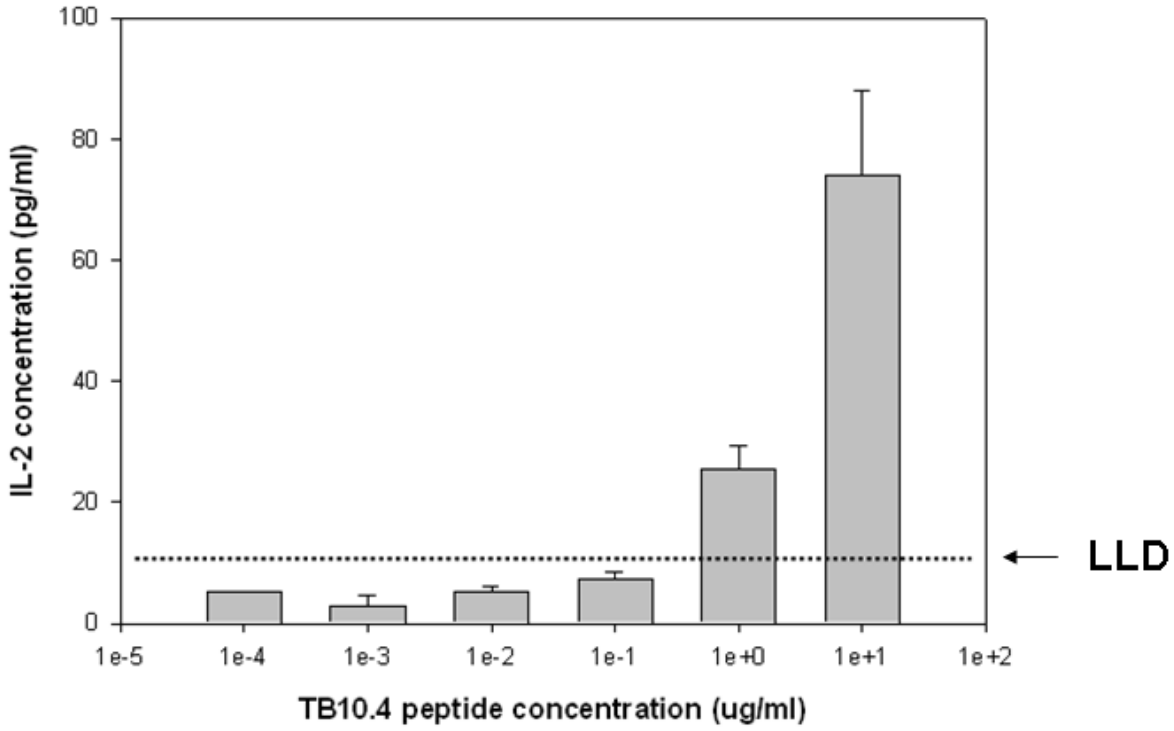

Figure 4.5 MHC I and II antigen presentation pathways

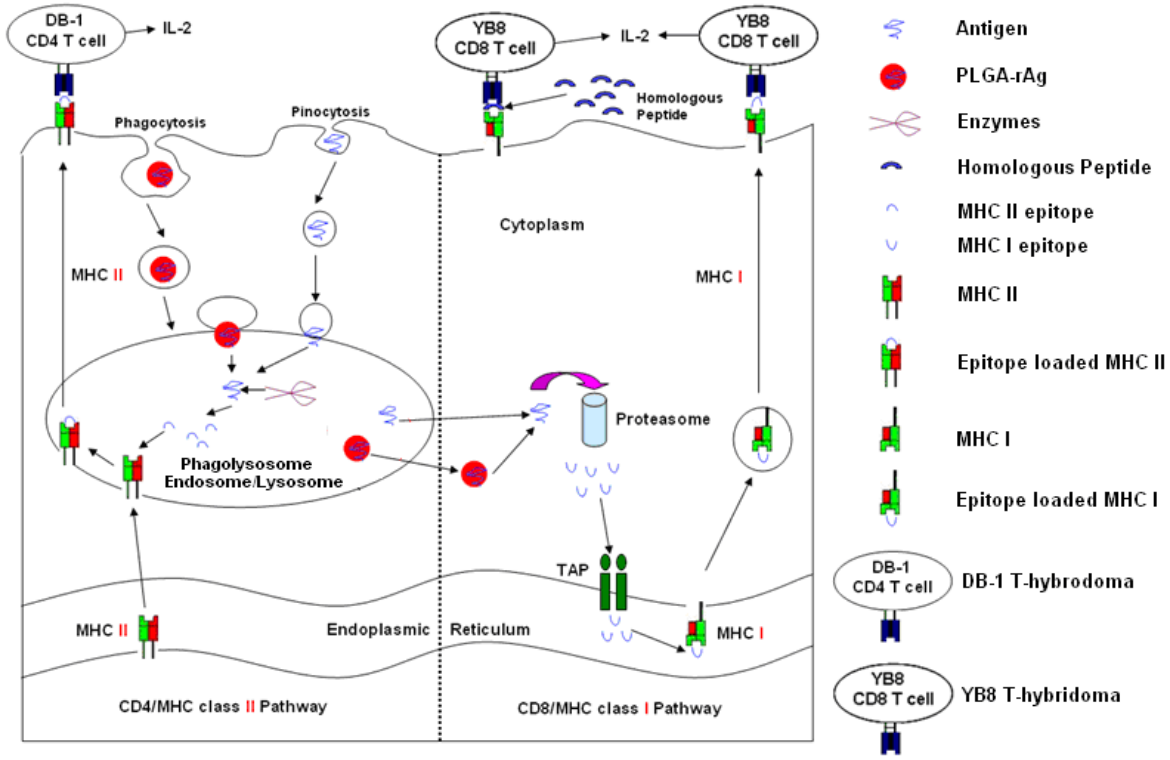

CHAPTER 5: DEVELOPMENT OF A PARTICLE SIZE COMPARATOR TO EVALUATE BATCH-TO-BATCH REPRODUCIBILITY OF INHALATION PRODUCTS

In previous chapters, recombinant TB antigens were designed and characterized; TB subunit vaccines were prepared by encapsulating recombinant antigens into PLGA microparticles; the efficacy of TB vaccines was evaluated by *in vitro* antigen presentation assays. This vaccine is intended to be delivered to the lungs *via* inhalation aerosols. Lung delivery requires an aerodynamic diameter in the range between 1 and 5 μm. Particles with larger sizes tend to deposit in the mouth and upper airways, whereas smaller particles tend to penetrate into deep lungs. Therefore, aerodynamic particle size distribution (APSD) of an aerosol is the key factor that determines mass deposition in the lungs. Cascade impaction experiment is routinely performed to characterize the aerodynamic size property of an aerosol. Typical experiment yields a series of mass deposition on different stages with defined aerodynamic cutoff size, once plotted, giving an APSD profile. A change of APSD profile may shift drug/vaccine deposition from the deep lung to the upper respiratory tract or even to the mouth and throat, which may eventually affect the site of action. Therefore, batch-to-batch reproducibility (equivalent APSD profiles) should be routinely examined to ensure the quality of an inhalation product. In the second scenario, if drug/vaccine manufacturers plan to develop a generic version of an inhalation product, an APSD profile sufficiently similar to that of the original product should be shown as an evidence of equivalence.

The purpose of this chapter is to develop a particle size comparator to evaluate batch-to-batch reproducibility or equivalence since there is no well-established comparator available so far. We investigated the performance of multivariate data analysis, especially orthogonal partial least square (OPLS) analysis, as a semi-quantitative tool to evaluate the reproducibility or equivalence of APSD profiles of orally inhaled and nasal drug products (OINDP). Monte Carlo simulation was employed to reconstitute APSD profiles based on 55 realistic scenarios proposed by the Product Quality Research Institute (PQRI) working group. OPLS analyses with different data pretreatment methods were performed on each of the reconstituted profiles. Compared to unit-variance scaling, equivalence determined based on OPLS analysis with Pareto scaling was shown to be more consistent with the working group assessment. Chi-square statistics was employed to compare the performance of OPLS analysis (Pareto scaling) with that of the combination test (i.e. chi-square ratio statistics and population bioequivalence test for impactor-sized mass) in terms of achieving greater consistency with the working group evaluation. A p-value of 0.036 suggested that OPLS analysis with Pareto scaling may be more predictive than the combination test with respect to consistency. Furthermore, OPLS analysis may also be employed to analyze part of the APSD profiles that contribute to the calculation of the mass median aerodynamic diameter (MMAD). Our results show that OPLS analysis performed on partial deposition sites doesn't interfere with the performance on all deposition sites.

5.1 Introduction

It is generally believed that aerosol particles greater than 10μm in aerodynamic diameter deposit primarily in the throat and are swallowed subsequently rather than reaching the lungs (196). Lung delivery requires particle size in the range of 1-5 μm (260-262), which

deposit either centrally or peripherally in the lungs depending on particle size. Therefore, aerodynamic particle size distribution (APSD) is an important *in vitro* characteristic of orally inhaled and nasal drug product (OINDP) because of a plausible link between particle size and eventual deposition in the respiratory tract. The interest to develop a statistical method to determine *in vitro* bioequivalence came from the practical need from both the regulators and the drug manufacturer. Once innovator companies make changes to a drug product or drug manufacturers plan to develop a generic version of a drug product, evidence should be provided to the regulators that the new or modified product has an APSD profiles sufficiently similar to that of the original product.

The chi-square ratio statistic (263) proposed in the 1999 US FDA guidance (40, 52) was developed using Anderson 8-stage cascade impactor (38) applied to albuterol metered-dose inhaler data. In order to study this test's applicability to a broad range of OINDP profiles, a working group involving scientists from industry, academia, FDA and US pharmacopeia was established through the Product Quality Research Institute (PQRI) (264). The working group expended a great effort in investigating this chi-square ratio statistics. The work began with developing a simulation method capable of modeling APSD profiles and translating the chi-square ratio statistics proposed by the FDA into an executable algorithm (44). The working group first studied the stability of the chi-square ratio test on pairs of identical profiles, which showed that the stability increased as the number of stages increases and less stable for profiles that are common to metered-dose inhalers (MDIs) and dry powder inhalers (DPIs) (194). The next study focused on pairs of profiles differing in a specified and systematic way on a single deposition site, which gave rise to a total number of 38 scenarios (39, 194). The findings from this study led the working group supplementing the

chi-square ratio statistics with a population bioequivalence (PBE) test based on impactor-sized mass (ISM) (45) in order to increase the discriminating ability of the overall statistical procedure (195). Based on the study of this combination test (i.e. chi-square ratio test and ISM-PBE test), the working group produced a final report in 2007 on a statistical procedure for determining equivalence (195). Due to the deficiencies of the combination test, no recommendations were made by the working group for APSD profiles comparison.

In this chapter, we proposed another method to evaluate the batch-to-batch reproducibility or equivalence of APSD profiles. The new method is based on multivariate data analysis, especially orthogonal partial least square (OPLS) analysis. Multivariate data analysis can be generally divided into two categories (265). One is the unsupervised method such as principal component analysis (PCA). The other one is the supervised method such as partial least square (PLS) analysis and orthogonal partial least square analysis. Principal component analysis is different from orthogonal partial least square analysis in that *a priori* knowledge of the identity of the profiles was not employed when patterns are assessed (265). Principal component analysis is generally employed as a pattern recognition tool before proceeding to the supervised method such as OPLS. Orthogonal partial least square analysis relates a matrix containing independent variables such as mass deposition on each deposition site to a matrix containing dependent variables such as profile membership. OPLS analysis is frequently employed as a discriminant analysis to retrieve information lying in independent variables that may result in class separation. However, the main objective is not to use OPLS analysis to dissect out the independent variables contributing to class separation. Rather, the capability to detect difference between test and reference profiles revealed by OPLS model fitting is our primary goal. There are three reasons for proposing this method: 1) an APSD

profile contains information from multiple deposition sites and, therefore, is a multivariate measurement (196); 2) mass deposition on each stage is not independent from each other. It has been suggested that the deposition on different stages may co-vary between each other (196) and this was indeed considered in the Monte Carlo simulation of 55 realistic scenarios provided by the working group (41, 42); 3) principal components calculated in the OPLS analysis are all orthogonal and thus can resolve the issue of covariance (265). We began our work with first reconstituting 55 realistic scenarios by Monte Carlo simulation. Profiles generated were subjected to OPLS analysis to derive a parameter Eq (standing for equivalence) as described in the methods. Finally, we compared the performance of the OPLS analysis with that of the combination test in terms of achieving greater consistency with the working group evaluation.

5.2 Methods

Monte Carlo Simulation

Monte Carlo simulation was performed in ADAPT II (University of Southern California) to reconstitute 55 aerodynamic particle size distribution (APSD) profiles provided by the Product Quality Research Institute (PQRI) working group (41, 42, 195). Information about the mean and standard deviation for mass deposition on each site were readily available from the profiles provided. They were used as parameters for Monte Carlo simulation in ADAPT II. Population simulation with output noise assuming normal distribution of mass deposition on each stage was adopted. Monte Carlo simulations with a number of 5,000 were performed and repeated three times for each of the 55 realistic scenarios of aerodynamic particle size distribution profiles. The averages were taken for each scenario. In some cases simulations with different numbers were performed for the purpose

of demonstration. Data generated were organized in Microsoft® Excel for each scenario.

Multivariate Data Analysis

Orthogonal partial least square (OPLS) analysis was carried out in SIMCA-P 11.5 (Umetrics) and was employed to compare test profiles with reference profiles in all scenarios. Mass deposition data (X variables) were pretreated with either Pareto scaling or unit-variance scaling in addition to mean centering. Reference and test profiles are coded as 0 and 1 (Y variables) respectively. In order to normalize mass deposition, absolute mass data were first normalized to percent mass deposition data in Excel before proceeding to OPLS analysis. The first two principal components are calculated in all cases for the convenience of plotting. However, the R^2 for OPLS model fitting based on the first principal component was recorded. Eq was defined as equal to $1\text{-}R^2$ and served as a measure of equivalence between test and reference profiles for all 55 scenarios.

Chi-square Test

Chi-square test was carried out in Minitab 14.1 (Minitab Inc.) to compare OPLS analysis (with Pareto scaling) with the combination test proposed by the Food and Drug Administration (FDA) and the PQRI working group. The difference (Δ) between the working group evaluation and Eq (by OPLS analysis) or proportion (by the combination test) was divided into three categories: $\Delta \geq 0.5$, $0.3 \leq \Delta < 0.5$ and $\Delta < 0.3$. A p-value less than 0.05 was considered as statistically significant.

5.3 Results and Discussions

5.3.1 Monte Carlo simulation to recover 55 realistic scenarios of aerodynamic particle size distribution profiles

All 55 realistic scenarios have been simulated by Monte Carlo simulation. Among

these profiles, only two scenarios were chosen to represent significant variability in the upper deposition sites between test and reference profiles in scenario 13c (figure 5.1a) as apposed to in the lower deposition sites in scenario 2bb2 (figure 5.1b). Profiles simulated here are slightly different in appearance from those provided by the Product Quality Research Institute (PQRI) working group (41, 42, 195). This is possibly due to the inherent variability of Monte Carlo simulation. A simulation number of 30 was chosen for both scenarios.

5.3.2 Comparison of chi-square ratio statistics and orthogonal partial least square analysis with respect to profile comparison

It was suggested that 30 each reference and test inhalers should be sampled individually and subject to chi-square ratio statistics (194-196). A sample size of 30 was considered necessary to represent the random sampling of a population of dry powder inhalers or metered-dose inhalers manufactured. In addition, this is also a practical number, which requires a considerable yet manageable amount of sampling work. Figure 5.2a shows the flowchart of the chi-square ratio statistics. Thirty reference and test inhalers are randomly sampled from corresponding populations (e.g. 5,000). Sample profiles for these 30 inhalers are collected and then subject to chi-square ratio statistics. In an attempt to set up an appropriate critical value for the chi-square ratio statistics, such statistical testing based on 30 samples is repeated hundreds of thousands of times to obtain a distribution of statistics, upon which a reasonable critical value may be chosen. It should be noted that the statistics obtained based on a sample size of 30 actually gives the possibility of equivalence between test and reference profiles from two corresponding populations rather than two samples. In contrast to chi-square ratio statistics, figure 5.2b shows the rationale for orthogonal partial least square (OPLS) analysis as an analytical tool to judge reproducibility or equivalence

between two populations. First, it should be emphasized that the method developed based on OPLS analysis is an analytical tool rather than a statistical test. There is no p-value associated with this method. R^2 or its derivative Eq was instead used as an indicator of reproducibility or equivalence between test and reference profiles (see explanation in the following section). This method also begins with a random sampling of 30 samples in consistent with the chi-square ratio statistics. The sample mean and standard deviation of mass at each deposition site was calculated based on impactor data from these 30 samples. Rather than statistical testing, the sample mean and standard deviation was used for Monte Carlo simulation to obtain simulated population profiles. Ideally, the population mean and standard deviation of mass deposition should be used for the population simulation. However, these numbers won't be known until all the inhalers are characterized, which are not practical. Therefore, we consider a sample size of 30 as both necessary and practical since the more samples collected the more accurately sample mean and standard deviation can represent population mean and standard deviation. The size for population simulation was also studied, which suggests that a population size of 5,000 may be relevant and more importantly the R^2 based on this size tends to stabilize. Consequently, the R^2 (or its derivative Eq) for OPLS model fitting based on 5,000 profiles may serve as an indicator of reproducibility or equivalence between test and reference populations of at least this size.

5.3.3 Orthogonal partial least square analysis of test and reference profiles

Profiles generated by Monte Carlo simulation were analyzed by OPLS analysis as described in methods. OPLS places the first principal component onto the largest difference between test and reference profiles. The successive principal components will span the difference which is not represented by the preceding component (265). Therefore, OPLS

score plot consisting of the first two components provides a visual impression of the comparability between test and reference profiles. The larger the difference between the test and reference profiles, the further they are separated from each other on the first principal component. However, this separation is only a qualitative impression rather than a quantitative measure. In order to derive a semi-quantitative parameter which may serve as a measure of equivalence, R^2 for OPLS model fitting (based on the first principal component) was initially selected. R^2 represents how well the model fits the data or how much variability in the data can be explained by the model (265). R^2 equals to 0 if test and reference profiles are identical; on the other hand, R^2 approaches 1 when test profiles are completely different from reference profiles assuming a right model is used. Apart from model fitting, R^2 also depends on the variability in the data as will be seen in the following section where different data pretreatment methods (i.e. different treatment of the variability) were employed. Based on this rationale, we define a parameter $Eq = 1-R^2$, which may be considered as a measure of equivalence or comparability for the test and reference profiles. Strictly speaking, Eq is not a statistical value that can be used for statistical testing but rather a semi-quantitative value defined by us for the purpose of interpretive evaluation of aerodynamic particle size distribution (APSD) profiles.

5.3.4 Studying 55 realistic scenarios with orthogonal partial least square analysis

Based on the description above and in the methods, OPLS analysis of 55 realistic scenarios was carried out with different data pretreatment methods. The absolute mass deposition data can be used as is or normalized to percent mass deposition data. All the data were mean centered to avoid greater deposition on particular sites dominating the whole distribution. To account for the variance on each deposition site, two scaling methods were

employed. One is unit-variance (UV) scaling in which the base weight is computed as the reciprocal of standard deviation and the other is Pareto scaling which gives the weight of the reciprocal of square root of standard deviation (265). Pareto scaling is between no scaling and UV scaling and gives the variable under evaluation a variance equal to its standard deviation instead of unit variance. The effect of both scaling methods was investigated comprehensively.

Before performing OPLS analysis on all realistic scenarios, we carried out a test analysis on the feasibility of this method. In figure 5.3a, Monte Carlo simulations were performed twice (5,000 for each) based on parameters from reference profiles in scenario 1a. The first simulation generates 5,000 reference profiles and the second simulation generates another 5,000 reference profiles yet considered as test profiles. Predictably, OPLS analysis on such reference and test profiles should yield a R^2 approaching 0 and both profiles should be completely mixed without any separation on the first principal component in the score plot. Indeed, we observed the same phenomenon as shown in figure 5.3a. Then OPLS analysis was performed for all realistic scenarios. Figure 5.3b-e represents such analysis for scenario 1a-1d, which was considered by the working group with decreasing similarity between test and reference profiles. OPLS analysis showed the same trend as evidenced by more and more separation between profiles on the first principal component in the score plot (figure 5.3b-e).

5.3.5 Effect of different data pretreatment methods on the performance of orthogonal partial least square analysis

The Eq value (defined as $1-R^2$) for each scenario computed by OPLS analysis based on different data pretreatment methods, the probability of equivalence derived from the combination test (chi-square+ISM-PBE), and the working group evaluation of equivalence

are all tabulated in table 5.1. It has been proposed by the working group that agreement to within 50% (or 0.5) of the overall frequency of equivalence declarations between the working group and the combination test was interpreted as adequate for the statistical procedure to make correct decisions (195). In cases where the differences were more than 0.5, the combination test was considered not be able to make the correct decisions and inputs from reviewers' experience were necessary to determine APSD equivalence. Similarly, we extended this criterion to the performance of the OPLS analysis (i.e. the difference between Eq value and the working group assessment less than 0.5 was considered adequate). The differences between the working group evaluation and the combination test are plotted in figure 5.4a. The difference between the working group assessment and OPLS analysis for each of the data pretreatment methods are plotted in figure 5.4b-e. We noticed that OPLS analysis with Pareto scaling works better than UV scaling as evidenced by less inconsistencies no matter whether absolute or normalized mass was used. However, UV scaling on normalized mass works better than the same scaling on absolute mass. The effect of different scaling methods on multivariate data analysis has been studied in other fields (266). Van de Berg showed in his metabolomic study that Pareto scaling, compared to unit-variance scaling, was more stable in terms of generating reliable rank of the most important metabolites (267). Noda examined two scaling techniques (Pareto scaling vs. unit-variance scaling) to enhance two-dimensional correlation Raman spectra and concluded that Pareto scaling was able to circumvent the amplification of noise by retaining a portion of magnitude information (268). Therefore, it is not to our surprise that Pareto scaling works better than UV scaling since the magnitude information about the mass deposition on each site was retained. Moreover, this magnitude information was not changed from absolute to

normalized mass deposition data when used with Pareto scaling. However, the inaccuracy of mass deposition may be amplified to a different extent with or without normalization since the magnitude information was completely lost in unit-variance scaling. This may provide a possible explanation for the different performance on normalized or absolute mass data with UV scaling. Finally, we compared the performance of the combination test with that of OPLS analysis based on Pareto scaling by chi-square statistical test according to the criterion proposed in the methods (figure 5.5). The p-value ($0.036<0.05$) suggested that multivariate data analysis may be more indicative than the combination test for the purpose of interpretive evaluation of reproducibility or equivalence of APSD profiles.

5.3.6 Three scenarios mis-predicted by orthogonal partial least square analysis

When OPLS analysis with Pareto Scaling was employed, three scenarios with differences exceeding 0.5 are 12a2, 12a3 and 12b1 (figure 5.4c and table 5.1). An impression of equivalent test and reference profiles was given when these scenarios were reconstituted by Monte Carlo simulation. However, OPLS analysis clearly separated the test profiles from the reference profiles in the score plot with large R^2 value (table 5.1) possibly because of very small standard deviation relative to the mean in certain deposition sites. OPLS analysis appeared to be sensitive to small standard deviation/mean ratios while at this stage no efforts haven been expended in correlating the sensitivity of OPLS analysis to the standard deviation/mean ratios. On the other hand, the combination test predicts pretty well in these three scenarios (figure 5.4a and table 5.1).

5.3.7 Orthogonal partial least square analysis of mass deposition on partial deposition sites

Comparison based on the whole deposition profiles was recommended by the FDA and

PQRI working group since a change in mass deposition outside the impactor may affect the performance of the drug product (196). However, researchers are sometimes interested in only a part of the APSD profiles (e.g. mass deposition inside impactors and on the filter (192)) for two reasons: 1) there was no clear cut-off size for mass deposition outside the impactor; 2) mass deposition on these sites is important for the calculation of mass median aerodynamic diameter (MMAD). Therefore, we performed OPLS analysis with Pareto scaling on mass deposition profiles inside the impactor for all 55 realistic scenarios. Then, we compared the R^2 obtained from partial deposition sites with that from all deposition sites. In scenario 13c, the R^2 for partial sites is 0.08 as opposed to 0.51 for all sites. This difference may be explained by the greater difference between test and reference profiles outside the impactor while the difference inside the impactor is very small (figure 5.1a). In scenario 2bb2, the major difference comes from the deposition inside the impactor while little difference exists outside the impactor. The R^2 for partial sites is 0.46 and 0.48 for all sites. This modest increase in R^2 is due to a mild contribution of small difference from deposition sites outside the impactor (figure 5.1b). Our analyses indicate that OPLS analysis performed on partial deposition sites doesn't interfere with the performance on all deposition sites.

5.4 Summary

Multivariate data analysis may open a new way for scientists in the field of pharmaceutical aerosol sciences to evaluate the batch-to-batch reproducibility or equivalence of aerodynamic particle size distribution profiles. Our study shows that orthogonal partial least square analysis coupled with Pareto scaling works best among all the data pretreatment methods investigated. It is not our intention to replace the combination test proposed by the FDA and PQRI working group; rather this new method may serve as a semi-quantitative tool

to evaluate particle size distribution profiles before a robust and well-established statistical test can be proposed. In addition, orthogonal partial least square analysis should be performed with caution in certain situations where the standard deviation/mean ratios are relatively small where the combination test or more statistically relevant test should be considered.

Table 5.1 Equivalence value determined from different analysis methods and the working group evaluation. Column I: scenario ID. Column II-V: equivalence (Eq value) determined based on orthogonal partial least square analysis with different data pretreatment methods. Eq values in column II-V are the average of three individual simulations (n=3, 5,000 each). Column VI: likelihood of equivalence based on the combination test proposed by the US FDA and the PQRI working group. Column VII: equivalence evaluated by the working group. The likelihood of equivalence from the working group evaluation and the combination test were retrieved from reference 195.

Scenario	UV-Abs	Par-Abs	UV-Nor	Par-Nor	Chi-2+ISM	WG
1a	0.64	0.73	0.68	0.77	0.70	1.00
1b	0.53	0.62	0.60	0.65	0.22	0.79
1c	0.34	0.46	0.42	0.47	0.01	0.07
1d	0.20	0.28	0.20	0.26	0.00	0.00
1aa	0.76	0.86	0.79	0.87	0.81	1.00
1bb	0.55	0.61	0.56	0.60	0.48	0.79
1cc	0.39	0.51	0.47	0.51	0.01	0.36
1dd	0.20	0.29	0.25	0.28	0.00	0.00
1ee	0.18	0.25	0.20	0.22	0.00	0.00
2a	0.67	0.74	0.68	0.78	0.89	0.79
2b	0.45	0.51	0.46	0.53	0.92	0.50
2c	0.43	0.46	0.44	0.47	0.89	0.21
2aa1	0.66	0.70	0.67	0.70	0.88	0.71
2bb1	0.47	0.51	0.49	0.60	0.80	0.64
2cc1	0.48	0.57	0.54	0.60	0.74	0.50
2dd1	0.46	0.55	0.48	0.54	0.89	0.29
2aa2	0.49	0.52	0.49	0.53	0.90	0.64
2bb2	0.48	0.51	0.49	0.52	0.89	0.29
2cc2	0.41	0.41	0.42	0.43	0.94	0.14
4a	0.90	0.93	0.91	0.94	0.88	1.00
4b	0.07	0.51	0.19	0.51	0.89	1.00
4c	0.08	0.26	0.11	0.26	0.68	0.21
4d	0.07	0.21	0.09	0.19	0.45	0.14
5a	0.72	0.78	0.74	0.80	0.89	0.93
5b	0.35	0.42	0.39	0.44	0.86	0.86
5c	0.12	0.16	0.15	0.16	0.50	0.29
7a	0.21	0.21	0.23	0.23	0.89	0.29
7b	0.44	0.48	0.49	0.53	0.95	0.50
7c	0.71	0.76	0.74	0.79	0.92	0.93
10a	0.18	0.17	0.17	0.16	1.00	0.14
10b	0.20	0.17	0.20	0.17	1.00	0.29
10c	0.41	0.41	0.41	0.41	1.00	0.50
10d	0.71	0.73	0.73	0.74	1.00	1.00
11a	0.36	0.39	0.49	0.51	0.78	0.64
11b	0.59	0.62	0.72	0.74	1.00	1.00
11c	0.82	0.84	0.83	0.87	1.00	1.00
12a0	0.05	0.06	0.05	0.06	0.07	0.07
12a1	0.07	0.09	0.07	0.10	0.82	0.14
12a2	0.10	0.15	0.10	0.16	1.00	0.86
12a3	0.12	0.27	0.13	0.29	1.00	1.00

12b0	0.11	0.16	0.11	0.17	0.03	0.29
12b1	0.17	0.26	0.19	0.31	0.93	0.86
12b2	0.25	0.44	0.27	0.47	1.00	0.86
12b3	0.31	0.55	0.33	0.56	1.00	1.00
13a	0.46	0.71	0.69	0.74	0.40	1.00
13b	0.29	0.60	0.43	0.65	0.38	0.57
13c	0.22	0.41	0.24	0.49	0.26	0.36
13d	0.12	0.38	0.29	0.43	0.00	0.21
13e	0.07	0.35	0.23	0.44	0.00	0.07
13f	0.38	0.87	0.50	0.90	0.84	0.93
13g	0.29	0.71	0.42	0.75	0.83	0.50
14a1	0.06	0.20	0.07	0.13	0.00	0.00
14a2	0.06	0.25	0.09	0.18	0.00	0.07
14a3	0.07	0.23	0.12	0.22	0.03	0.43
14a4	0.07	0.26	0.15	0.28	0.37	0.71

UV-Abs: absolute mass data were pretreated with unit-variance scaling
Par-Abs: absolute mass data were pretreated with Pareto scaling
UV-Nor: normalized percent mass data were pretreated with unit-variance scaling
Par-Nor: normalized percent mass data were pretreated with Pareto scaling
Chi-2+ISM: chi-square ratio statistics supplemented by a population bioequivalence test for impactor-sized mass
WG: working group evaluation

Figure 5.1 Reconstituted aerodynamic particle size distribution profiles for scenario 13c and scenario 2bb2 (Monte Carlo simulations with a number of 30 were generated for each reference and test profiles). a, Scenario 13c; b, Scenario 2bb2.

a

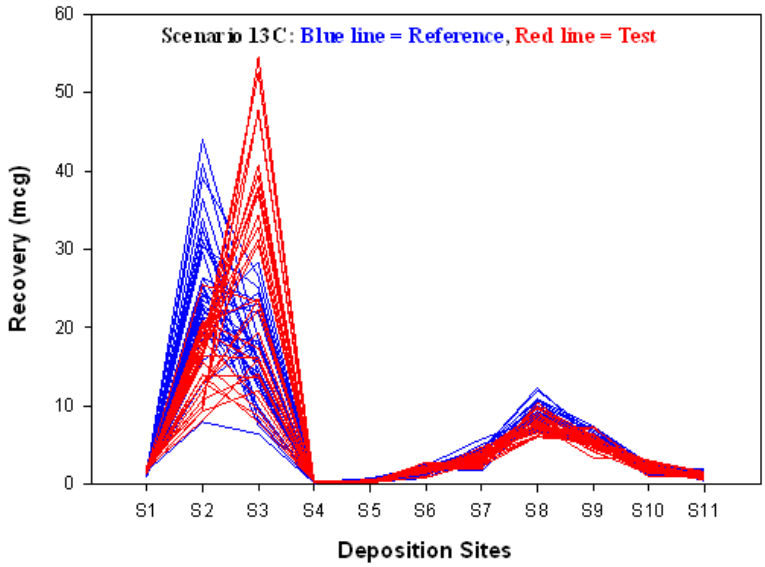

b

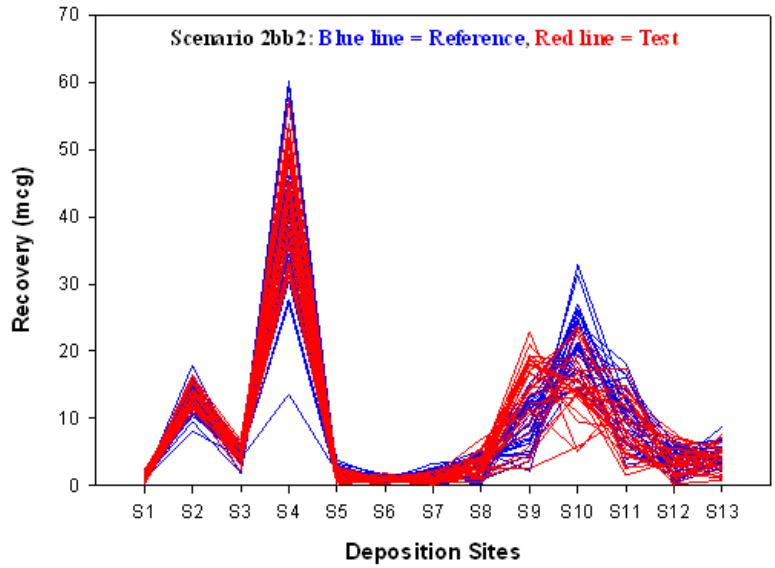

Figure 5.2 Comparison of chi-square ratio statistics and orthogonal partial least square analysis with respect to profile comparison. a, flowchart of the chi-square ratio statistics developed by the PQRI working group; b, flowchart of the orthogonal partial least square analysis developed in our group.

a

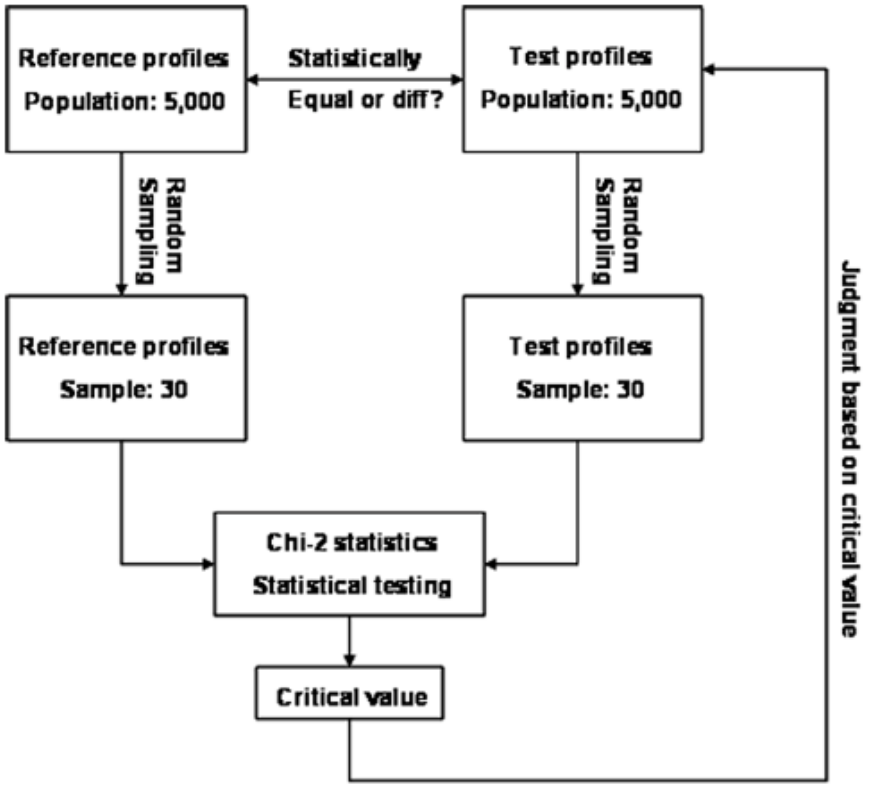

b

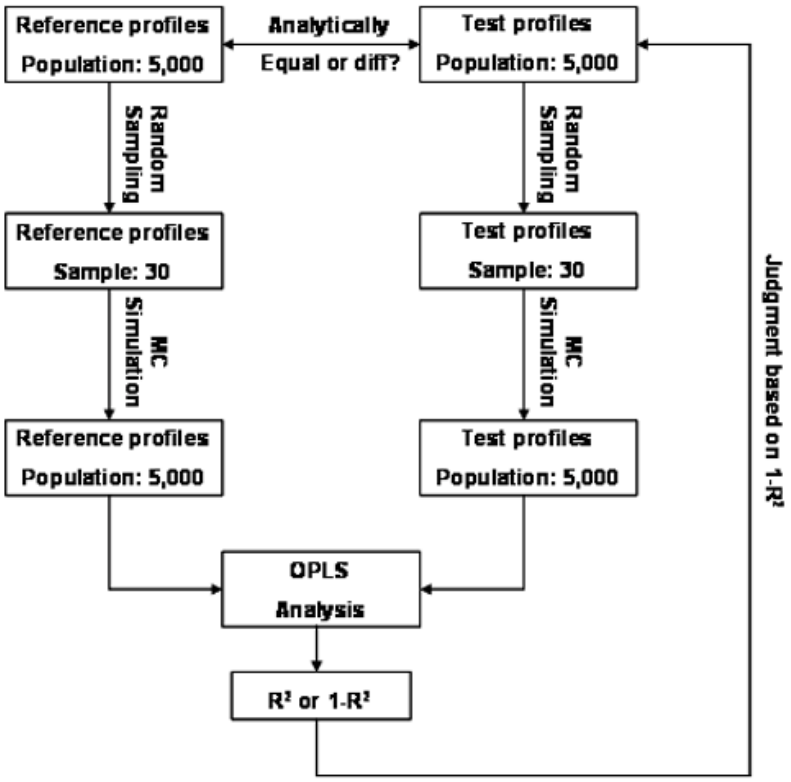
Reference profiles
Population: 5,000
Analytically
Equal or diff?
Test profiles
Population: 5,000
Random Sampling
Random Sampling
Reference profiles
Sample: 30
Test profiles
Sample: 30
MC Simulation
MC Simulation
Reference profiles
Population: 5,000
Test profiles
Population: 5,000
OPLS
Analysis
R² or 1-R²
Judgment based on 1-R²

Figure 5.3 Score plot of orthogonal partial least square analysis to compare reference and test profiles generated by Monte Carlo simulation (5,000). Each data point in the score plot represents a whole profile (deposition on all sites). Reference profiles are colored blue and test profiles are colored red. a, reference profiles from scenario 1a were compared with itself (two separate simulations); b-e, reference profiles were compared with test profiles from scenario 1a, 1b, 1c and 1d respectively.

a

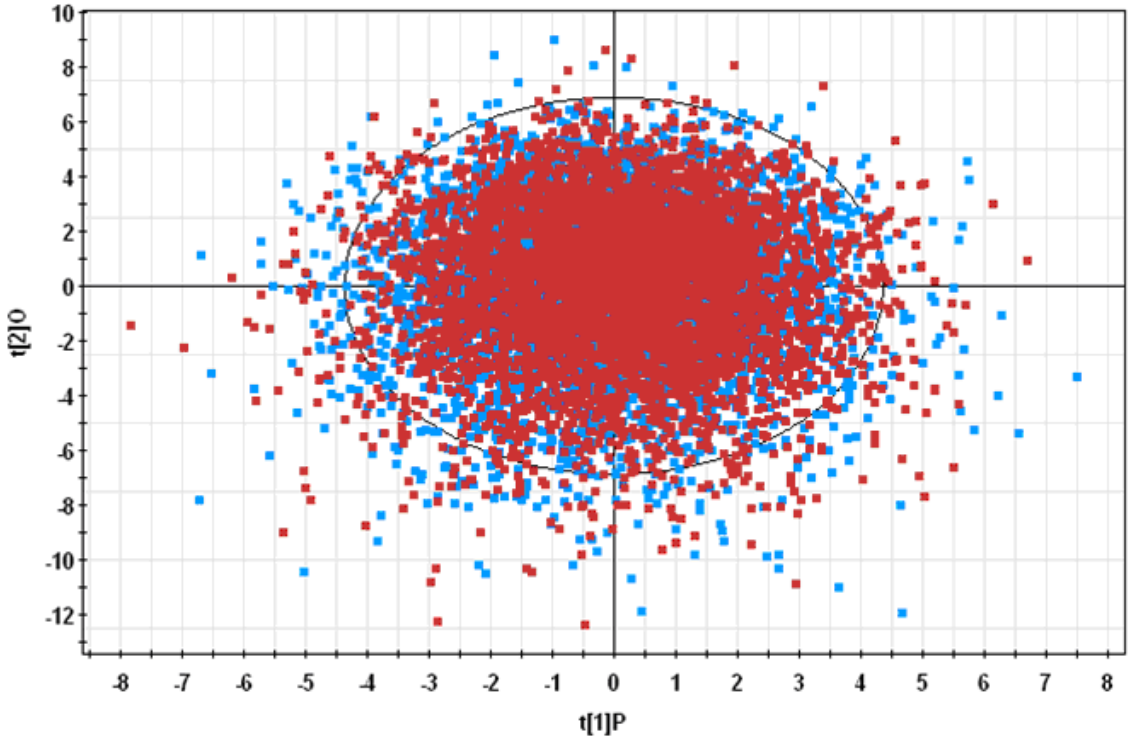

b

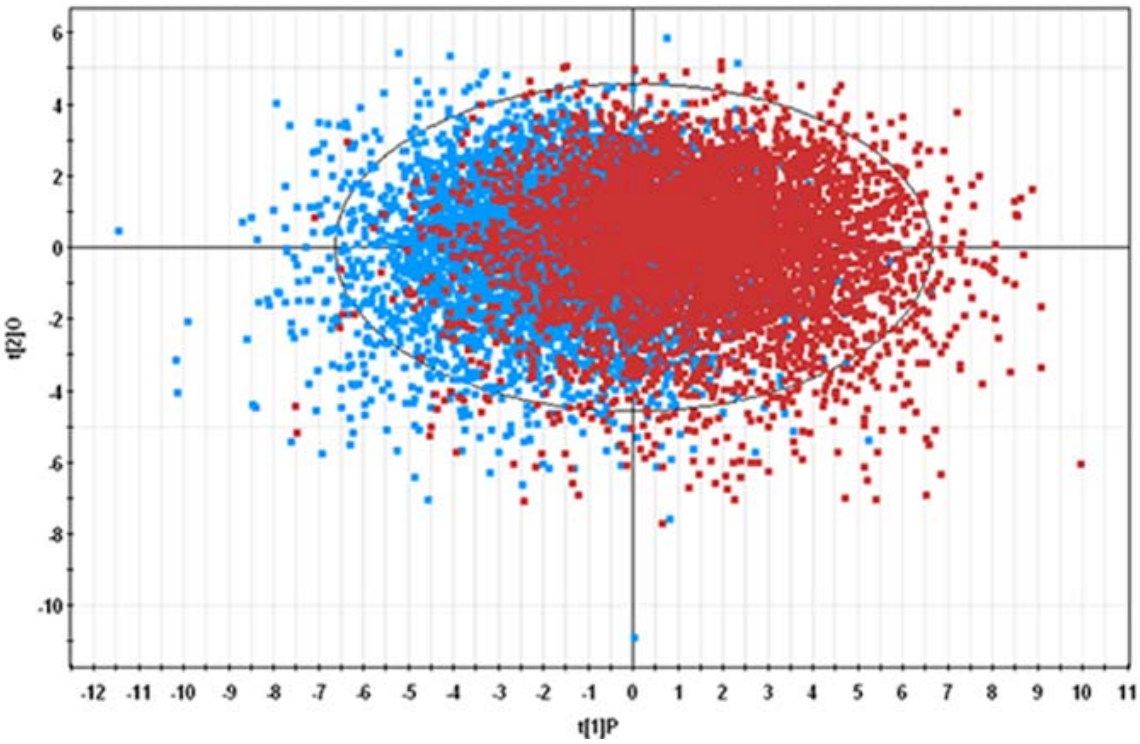

c

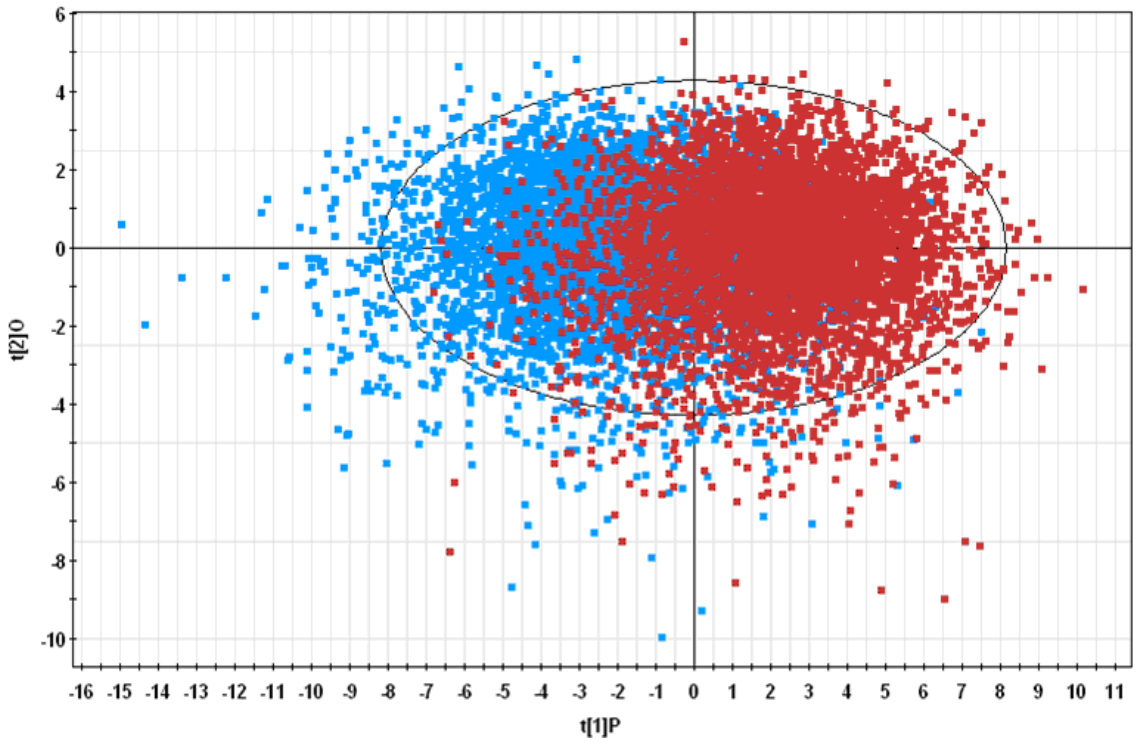

d

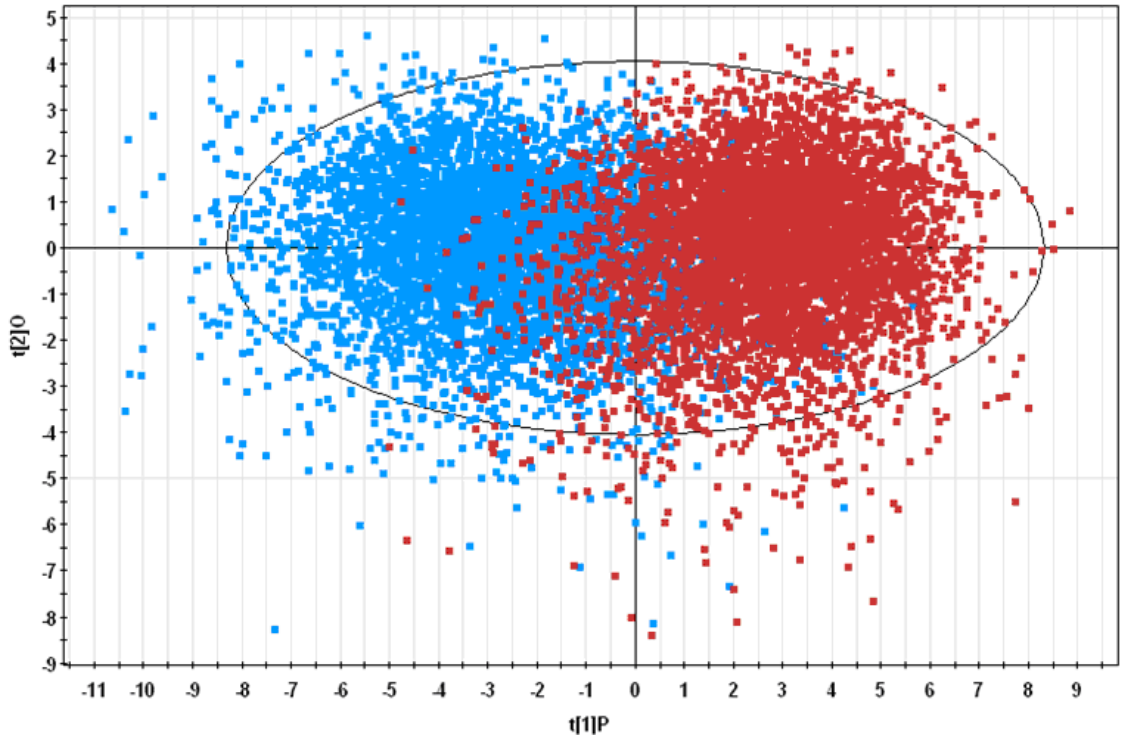

e

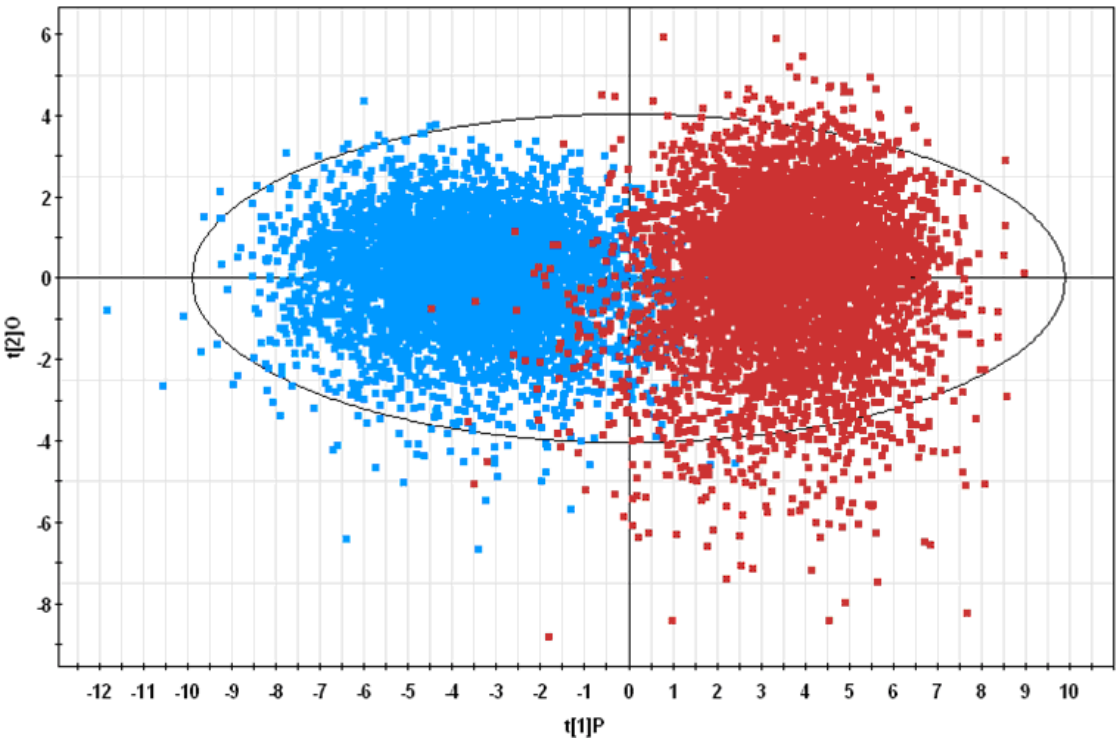

Figure 5.4 Differences between the working group (WG) assessment and statistical analyses based on different methods and data pretreatment. a, differences between the WG assessment and the combination test (chi-square plus ISM-PBE); b, differences between the WG assessment and the OPLS analysis based on unit-variance scaling on absolute mass data; c, same as b except that Pareto scaling was used; d, same as b but absolute mass data was first normalized to the percent mass data; e, same as d but Pareto scaling was used. The working group evaluation and possibility of equivalence from the combination test were retrieved from reference 195.

a

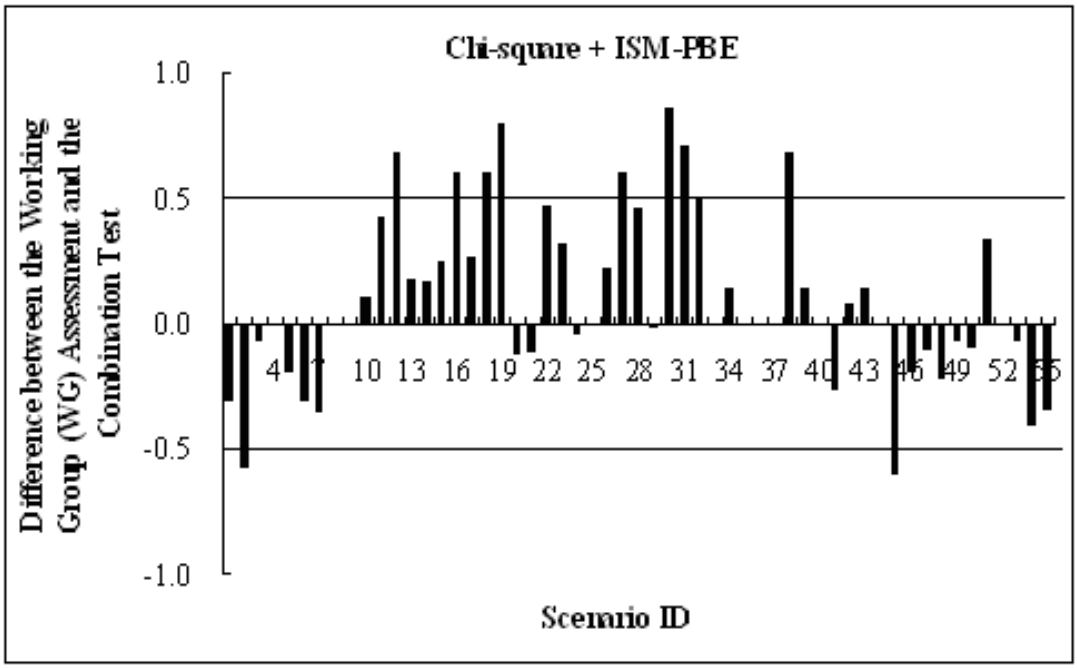

b

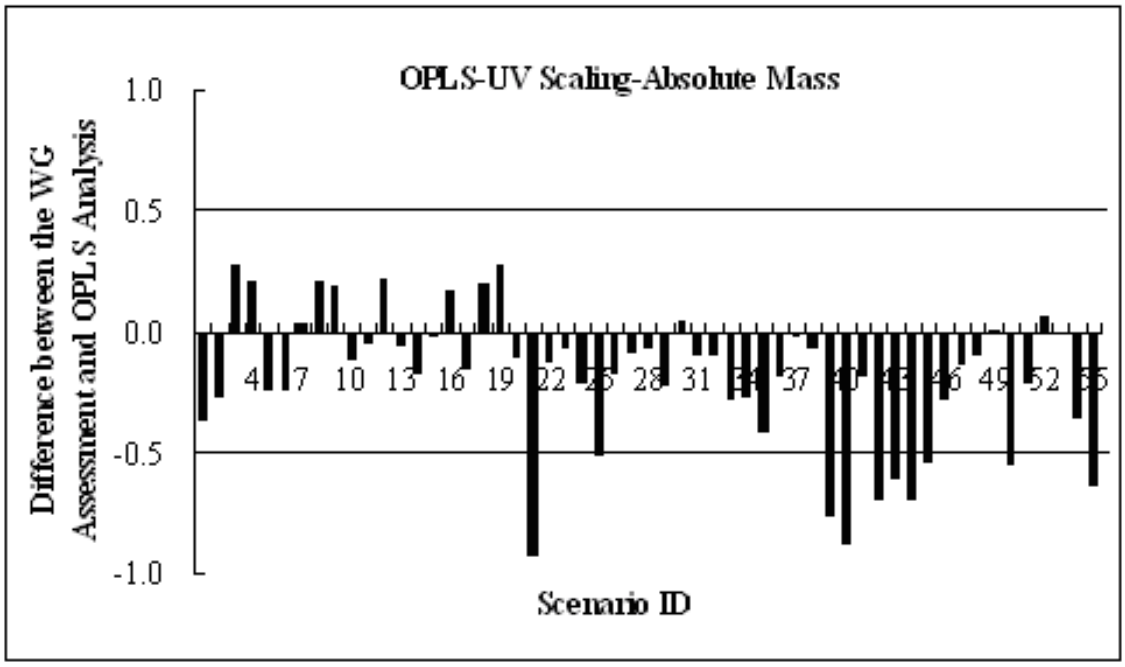
OPLS-UV Scaling-Absolute Mass
Difference between the WG Assessment and OPLS Analysis
1.0
0.5
0.0
-0.5
-1.0
4
7
10
13
16
19
22
28
31
37
46
49
52
Scenario ID

c

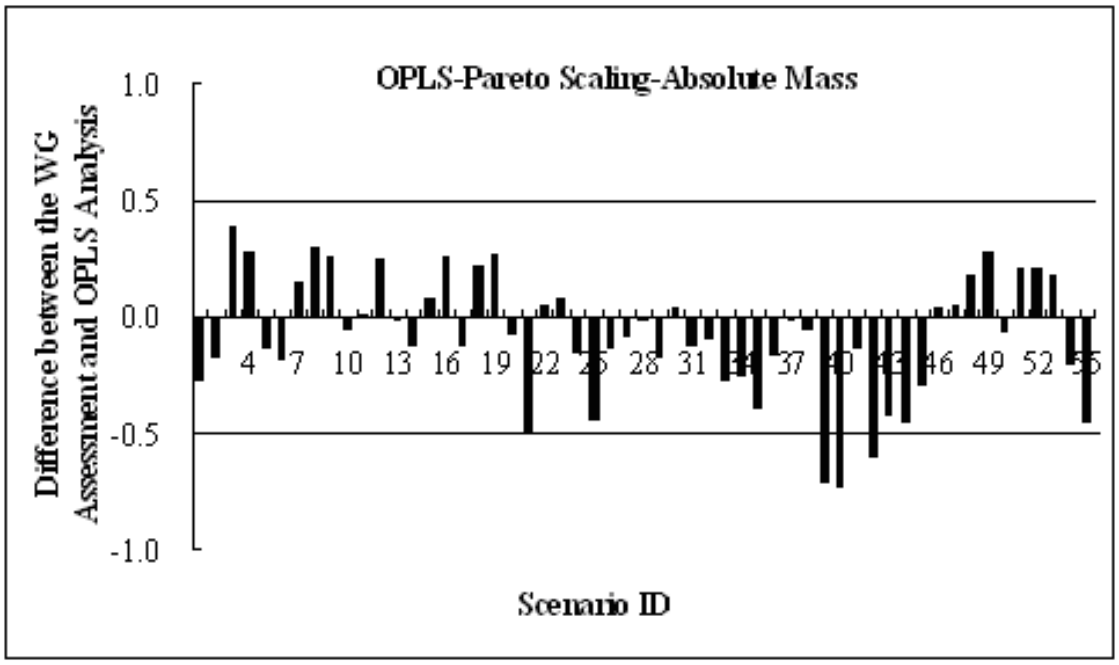
OPLS-Pareto Scaling-Absolute Mass
Difference between the WG Assessment and OPLS Analysis
1.0
0.5
0.0
-0.5
-1.0
4
7
10
13
16
19
22
28
31
37
46
49
52
Scenario ID

d

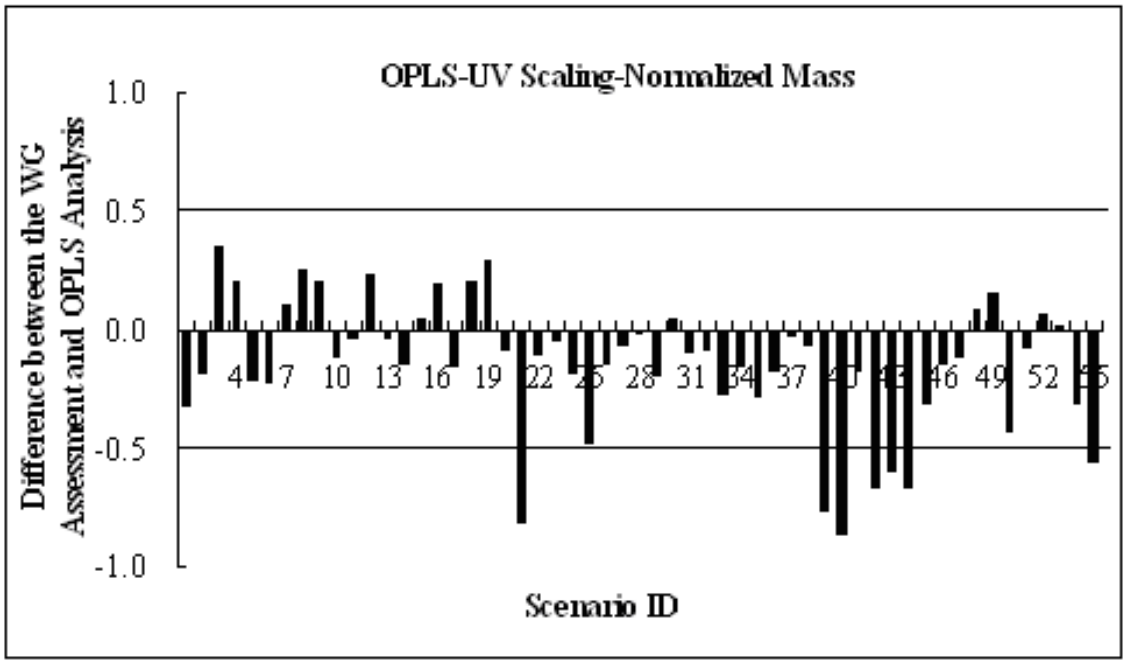
OPLS-UV Scaling-Normalized Mass
Difference between the WG Assessment and OPLS Analysis
1.0
0.5
0.0
-0.5
-1.0
4 7 10 13 16 19 22 25 28 31 34 37 40 43 46 49 52 55
Scenario ID

e

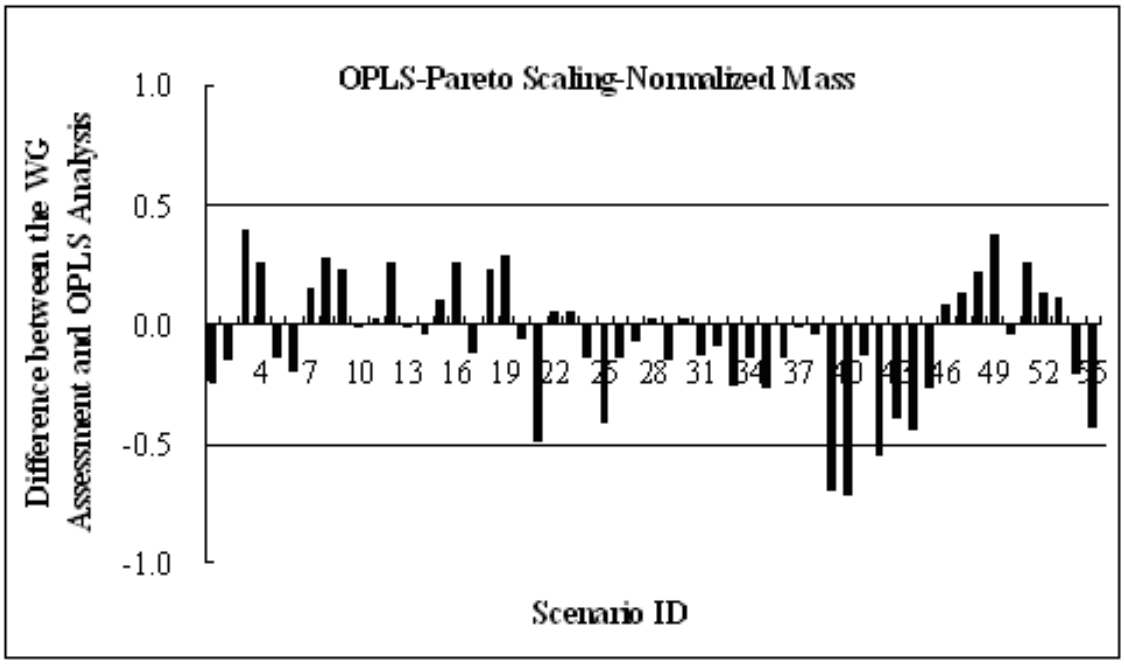
OPLS-Pareto Scaling-Normalized Mass
Difference between the WG Assessment and OPLS Analysis
1.0
0.5
0.0
-0.5
-1.0
4 7 10 13 16 19 22 25 28 31 34 37 40 43 46 49 52 55
Scenario ID

Figure 5.5 Comparison of the performance of the combination test (chi-square plus ISM-PBE) with that of orthogonal partial least square analysis based on Pareto scaling. The difference (Δ) between the working group evaluation and each of the two analysis methods was placed into three categories as labeled in figure 5.5. The number of scenarios falls into each category was plotted in the y-axis and labeled above corresponding bar. Chi-square statistical test was then performed to compare the two methods in terms of achieving greater consistencies (Chi-Sq = 6.632, p-Value = 0.036). The working group assessment and the possibility of equivalence from the combination test were retrieved from reference 195.

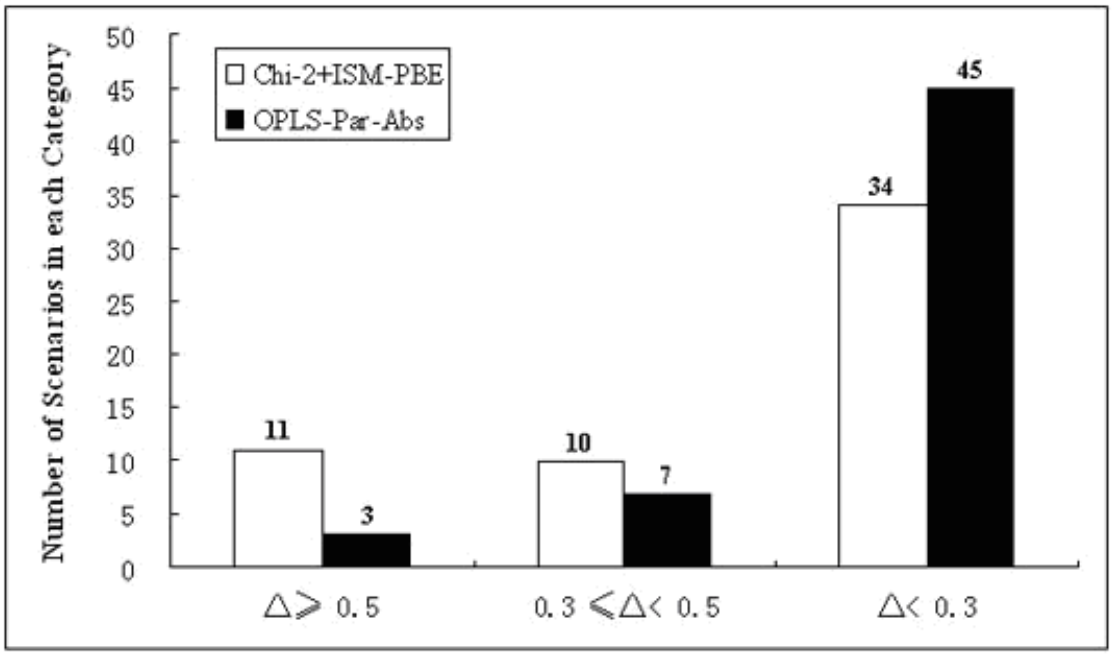

CHAPTER 6: DISCUSSION AND FUTURE STUDIES

Tuberculosis (TB) is one of the leading causes of mortality in the world. The only commercially available prophylactic vaccine for TB is BCG. However, there are several shortcomings associated with this attenuated live bacterial vaccine such as waning protection over time, variable efficacy in different populations, interference by environmental mycobacteria, and inability to be used in immunocompromised patients. There has been long interest in developing the second-generation TB vaccines, among which subunit vaccine has drawn significant attention from researchers in this field due to its simplicity and safety. Various TB antigens have been identified so far and characterized both biochemically and immunologically. These antigens or antigen combinations were incorporated into appropriate formulations for the development of TB subunit vaccine. Particulate system was mostly studied as the delivery vehicle for subunit vaccines since it contributes to both dosage forms and adjuvancy of the subunit vaccine. Moreover, the characteristics of a particulate system determine the flow property of the powdered vaccine, which is particularly important for vaccines intended for pulmonary delivery. Since particle size distribution plays an essential role in vaccine delivery into the lungs, the batch-to-batch reproducibility of vaccine powders should be examined, which requires the development of a particle size comparator to evaluate the aerodynamic particle size distribution (APSD) profiles.

The research described in this dissertation began with recombinant TB antigen design, expression, purification and characterization (chapter 2); purified antigens were then encapsulated into PLGA microparticle formulations at optimized spray-drying conditions

followed by comprehensive formulation characterization (chapter 3); the efficacy of vaccine formulations was subsequently evaluated by *in vitro* antigen presentation assays to understand the nature of induced immune response (chapter 4); to examine the batch-to-batch reproducibility, a particle size comparator based on orthogonal partial least square analysis (OPLS) was developed (chapter 5). The overall goal of this research is to compare the *in vitro* immune response of newly designed respirable TB subunit vaccines based on Ag85B/TB10.4 and their different combinations in order to make a recommendation of the best antigen/antigen combination for future animal protection study. The second goal is to develop a particle size comparator to evaluate the batch-to-batch reproducibility of inhalation products with an ultimate goal to use it as a quality evaluation tool for making highly reproducible TB subunit vaccines suitable for lung delivery and immunization.

There were four specific aims in this research and four corresponding hypotheses associated with each specific aim. The results and achievement for each specific aim were comprehensively documented in each previous chapter and will not be reiterated here. Rather, discussions in this chapter will focus on four hypotheses proposed.

- H1: Milligram quantities of soluble recombinant antigens can be obtained by rational design of the expression constructs.
- H2: Respirable PLGA-rAg microparticles can be manufactured with a target size by optimizing the spray-drying parameters.
- H3: PLGA-rAg microparticles can induce stronger and prolonged immune response *in vitro* compared to antigen solutions.
- H4: Particle size comparator constructed on the basis of orthogonal partial least square analysis has a better performance than that developed on the basis of chi-square ratio

statistics.

6.1 Milligram quantities of soluble recombinant antigens can be obtained by rational design of the expression constructs

This hypothesis was successfully addressed in chapter two. The expression of TB10.4 on its own led to the exclusive formation of inclusion bodies. Similarly, Ag85B-TB10.4 or TB10.4-Ag85B, when expressed on their own, was found exclusively in the inclusion bodies. However, N-terminal fusion of thioredoxin to TB10.4 (Trx-TB10.4) dramatically increased its solubility with a yield of approximately 14mg/L when overexpressed in *E. coli* culture. This initial success with TB10.4 stimulated our effort to improve the solubility of the fusion antigen by the same strategy. However, the fact that N-terminal fusion of thioredoxin to Ag85B-TB10.4 only slightly increased its solubility requires further optimization of the expression construct by rational design. The construct was redesigned to change the order of fusion to TB10.4-Ag85B. The resulting protein (Trx-TB10.4-Ag85B) showed significantly increased solubility with a yield of approximately 2.5mg/L. Interestingly, free TB10.4 and TB10.4-Ag85B could be released after protease treatment without compromising their solubility. The yields for these two proteins are approximately 4mg/L and 1mg/L respectively.

Purifying recombinant proteins from the soluble fraction of *E. coli* culture is highly preferred for several reasons such as the ease of purification, better chance to retain native conformation, and cost saving. Among them, a better chance to retain native conformation is the mostly favored property since these proteins are intended for use as antigens to develop TB subunit vaccine. Antigen conformations are mostly likely to be associated with their immunogenicity in terms of both humoral and cell-mediated immunity. To better mimic

pathogen invasion, antigens delivered from the subunit vaccine should better adopt a conformation sufficiently similar to that of native TB proteins. This research represents one of few studies that used soluble recombinant TB antigens to develop the subunit vaccine.

The success is based on a good understanding of protein structure. Two mechanisms were proposed in chapter two to explain the increased solubility and yield of Trx-TB10.4-Ag85B in comparing to Trx-Ag85B-TB10.4. The spatial effect suggests that direct solubilization effect of thioredoxin on TB10.4 is important, which may be compromised by the long spacer Ag85B in the Trx-Ag85B-TB10.4 design. The linker effect suggests that the shorter flexible linker (between Ag85B and TB10.4) in Trx-Ag85B-TB10.4 design may compromise the folding of the two fusion partners and thus leading to poor solubility. Although the validity of proposed mechanisms should be addressed in the future, they did play a pivotal role in guiding our successful design of a novel recombinant TB antigen TB10.4-Ag85B with great solubility.

6.2 Respirable PLGA-rAg microparticles can be manufactured with a target size by optimizing the spray-drying parameters

This hypothesis was successfully addressed in chapter three. Highly reproducible PLGA-rAg microparticles were prepared by emulsion/spray-drying method with very similar particle size and distribution, surface charge and morphology and thermal characteristics. The concept of Quality-by-Design (QbD) rather than trial-by-error was employed for the optimization of spray-drying parameters. Five process variables including atomization pressure, spray flow, aspirator flow, inlet temperature and pump feeding rate were optimized with respect to two response variables, i.e. particle size and yield. The optimization criteria were as follows: a) a VMD around 3μm (greater macrophage uptake), b) a yield greater than

15% (cost saving), c) a single mode of size distribution and a span less than 1 (uniformity) and d) mass median aerodynamic diameter (MMAD) between 1 and 5μm (aerosol delivery to the lung).

A half-factorial design (2^{5-1}) was chosen for this optimization with reduced number of experiments by half yet without losing statistical powder to dissect out significant main effects and two-way interactions. This was again determined by the high-resolution nature of this particular design. Under optimized spray-drying conditions with atomization pressure (3 bars), spray flow (700 L/hr), pump feeding rate (4 ml/min), aspirator flow (100%) and inlet temperature (55 ˚C), manufactured particles showed a unimodal and narrow size distribution, which meet the proposed criteria for optimization. The VMD is approximately 3 μm, a yield of approximately 18%, and an MMAD of 3.3μm.

The VMD was successfully optimized to the target size ideal for alveolar macrophage uptake. The yield of 18% is relatively low possibly due to the small bench scale but could be much higher once this process is scaled up. An MMAD of 3.3μm falls within the range of 1 to 5μm, considered as suitable for pulmonary delivery. Moreover, the fine particle fraction (FPF) of the emitted dose was 61.5±6.4% and FPF of the total dose was 37.0±5.5%, which suggested that optimized formulations could be effectively delivered into deep lungs where alveolar macrophages are populated without the need of carrier excipient (e.g. lactose) in the formulation.

The successful manufacture of respirable PLGA-rAg microparticles can be attributable to, among others, the selection of an appropriate solvent (dichloromethane in our study) to dissolve PLGA and the selection of an appropriate statistical design with a high-resolution nature.

6.3 PLGA-rAg microparticles can induce stronger and prolonged immune response *in vitro* compared to antigen solutions

This hypothesis was addressed in chapter four. PLGA-rAg induced much stronger Ag85B specific MHC II immune response than antigen solutions. At the same antigen concentration as in PLGA-rAg formulation, the solution formulation failed to induce any detectable IL-2 secretion. Antigen solution induced response could only be observed at very high antigen concentration. Therefore, encapsulation of antigens into PLGA microparticles dramatically increased the potency of antigens. Second, PLGA-rAg induced prolonged Ag85B specific MHC II immune response than antigen solutions, which may be correlated with the sustained protein release from PLGA microparticles.

6.4 Particle size comparator constructed on the basis of orthogonal partial least square analysis has a better performance than that developed on the basis of chi-square ratio statistics

This hypothesis was addressed in chapter five. The major difference between the two comparators lies in their underlying mechanisms. Comparator developed on the basis of orthogonal partial least square analysis (OPLS) is an analytical tool rather than statistics. Therefore, no statistical inference could be made by using this comparator. Rather, this comparator gives an equivalence value based on OPLS model fitting, which can be used to judge equivalence or batch-to-batch reproducibility. The performance of OPLS method was superior to that of chi-square ratio statistics. However, rigorous validation is required in the future to further develop this comparator.

6.5 General conclusions

The first research goal was to compare the *in vitro* immune response of newly designed

respirable TB subunit vaccines based on Ag85B/TB10.4 and their different combinations in order to make a recommendation of the best antigen/antigen combination for future animal protection study. To make a fair comparison, antigens should be prepared from the same source, either from native antigens, inclusion bodies or soluble recombinants. Since Ag85B is a soluble recombinant protein purified previously in our lab, extensive efforts were first spent to make other antigen or antigen combinations soluble as well. With rational design, TB10.4 and the fusion antigen TB10.4-Ag85B were successfully expressed as soluble proteins and purified in milligram quantities. This achievement made it possible to make appropriate comparisons among Ag85B, TB10.4, Ag85B+TB10.4 and TB0.4-Ag85B. Useful physicochemical information was obtained by characterizing newly designed antigens such as pH-stability and temperature-dependent stability, which offered invaluable information for vaccine formulation development.

PLGA microparticle formulation was selected to manufacture TB subunit vaccine by encapsulating prepared antigens into PLGA polymers for several reasons such as potency, delivery, targeting, and sustained release. PLGA-rAgs were successfully manufactured with a target size of 3 μm by systematic optimization of spray-drying parameters and at the same time a thorough knowledge of particle engineering with spray-drying technique was developed. To ensure prepared PLGA-rAgs have similar physicochemical properties, these microparticles were characterized with respect to particle size and distribution, surface energy, charge and morphology, flow property, thermal behaviors and release profiles. Although different antigens were encapsulated, PLGA-rAgs showed highly reproducible physicochemical properties as mentioned above. This achievement justifies a fair comparison of different antigens or antigen combinations by *in vitro* efficacy evaluation.

The efficacy of PLGA-rAgs was evaluated by *in vitro* antigen presentation assays. It was shown that PLGA microparticle formulation significantly increased the potency of encapsulated antigens and improved the kinetics of antigen presentation. A comparison of antigen blend (Ag85B+TB10.4) and antigen fusion (TB10.4-Ag85B) with respect to Ag85B specific MHC II response suggested that antigen blend should better be chosen for future animal protection study.

The second research goal was to develop a particle size comparator to evaluate the batch-to-batch reproducibility of inhalation products with an ultimate goal to use it as a quality evaluation tool for making highly reproducible TB subunit vaccines suitable for lung delivery and immunization. A particle size comparator was developed with some success by employing orthogonal partial least square analysis (OPLS). A comparison to chi-square ratio statistics suggested that OPLS method has a better performance which deserved further development. A successful particle size comparator is highly desirable which will serve as a quality control tool for particle engineering in the future.

6.6 Future studies

Some questions emerging from the present research need to be addressed in the future.

a) Antigen structure after PLGA encapsulation

The secondary structure of Ag85B, TB10.4 and TB10.4-Ag85B were studied by circular dichroism before PLGA encapsulation. It is not clear whether PLGA encapsulation or spray drying will alter the secondary structure of encapsulated antigens. The SDS-PAGE experiment in chapter three suggested that the formulation process didn't compromise the integrity of encapsulated antigens; however, this experiment didn't provide information on antigen secondary structure. An experiment in the future should address this question. It will

be ideal to study antigen secondary structure in the PLGA microparticles rather than the released form. This is because factors such as pH change, temperature fluctuation and agitation during antigen release will most likely to affect the secondary structure of released antigens. FTIR experiment may be performed with PLGA microparticles as the reference and PLGA-rAg as the test sample. After appropriate subtraction, the secondary structure of encapsulated antigens may be deconvoluted. This structure information can then be compared to that of soluble antigens to make a conclusion.

b) Structure comparison of soluble TB10.4 and TB10.4 purified from inclusion bodies

TB10.4 will be needed in large quantities in the future since antigen blend (Ag85B+TB10.4) was recommended for animal protection studies. Although the solubility and yield of TB10.4 have been improved dramatically by rational design of the expression construct, the purification procedure is still laborious which include three chromatographic steps and one enzymatic treatment. If TB10.4 can be purified from inclusion bodies with verified the same secondary/tertiary structure as of soluble TB10.4, this antigen can be directly purified from inclusion bodies in the future without tedious purification procedure. Therefore, an experiment will be extremely useful to compare the secondary structure of TB10.4 refolded from the inclusion body to that of its soluble counterpart by circular dichroism.

c) Manufacture of PLGA microparticles

In this study, primary emulsion/spray-drying was used to manufacture PLGA microparticles. Antigens and MDP were dissolved in an aqueous phase while PLGA was dissolved in dichloromethane. Both antigens and MDP were not soluble in dichloromethane and, therefore, emulsion was performed to disperse antigen/MDP into PLGA solution. This

emulsion procedure is difficult to scale up, which may result in heterogeneous particle distributions. In the future, PLGA may be dissolved in a water-miscible organic solvent such as acetone so that water soluble antigens and MDP may be simply mixed with acetone dissolved PLGA. Compared to emulsion, this process can be scaled up very easily. However, spray-drying should be performed in a closed system with nitrogen as the drying gas rather than air since acetone is extremely flammable when spray-drying is operated in an open system as we did with dichloromethane.

d) Improvement of release profile

PLGA microparticles manufactured under current protocol resulted in a poor release profile of MDP. This molecule displayed an almost complete burst release during the first half hour. Studies in the future should first verify the necessity to include this molecule in the vaccine formulation. If this molecule is beneficial for the potency of TB subunit vaccine, effort should be spent to improve its release profile. The method mentioned in the last paragraph may improve MDP release since MDP and PLGA are co-dissolved in the water/acetone system.

e) Improve TB10.4 antigen presentation assay

We were not able to evaluate TB10.4 specific MHC I epitope presentation of manufactured TB subunit vaccines due to the lack of assay sensitivity under current experimental conditions in our lab. An existing radioactive assay was considered and in consultation with immunology faculty at University of North Carolina and Dr. Majlessi it was concluded that no better sensitivity could be achieved than with the ELISA. Future collaboration with Dr. Laleh Majlessi may address this problem since this assay was originally developed in her group with sufficient sensitivity.

f) Study of TB10.4 specific MHC II immune response

We were not able to study TB10.4 specific MHC II immune response since there is no TB10.4 specific CD4 T-hybridoma available at the moment. This hybridoma can be developed in the future to evaluate TB10.4 response by *in vitro* antigen presentation assay. Alternatively, TB10.4 specific MHC II immune response can be studied by immunization of animals with PLGA-rAg. T-lymphocytes from vaccinated mice may be isolated from the spleen followed by *in vitro* stimulation of T cells with TB10.4 specific MHC II epitope. After activation, T cells will undergo clonal expansion, which results in an increase of T cell numbers. This increase can be quantified by flowcytometry.

g) Study of Ag85B specific MHC I immune response

We were not able to study Ag85B specific MHC I immune response in this research since Ag85B specific CD8 T-hybridoma was not available to us at the moment. This hybridoma may be developed in the future to evaluate Ag85B response by *in vitro* antigen presentation assay. Alternatively, Ag85B specific MHC I immune response can be studied by immunization of animals with PLGA-rAg. T-lymphocytes from vaccinated mice are isolated from the spleen followed by *in vitro* stimulation of T cells with Ag85B specific MHC I epitope. After activation, T cells will undergo clonal expansion, which results in an increase of T cell numbers. This increase can be quantified by flowcytometry.

h) Optimization of molar ratios of the two antigens

In this study, Ag85B and TB10.4 were used at a molar ratio of 1:1. In the future study, different ratios of two antigens can be investigated.

i) Formulation optimization

In this study, MDP was the only adjuvant used in the subunit vaccine formulation.

Other adjuvants such as IL-2, IL-12, IC31, MPL (monophosphoryl lipid A), DDA (dimethyldioctadecylammonium), TDB (trehalose 6, 6'-dibehenate) could be screened systematically with antigens in order to find the best subunit vaccine formulation.

j) Animal protection experiment

After the formulation is optimized, animal protection experiment could be planned. First, the efficacy of subunit vaccine by itself should be compared to BCG. Multiple doses of subunit vaccine may be needed for effective immunization. Second, the efficacy of subunit vaccine as a BCG booster can be studied in a heterologous prime-boost protocol. To be valuable, TB subunit vaccines should at least offer some protection by itself and provide improved protection once given as a booster to BCG.

k) Further development of particle size comparator

In the present study, a particle size comparator was developed based on orthogonal partial least square analysis. It showed better performance than chi-square ratio statistics. However, the equivalence criterion was not proposed in this study and should be studied in the future. In addition, a larger validation dataset are needed to validate this method.

6.7 Concluding remarks

The current study of TB subunit vaccine with different recombinant antigens, Ag85B, TB10.4, TB10.4-Ag85B (fusion), and Ag85B/TB10.4 (blend), clearly suggests that antigen blend is a better option for multiple-antigen vaccine development. Microparticulate system not only served as a delivery vehicle for aerosol dispersion but also dramatically improved the potency and kinetics of encapsulated antigens. A thorough knowledge of spray-drying technique was developed in this study, which may help the scale-up of vaccine manufacturing in the future. A particle size comparator was developed with some success

and may serve as a quality evaluation tool to ensure batch-to-batch reproducibility of manufactured TB subunit vaccines.

REFERENCES

1. WHO. Tuberculosis. 2009. Available from http://www.who.int/tb/publications/global_report/2009/en/index.html.

2. Deribew A., Tesfay M., Hailemichael Y., Negussu N., Daba S., Woji A., Belachew T., Apers L., Robert C. Tuberculosis and HIV co-infection: its impact on quality of life. Health Qual Life Outcomes. 7:105 (2009).

3. Espinal M.A., Laszlo A., Simonsen L., Boulahbal F., Kim S.J., Reniero A., Hoffner S., Rieder H.L., Binkin N., Dye C., Williams R., Raviglione M.C. Global trends in resistance to antituberculosis drugs. World Health Organization-International Union against Tuberculosis and Lung Disease Working Group on Anti-Tuberculosis Drug Resistance Surveillance. N Engl J Med. 344:1294-303 (2001).

4. Baghaei P., Tabarsi P., Dorriz D., Marjani M., Shamaei M., Pooramiri M.V., Mansouri D., Farnia P., Masjedi M., Velayati A. Adverse Effects of Multidrug-Resistant Tuberculosis Treatment With a Standardized Regimen: A Report From Iran. Am J Ther. (2009).

5. Riccardi G., Pasca M.R., Buroni S. Mycobacterium tuberculosis: drug resistance and future perspectives. Future Microbiol. 4:597-614 (2009).

6. Pillay M., Sturm A.W. Evolution of the extensively drug-resistant F15/LAM4/KZN strain of Mycobacterium tuberculosis in KwaZulu-Natal, South Africa. Clin Infect Dis. 45:1409-14 (2007).

7. Ioerger T.R., Koo S., No E.G., Chen X., Larsen M.H., Jacobs W.R., Jr., Pillay M., Sturm A.W., Sacchettini J.C. Genome analysis of multi- and extensively-drug-resistant tuberculosis from KwaZulu-Natal, South Africa. PLoS One. 4:e7778 (2009).

8. Ramaswamy S., Musser J.M. Molecular genetic basis of antimicrobial agent resistance in Mycobacterium tuberculosis: 1998 update. Tuber Lung Dis. 79:3-29 (1998).

9. Chan E.D., Iseman M.D. Multidrug-resistant and extensively drug-resistant tuberculosis: a review. Curr Opin Infect Dis. 21:587-95 (2008).

10. Verma I., Grover A. Antituberculous vaccine development: a perspective for the endemic world. Expert Rev Vaccines. 8:1547-53 (2009).

11. Sterne J.A., Rodrigues L.C., Guedes I.N. Does the efficacy of BCG decline with time since vaccination? Int. J. Tuberc. Lung Dis. 2:200-207 (1998).

12. Rodrigues L.C., Pereira S.M., Cunha S.S., Genser B., Ichihara M.Y., de Brito S.C., Hijjar M.A., Dourado I., Cruz A.A., Sant'Anna C., Bierrenbach A.L., Barreto M.L.

Effect of BCG revaccination on incidence of tuberculosis in school-aged children in Brazil: the BCG-REVAC cluster-randomised trial. Lancet. 366:1290-5 (2005).

13. Horwitz M.A., Harth G. A new vaccine against tuberculosis affords greater survival after challenge than the current vaccine in the guinea pig model of pulmonary tuberculosis. Infect Immun. 71:1672-9 (2003).

14. Horwitz M.A., Harth G., Dillon B.J., Maslesa-Galic S. Recombinant bacillus calmette-guerin (BCG) vaccines expressing the Mycobacterium tuberculosis 30-kDa major secretory protein induce greater protective immunity against tuberculosis than conventional BCG vaccines in a highly susceptible animal model. Proc Natl Acad Sci U S A. 97:13853-8 (2000).

15. Perez E., Samper S., Bordas Y., Guilhot C., Gicquel B., Martin C. An essential role for phoP in Mycobacterium tuberculosis virulence. Mol Microbiol. 41:179-87 (2001).

16. Soto C.Y., Menendez M.C., Perez E., Samper S., Gomez A.B., Garcia M.J., Martin C. IS6110 mediates increased transcription of the phoP virulence gene in a multidrug-resistant clinical isolate responsible for tuberculosis outbreaks. J Clin Microbiol. 42:212-9 (2004).

17. Lowrie D.B., Silva C.L., Tascon R.E. Progress towards a new tuberculosis vaccine. BioDrugs. 10:201-13 (1998).

18. Havenga M., Vogels R., Zuijdgeest D., Radosevic K., Mueller S., Sieuwerts M., Weichold F., Damen I., Kaspers J., Lemckert A., van Meerendonk M., van der Vlugt R., Holterman L., Hone D., Skeiky Y., Mintardjo R., Gillissen G., Barouch D., Sadoff J., Goudsmit J. Novel replication-incompetent adenoviral B-group vectors: high vector stability and yield in PER.C6 cells. J Gen Virol. 87:2135-43 (2006).

19. Dietrich J., Aagaard C., Leah R., Olsen A.W., Stryhn A., Doherty T.M., Andersen P. Exchanging ESAT6 with TB10.4 in an Ag85B fusion molecule-based tuberculosis subunit vaccine: efficient protection and ESAT6-based sensitive monitoring of vaccine efficacy. J Immunol. 174:6332-9 (2005).

20. Grosset J.H. Bacteriology of tuberculosis. In: Reichman L., Hershfield E.S. (eds.), Tuberculosis: A comprehensive international approach, Marcel Dekker, Inc, New York, 1993, p. 49-74.

21. Ryan K.J., Ray C.G., (eds). Sherris Medical Microbiology. 4th ed., McGraw Hill, 2004.

22. Murray P.R., Rosenthal K.S., Pfaller M.A. Medical Microbiology. Elsevier Mosby, 2005.

23. Kaur D., Guerin M.E., Skovierova H., Brennan P.J., Jackson M. Chapter 2:

Biogenesis of the cell wall and other glycoconjugates of Mycobacterium tuberculosis. Adv Appl Microbiol. 69:23-78 (2009).

24. Besra G.S., Chatterjee D. Lipids and carbohydrates of Mycobacterium tuberculosis. In: Bloom B. (eds.), Tuberculosis: Pathogenesis, Protection and Control, ASM Press, Washington, DC, 1994, p. 285-306.

25. WHO. Tuberculosis. 2007. Available from: http://www.who.int/mediacentre/factsheets/fs104/en/index.html.

26. Smith P.G., Moss A.R. In: Bloom B. (eds.), Tuberculosis: Pathogenesis, Protection and Control, ASM Press, Washington DC, 1994, p. 47-59.

27. Dannenberg A.M.J., Rook G.A.W. Pathogenesis of pulmonary tuberculosis: an interplay of tissue-damaging and macrophage-activating immune responses-Dual mechanisms that control bacillary multiplication. In: Bloom B. (eds.), Tuberculosis: Pathogenesis, Protection and Control, ASM Press, Washington DC, 1994, p. 459-483.

28. Flynn J.L., Chan J. Immunology of tuberculosis. Annu Rev Immunol. 19:93-129 (2001).

29. Kang P.B., Azad A.K., Torrelles J.B., Kaufman T.M., Beharka A., Tibesar E., DesJardin L.E., Schlesinger L.S. The human macrophage mannose receptor directs Mycobacterium tuberculosis lipoarabinomannan-mediated phagosome biogenesis. J Exp Med. 202:987-99 (2005).

30. Schlesinger L.S. Macrophage phagocytosis of virulent but not attenuated strains of Mycobacterium tuberculosis is mediated by mannose receptors in addition to complement receptors. J Immunol. 150:2920-30 (1993).

31. Heldwein K.A., Fenton M.J. The role of Toll-like receptors in immunity against mycobacterial infection. Microbes Infect. 4:937-44 (2002).

32. Drennan M.B., Nicolle D., Quesniaux V.J., Jacobs M., Allie N., Mpagi J., Fremond C., Wagner H., Kirschning C., Ryffel B. Toll-like receptor 2-deficient mice succumb to Mycobacterium tuberculosis infection. Am J Pathol. 164:49-57 (2004).

33. Means T.K., Wang S., Lien E., Yoshimura A., Golenbock D.T., Fenton M.J. Human toll-like receptors mediate cellular activation by Mycobacterium tuberculosis. J Immunol. 163:3920-7 (1999).

34. Underhill D.M., Ozinsky A., Hajjar A.M., Stevens A., Wilson C.B., Bassetti M., Aderem A. The Toll-like receptor 2 is recruited to macrophage phagosomes and discriminates between pathogens. Nature. 401:811-5 (1999).

35. Underhill D.M., Ozinsky A., Smith K.D., Aderem A. Toll-like receptor-2 mediates

mycobacteria-induced proinflammatory signaling in macrophages. Proc Natl Acad Sci U S A. 96:14459-63 (1999).

36. Brightbill H.D., Libraty D.H., Krutzik S.R., Yang R.B., Belisle J.T., Bleharski J.R., Maitland M., Norgard M.V., Plevy S.E., Smale S.T., Brennan P.J., Bloom B.R., Godowski P.J., Modlin R.L. Host defense mechanisms triggered by microbial lipoproteins through toll-like receptors. Science. 285:732-6 (1999).

37. Thoma-Uszynski S., Stenger S., Takeuchi O., Ochoa M.T., Engele M., Sieling P.A., Barnes P.F., Rollinghoff M., Bolcskei P.L., Wagner M., Akira S., Norgard M.V., Belisle J.T., Godowski P.J., Bloom B.R., Modlin R.L. Induction of direct antimicrobial activity through mammalian toll-like receptors. Science. 291:1544-7 (2001).

38. Liu P.T., Stenger S., Li H., Wenzel L., Tan B.H., Krutzik S.R., Ochoa M.T., Schauber J., Wu K., Meinken C., Kamen D.L., Wagner M., Bals R., Steinmeyer A., Zugel U., Gallo R.L., Eisenberg D., Hewison M., Hollis B.W., Adams J.S., Bloom B.R., Modlin R.L. Toll-like receptor triggering of a vitamin D-mediated human antimicrobial response. Science. 311:1770-3 (2006).

39. Meylan E., Tschopp J., Karin M. Intracellular pattern recognition receptors in the host response. Nature. 442:39-44 (2006).

40. Chamaillard M., Girardin S.E., Viala J., Philpott D.J. Nods, Nalps and Naip: intracellular regulators of bacterial-induced inflammation. Cell Microbiol. 5:581-92 (2003).

41. Girardin S.E., Boneca I.G., Viala J., Chamaillard M., Labigne A., Thomas G., Philpott D.J., Sansonetti P.J. Nod2 is a general sensor of peptidoglycan through muramyl dipeptide (MDP) detection. J Biol Chem. 278:8869-72 (2003).

42. Kobayashi K.S., Chamaillard M., Ogura Y., Henegariu O., Inohara N., Nunez G., Flavell R.A. Nod2-dependent regulation of innate and adaptive immunity in the intestinal tract. Science. 307:731-4 (2005).

43. Ferwerda G., Girardin S.E., Kullberg B.J., Le Bourhis L., de Jong D.J., Langenberg D.M., van Crevel R., Adema G.J., Ottenhoff T.H., Van der Meer J.W., Netea M.G. NOD2 and toll-like receptors are nonredundant recognition systems of Mycobacterium tuberculosis. PLoS Pathog. 1:279-85 (2005).

44. Chan J., Xing Y., Magliozzo R.S., Bloom B.R. Killing of virulent Mycobacterium tuberculosis by reactive nitrogen intermediates produced by activated murine macrophages. J Exp Med. 175:1111-22 (1992).

45. MacMicking J.D., North R.J., LaCourse R., Mudgett J.S., Shah S.K., Nathan C.F. Identification of nitric oxide synthase as a protective locus against tuberculosis. Proc

Natl Acad Sci U S A. 94:5243-8 (1997).

46. Chan J., Tanaka K., Carroll D., Flynn J., Bloom B.R. Effects of nitric oxide synthase inhibitors on murine infection with Mycobacterium tuberculosis. Infect Immun. 63:736-40 (1995).

47. Rockett K.A., Brookes R., Udalova I., Vidal V., Hill A.V., Kwiatkowski D. 1,25-Dihydroxyvitamin D3 induces nitric oxide synthase and suppresses growth of Mycobacterium tuberculosis in a human macrophage-like cell line. Infect Immun. 66:5314-21 (1998).

48. Gutierrez M.G., Master S.S., Singh S.B., Taylor G.A., Colombo M.I., Deretic V. Autophagy is a defense mechanism inhibiting BCG and Mycobacterium tuberculosis survival in infected macrophages. Cell. 119:753-66 (2004).

49. Alonso S., Pethe K., Russell D.G., Purdy G.E. Lysosomal killing of Mycobacterium mediated by ubiquitin-derived peptides is enhanced by autophagy. Proc Natl Acad Sci U S A. 104:6031-6 (2007).

50. Rook G.A., Steele J., Fraher L., Barker S., Karmali R., O'Riordan J., Stanford J. Vitamin D3, gamma interferon, and control of proliferation of Mycobacterium tuberculosis by human monocytes. Immunology. 57:159-63 (1986).

51. Crowle A.J., Ross E.J., May M.H. Inhibition by 1,25(OH)2-vitamin D3 of the multiplication of virulent tubercle bacilli in cultured human macrophages. Infect Immun. 55:2945-50 (1987).

52. Sly L.M., Lopez M., Nauseef W.M., Reiner N.E. 1alpha,25-Dihydroxyvitamin D3-induced monocyte antimycobacterial activity is regulated by phosphatidylinositol 3-kinase and mediated by the NADPH-dependent phagocyte oxidase. J Biol Chem. 276:35482-93 (2001).

53. Ly L.H., McMurray D.N. The Yin-Yang of TNFalpha in the guinea pig model of tuberculosis. Indian J Exp Biol. 47:432-9 (2009).

54. Ding A.H., Nathan C.F., Stuehr D.J. Release of reactive nitrogen intermediates and reactive oxygen intermediates from mouse peritoneal macrophages. Comparison of activating cytokines and evidence for independent production. J Immunol. 141:2407-12 (1988).

55. Flesch I.E., Hess J.H., Oswald I.P., Kaufmann S.H. Growth inhibition of Mycobacterium bovis by IFN-gamma stimulated macrophages: regulation by endogenous tumor necrosis factor-alpha and by IL-10. Int Immunol. 6:693-700 (1994).

56. Bean A.G., Roach D.R., Briscoe H., France M.P., Korner H., Sedgwick J.D., Britton

W.J. Structural deficiencies in granuloma formation in TNF gene-targeted mice underlie the heightened susceptibility to aerosol Mycobacterium tuberculosis infection, which is not compensated for by lymphotoxin. J Immunol. 162:3504-11 (1999).

57. Flynn J.L., Goldstein M.M., Chan J., Triebold K.J., Pfeffer K., Lowenstein C.J., Schreiber R., Mak T.W., Bloom B.R. Tumor necrosis factor-alpha is required in the protective immune response against Mycobacterium tuberculosis in mice. Immunity. 2:561-72 (1995).

58. Keane J., Gershon S., Wise R.P., Mirabile-Levens E., Kasznica J., Schwieterman W.D., Siegel J.N., Braun M.M. Tuberculosis associated with infliximab, a tumor necrosis factor alpha-neutralizing agent. N Engl J Med. 345:1098-104 (2001).

59. Feng C.G., Kaviratne M., Rothfuchs A.G., Cheever A., Hieny S., Young H.A., Wynn T.A., Sher A. NK cell-derived IFN-gamma differentially regulates innate resistance and neutrophil response in T cell-deficient hosts infected with Mycobacterium tuberculosis. J Immunol. 177:7086-93 (2006).

60. Cooper A.M., Dalton D.K., Stewart T.A., Griffin J.P., Russell D.G., Orme I.M. Disseminated tuberculosis in interferon gamma gene-disrupted mice. J Exp Med. 178:2243-7 (1993).

61. Flynn J.L., Chan J., Triebold K.J., Dalton D.K., Stewart T.A., Bloom B.R. An essential role for interferon gamma in resistance to Mycobacterium tuberculosis infection. J Exp Med. 178:2249-54 (1993).

62. Fraser D.A., Bulat-Kardum L., Knezevic J., Babarovic P., Matakovic-Mileusnic N., Dellacasagrande J., Matanic D., Pavelic J., Beg-Zec Z., Dembic Z. Interferon-gamma receptor-1 gene polymorphism in tuberculosis patients from Croatia. Scand J Immunol. 57:480-4 (2003).

63. Cooke G.S., Campbell S.J., Sillah J., Gustafson P., Bah B., Sirugo G., Bennett S., McAdam K.P., Sow O., Lienhardt C., Hill A.V. Polymorphism within the interferon-gamma/receptor complex is associated with pulmonary tuberculosis. Am J Respir Crit Care Med. 174:339-43 (2006).

64. Lio D., Marino V., Serauto A., Gioia V., Scola L., Crivello A., Forte G.I., Colonna-Romano G., Candore G., Caruso C. Genotype frequencies of the +874T-->A single nucleotide polymorphism in the first intron of the interferon-gamma gene in a sample of Sicilian patients affected by tuberculosis. Eur J Immunogenet. 29:371-4 (2002).

65. Vidyarani M., Selvaraj P., Prabhu Anand S., Jawahar M.S., Adhilakshmi A.R., Narayanan P.R. Interferon gamma (IFNgamma) & interleukin-4 (IL-4) gene variants & cytokine levels in pulmonary tuberculosis. Indian J Med Res. 124:403-10 (2006).

66. Jiao X., Lo-Man R., Guermonprez P., Fiette L., Deriaud E., Burgaud S., Gicquel B., Winter N., Leclerc C. Dendritic cells are host cells for mycobacteria in vivo that trigger innate and acquired immunity. J Immunol. 168:1294-301 (2002).

67. Tian T., Woodworth J., Skold M., Behar S.M. In vivo depletion of CD11c+ cells delays the CD4+ T cell response to Mycobacterium tuberculosis and exacerbates the outcome of infection. J Immunol. 175:3268-72 (2005).

68. Tsuji S., Matsumoto M., Takeuchi O., Akira S., Azuma I., Hayashi A., Toyoshima K., Seya T. Maturation of human dendritic cells by cell wall skeleton of Mycobacterium bovis bacillus Calmette-Guerin: involvement of toll-like receptors. Infect Immun. 68:6883-90 (2000).

69. Prigozy T.I., Sieling P.A., Clemens D., Stewart P.L., Behar S.M., Porcelli S.A., Brenner M.B., Modlin R.L., Kronenberg M. The mannose receptor delivers lipoglycan antigens to endosomes for presentation to T cells by CD1b molecules. Immunity. 6:187-97 (1997).

70. Nigou J., Zelle-Rieser C., Gilleron M., Thurnher M., Puzo G. Mannosylated lipoarabinomannans inhibit IL-12 production by human dendritic cells: evidence for a negative signal delivered through the mannose receptor. J Immunol. 166:7477-85 (2001).

71. Tailleux L., Gicquel B., Neyrolles O. [DC-SIGN, a key receptor of Mycobacterium tuberculosis?]. Med Sci (Paris). 19:658-60 (2003).

72. Tailleux L., Schwartz O., Herrmann J.L., Pivert E., Jackson M., Amara A., Legres L., Dreher D., Nicod L.P., Gluckman J.C., Lagrange P.H., Gicquel B., Neyrolles O. DC-SIGN is the major Mycobacterium tuberculosis receptor on human dendritic cells. J Exp Med. 197:121-7 (2003).

73. van Kooyk Y., Geijtenbeek T.B. DC-SIGN: escape mechanism for pathogens. Nat Rev Immunol. 3:697-709 (2003).

74. Divangahi M., Chen M., Gan H., Desjardins D., Hickman T.T., Lee D.M., Fortune S., Behar S.M., Remold H.G. Mycobacterium tuberculosis evades macrophage defenses by inhibiting plasma membrane repair. Nat Immunol. 10:899-906 (2009).

75. Fenton M.J. Macrophages and tuberculosis. Curr Opin Hematol. 5:72-8 (1998).

76. Kaufmann S.H. How can immunology contribute to the control of tuberculosis? Nat Rev Immunol. 1:20-30 (2001).

77. Rescigno M., Martino M., Sutherland C.L., Gold M.R., Ricciardi-Castagnoli P. Dendritic cell survival and maturation are regulated by different signaling pathways. J Exp Med. 188:2175-80 (1998).

78. Hickman S.P., Chan J., Salgame P. Mycobacterium tuberculosis induces differential cytokine production from dendritic cells and macrophages with divergent effects on naive T cell polarization. J Immunol. 168:4636-42 (2002).

79. Giacomini E., Iona E., Ferroni L., Miettinen M., Fattorini L., Orefici G., Julkunen I., Coccia E.M. Infection of human macrophages and dendritic cells with Mycobacterium tuberculosis induces a differential cytokine gene expression that modulates T cell response. J Immunol. 166:7033-41 (2001).

80. Henderson R.A., Watkins S.C., Flynn J.L. Activation of human dendritic cells following infection with Mycobacterium tuberculosis. J Immunol. 159:635-43 (1997).

81. Kim K.D., Lee H.G., Kim J.K., Park S.N., Choe I.S., Choe Y.K., Kim S.J., Lee E., Lim J.S. Enhanced antigen-presenting activity and tumour necrosis factor-alpha-independent activation of dendritic cells following treatment with Mycobacterium bovis bacillus Calmette-Guerin. Immunology. 97:626-33 (1999).

82. Banchereau J., Steinman R.M. Dendritic cells and the control of immunity. Nature. 392:245-52 (1998).

83. Ehlers S. Lazy, dynamic or minimally recrudescent? On the elusive nature and location of the mycobacterium responsible for latent tuberculosis. Infection. 37:87-95 (2009).

84. Lazarevic V., Flynn J. CD8+ T cells in tuberculosis. Am J Respir Crit Care Med. 166:1116-21 (2002).

85. Flynn J.L., Goldstein M.M., Triebold K.J., Koller B., Bloom B.R. Major histocompatibility complex class I-restricted T cells are required for resistance to Mycobacterium tuberculosis infection. Proc Natl Acad Sci U S A. 89:12013-7 (1992).

86. Mogues T., Goodrich M.E., Ryan L., LaCourse R., North R.J. The relative importance of T cell subsets in immunity and immunopathology of airborne Mycobacterium tuberculosis infection in mice. J Exp Med. 193:271-80 (2001).

87. Stenger S., Mazzaccaro R.J., Uyemura K., Cho S., Barnes P.F., Rosat J.P., Sette A., Brenner M.B., Porcelli S.A., Bloom B.R., Modlin R.L. Differential effects of cytolytic T cell subsets on intracellular infection. Science. 276:1684-7 (1997).

88. Stenger S., Hanson D.A., Teitelbaum R., Dewan P., Niazi K.R., Froelich C.J., Ganz T., Thoma-Uszynski S., Melian A., Bogdan C., Porcelli S.A., Bloom B.R., Krensky A.M., Modlin R.L. An antimicrobial activity of cytolytic T cells mediated by granulysin. Science. 282:121-5 (1998).

89. Fine P.E., Rodrigues L.C. Modern vaccines. Mycobacterial diseases. Lancet. 335:1016-20 (1990).

90. Rodrigues L.C., Diwan V.K., Wheeler J.G. Protective effect of BCG against tuberculous meningitis and miliary tuberculosis: a meta-analysis. Int J Epidemiol. 22:1154-8 (1993).

91. Behr M.A. BCG--different strains, different vaccines? Lancet Infect Dis. 2:86-92 (2002).

92. Behr M.A., Small P.M. Has BCG attenuated to impotence? Nature. 389:133-4 (1997).

93. Fine P.E. Variation in protection by BCG: implications of and for heterologous immunity. Lancet. 346:1339-45 (1995).

94. Mahairas G.G., Sabo P.J., Hickey M.J., Singh D.C., Stover C.K. Molecular analysis of genetic differences between Mycobacterium bovis BCG and virulent M. bovis. J Bacteriol. 178:1274-82 (1996).

95. Hess J., Kaufmann S.H. Live antigen carriers as tools for improved anti-tuberculosis vaccines. FEMS Immunol Med Microbiol. 23:165-73 (1999).

96. Brewer T.F., Colditz G.A. Relationship between bacille Calmette-Guerin (BCG) strains and the efficacy of BCG vaccine in the prevention of tuberculosis. Clin Infect Dis. 20:126-35 (1995).

97. Brosch R., Gordon S.V., Pym A., Eiglmeier K., Garnier T., Cole S.T. Comparative genomics of the mycobacteria. Int J Med Microbiol. 290:143-52 (2000).

98. Horwitz M.A. Recombinant BCG expressing Mycobacterium tuberculosis major extracellular proteins. Microbes Infect. 7:947-54 (2005).

99. Horwitz M.A., Harth G., Dillon B.J., Maslesa-Galic S. A novel live recombinant mycobacterial vaccine against bovine tuberculosis more potent than BCG. Vaccine. 24:1593-600 (2006).

100. Portnoy D.A., Tweten R.K., Kehoe M., Bielecki J. Capacity of listeriolysin O, streptolysin O, and perfringolysin O to mediate growth of Bacillus subtilis within mammalian cells. Infect Immun. 60:2710-7 (1992).

101. Mazzaccaro R.J., Gedde M., Jensen E.R., van Santen H.M., Ploegh H.L., Rock K.L., Bloom B.R. Major histocompatibility class I presentation of soluble antigen facilitated by Mycobacterium tuberculosis infection. Proc Natl Acad Sci U S A. 93:11786-91 (1996).

102. Hess J., Miko D., Catic A., Lehmensiek V., Russell D.G., Kaufmann S.H. Mycobacterium bovis Bacille Calmette-Guerin strains secreting listeriolysin of Listeria monocytogenes. Proc Natl Acad Sci U S A. 95:5299-304 (1998).

103. Camacho L.R., Ensergueix D., Perez E., Gicquel B., Guilhot C. Identification of a virulence gene cluster of Mycobacterium tuberculosis by signature-tagged transposon mutagenesis. Mol Microbiol. 34:257-67 (1999).

104. Ranganathan U.D., Larsen M.H., Kim J., Porcelli S.A., Jacobs W.R., Jr., Fennelly G.J. Recombinant pro-apoptotic Mycobacterium tuberculosis generates CD8+ T cell responses against human immunodeficiency virus type 1 Env and M. tuberculosis in neonatal mice. Vaccine. 28:152-61 (2009).

105. Sheridan J.P., Marsters S.A., Pitti R.M., Gurney A., Skubatch M., Baldwin D., Ramakrishnan L., Gray C.L., Baker K., Wood W.I., Goddard A.D., Godowski P., Ashkenazi A. Control of TRAIL-induced apoptosis by a family of signaling and decoy receptors. Science. 277:818-21 (1997).

106. Chattergoon M.A., Kim J.J., Yang J.S., Robinson T.M., Lee D.J., Dentchev T., Wilson D.M., Ayyavoo V., Weiner D.B. Targeted antigen delivery to antigen-presenting cells including dendritic cells by engineered Fas-mediated apoptosis. Nat Biotechnol. 18:974-9 (2000).

107. Behr M.A., Wilson M.A., Gill W.P., Salamon H., Schoolnik G.K., Rane S., Small P.M. Comparative genomics of BCG vaccines by whole-genome DNA microarray. Science. 284:1520-3 (1999).

108. Gordon S.V., Brosch R., Billault A., Garnier T., Eiglmeier K., Cole S.T. Identification of variable regions in the genomes of tubercle bacilli using bacterial artificial chromosome arrays. Mol Microbiol. 32:643-55 (1999).

109. Salamon H., Kato-Maeda M., Small P.M., Drenkow J., Gingeras T.R. Detection of deleted genomic DNA using a semiautomated computational analysis of GeneChip data. Genome Res. 10:2044-54 (2000).

110. Skeiky Y.A., Sadoff J.C. Advances in tuberculosis vaccine strategies. Nat Rev Microbiol. 4:469-76 (2006).

111. Sambandamurthy V.K., Jacobs W.R., Jr. Live attenuated mutants of Mycobacterium tuberculosis as candidate vaccines against tuberculosis. Microbes Infect. 7:955-61 (2005).

112. Sambandamurthy V.K., Derrick S.C., Jalapathy K.V., Chen B., Russell R.G., Morris S.L., Jacobs W.R., Jr. Long-term protection against tuberculosis following vaccination with a severely attenuated double lysine and pantothenate auxotroph of Mycobacterium tuberculosis. Infect Immun. 73:1196-203 (2005).

113. Hernandez-Pando R., Pavon L., Arriaga K., Orozco H., Madrid-Marina V., Rook G. Pathogenesis of tuberculosis in mice exposed to low and high doses of an environmental mycobacterial saprophyte before infection. Infect Immun. 65:3317-27

(1997).

114. Agger E.M., Andersen P. A novel TB vaccine; towards a strategy based on our understanding of BCG failure. Vaccine. 21:7-14 (2002).

115. Wang J., Thorson L., Stokes R.W., Santosuosso M., Huygen K., Zganiacz A., Hitt M., Xing Z. Single mucosal, but not parenteral, immunization with recombinant adenoviral-based vaccine provides potent protection from pulmonary tuberculosis. J Immunol. 173:6357-65 (2004).

116. Holterman L., Vogels R., van der Vlugt R., Sieuwerts M., Grimbergen J., Kaspers J., Geelen E., van der Helm E., Lemckert A., Gillissen G., Verhaagh S., Custers J., Zuijdgeest D., Berkhout B., Bakker M., Quax P., Goudsmit J., Havenga M. Novel replication-incompetent vector derived from adenovirus type 11 (Ad11) for vaccination and gene therapy: low seroprevalence and non-cross-reactivity with Ad5. J Virol. 78:13207-15 (2004).

117. Mollenkopf H.J., Grode L., Mattow J., Stein M., Mann P., Knapp B., Ulmer J., Kaufmann S.H. Application of mycobacterial proteomics to vaccine design: improved protection by Mycobacterium bovis BCG prime-Rv3407 DNA boost vaccination against tuberculosis. Infect Immun. 72:6471-9 (2004).

118. Andersen A.B., Hansen E.B. Structure and mapping of antigenic domains of protein antigen b, a 38,000-molecular-weight protein of Mycobacterium tuberculosis. Infect Immun. 57:2481-8 (1989).

119. Nagai S., Wiker H.G., Harboe M., Kinomoto M. Isolation and partial characterization of major protein antigens in the culture fluid of Mycobacterium tuberculosis. Infect Immun. 59:372-82 (1991).

120. Young D.B., Garbe T.R. Lipoprotein antigens of Mycobacterium tuberculosis. Res Microbiol. 142:55-65 (1991).

121. Andersen P., Andersen A.B., Sorensen A.L., Nagai S. Recall of long-lived immunity to Mycobacterium tuberculosis infection in mice. J Immunol. 154:3359-72 (1995).

122. Skjot R.L., Oettinger T., Rosenkrands I., Ravn P., Brock I., Jacobsen S., Andersen P. Comparative evaluation of low-molecular-mass proteins from Mycobacterium tuberculosis identifies members of the ESAT-6 family as immunodominant T-cell antigens. Infect Immun. 68:214-20 (2000).

123. Skeiky Y.A., Lodes M.J., Guderian J.A., Mohamath R., Bement T., Alderson M.R., Reed S.G. Cloning, expression, and immunological evaluation of two putative secreted serine protease antigens of Mycobacterium tuberculosis. Infect Immun. 67:3998-4007 (1999).

124. Dillon D.C., Alderson M.R., Day C.H., Lewinsohn D.M., Coler R., Bement T., Campos-Neto A., Skeiky Y.A., Orme I.M., Roberts A., Steen S., Dalemans W., Badaro R., Reed S.G. Molecular characterization and human T-cell responses to a member of a novel Mycobacterium tuberculosis mtb39 gene family. Infect Immun. 67:2941-50 (1999).

125. Lu D., Garcia-Contreras L., Xu D., Kurtz S.L., Liu J., Braunstein M., McMurray D.N., Hickey A.J. Poly (lactide-co-glycolide) microspheres in respirable sizes enhance an in vitro T cell response to recombinant Mycobacterium tuberculosis antigen 85B. Pharm Res. 24:1834-43 (2007).

126. Skeiky Y.A., Alderson M.R., Ovendale P.J., Guderian J.A., Brandt L., Dillon D.C., Campos-Neto A., Lobet Y., Dalemans W., Orme I.M., Reed S.G. Differential immune responses and protective efficacy induced by components of a tuberculosis polyprotein vaccine, Mtb72F, delivered as naked DNA or recombinant protein. J Immunol. 172:7618-28 (2004).

127. Weinrich Olsen A., van Pinxteren L.A., Meng Okkels L., Birk Rasmussen P., Andersen P. Protection of mice with a tuberculosis subunit vaccine based on a fusion protein of antigen 85b and esat-6. Infect Immun. 69:2773-8 (2001).

128. Brandt L., Skeiky Y.A., Alderson M.R., Lobet Y., Dalemans W., Turner O.C., Basaraba R.J., Izzo A.A., Lasco T.M., Chapman P.L., Reed S.G., Orme I.M. The protective effect of the Mycobacterium bovis BCG vaccine is increased by coadministration with the Mycobacterium tuberculosis 72-kilodalton fusion polyprotein Mtb72F in M. tuberculosis-infected guinea pigs. Infect Immun. 72:6622-32 (2004).

129. Olsen A.W., Williams A., Okkels L.M., Hatch G., Andersen P. Protective effect of a tuberculosis subunit vaccine based on a fusion of antigen 85B and ESAT-6 in the aerosol guinea pig model. Infect Immun. 72:6148-50 (2004).

130. Olsen A.W., Hansen P.R., Holm A., Andersen P. Efficient protection against Mycobacterium tuberculosis by vaccination with a single subdominant epitope from the ESAT-6 antigen. Eur J Immunol. 30:1724-32 (2000).

131. Belisle J.T., Vissa V.D., Sievert T., Takayama K., Brennan P.J., Besra G.S. Role of the major antigen of Mycobacterium tuberculosis in cell wall biogenesis. Science. 276:1420-2 (1997).

132. Anderson D.H., Harth G., Horwitz M.A., Eisenberg D. An interfacial mechanism and a class of inhibitors inferred from two crystal structures of the Mycobacterium tuberculosis 30 kDa major secretory protein (Antigen 85B), a mycolyl transferase. J Mol Biol. 307:671-81 (2001).

133. Ronning D.R., Vissa V., Besra G.S., Belisle J.T., Sacchettini J.C. Mycobacterium

tuberculosis antigen 85A and 85C structures confirm binding orientation and conserved substrate specificity. J Biol Chem. 279:36771-7 (2004).

134. Ronning D.R., Klabunde T., Besra G.S., Vissa V.D., Belisle J.T., Sacchettini J.C. Crystal structure of the secreted form of antigen 85C reveals potential targets for mycobacterial drugs and vaccines. Nat Struct Biol. 7:141-6 (2000).

135. Jackson M., Raynaud C., Laneelle M.A., Guilhot C., Laurent-Winter C., Ensergueix D., Gicquel B., Daffe M. Inactivation of the antigen 85C gene profoundly affects the mycolate content and alters the permeability of the Mycobacterium tuberculosis cell envelope. Mol Microbiol. 31:1573-87 (1999).

136. Majlessi L., Rojas M.J., Brodin P., Leclerc C. CD8+-T-cell responses of Mycobacterium-infected mice to a newly identified major histocompatibility complex class I-restricted epitope shared by proteins of the ESAT-6 family. Infect Immun. 71:7173-7 (2003).

137. Billeskov R., Vingsbo-Lundberg C., Andersen P., Dietrich J. Induction of CD8 T cells against a novel epitope in TB10.4: correlation with mycobacterial virulence and the presence of a functional region of difference-1. J Immunol. 179:3973-81 (2007).

138. Lu D., Hickey A.J. Pulmonary vaccine delivery. Expert Rev Vaccines. 6:213-26 (2007).

139. Sullivan V.J., Mikszta J.A., Laurent P., Huang J., Ford B. Noninvasive delivery technologies: respiratory delivery of vaccines. Expert Opin Drug Deliv. 3:87-95 (2006).

140. Holmgren J., Czerkinsky C. Mucosal immunity and vaccines. Nat Med. 11:S45-53 (2005).

141. Pulliam B., Sung J.C., Edwards D.A. Design of nanoparticle-based dry powder pulmonary vaccines. Expert Opin Drug Deliv. 4:651-63 (2007).

142. LiCalsi C., Christensen T., Bennett J.V., Phillips E., Witham C. Dry powder inhalation as a potential delivery method for vaccines. Vaccine. 17:1796-803 (1999).

143. Mestecky J., ed. Mucosal Immunology. Academic Press, San Diego, 2005.

144. Kunkel E.J., Butcher E.C. Plasma-cell homing. Nat Rev Immunol. 3:822-9 (2003).

145. Garcia-Contreras L., Wong Y.L., Muttil P., Padilla D., Sadoff J., Derousse J., Germishuizen W.A., Goonesekera S., Elbert K., Bloom B.R., Miller R., Fourie P.B., Hickey A., Edwards D. Immunization by a bacterial aerosol. Proc Natl Acad Sci U S A. 105:4656-60 (2008).

146. Aleksandrov N.I., Gefen N.E. Physiological methods of immunization and possibilities of their improvement. Voen Med Zh. 8:82-7 (1958).

147. Aleksandrov N.I., Gefen N.E., Garin N.S., Gapochko K.G., Sergev V.M., Smirnov M.S., Tamarin A.L., Shliakhov E.N. Experience in massive aerogenic vaccination against anthrax. Voen Med Zh. 8:27-32 (1959).

148. Rosenthal S.R., McEnery J.T., Raisys N. Aerogenic BCG vaccination against tuberculosis in animal and human subjects. J Asthma Res. 5:309-23 (1968).

149. Hornick R.B., Eigelsbach H.T. Aerogenic immunization of man with live Tularemia vaccine. Bacteriol Rev. 30:532-8 (1966).

150. Cutts F.T., Clements C.J., Bennett J.V. Alternative routes of measles immunization: a review. Biologicals. 25:323-38 (1997).

151. Bennett J.V., Fernandez de Castro J., Valdespino-Gomez J.L., Garcia-Garcia Mde L., Islas-Romero R., Echaniz-Aviles G., Jimenez-Corona A., Sepulveda-Amor J. Aerosolized measles and measles-rubella vaccines induce better measles antibody booster responses than injected vaccines: randomized trials in Mexican schoolchildren. Bull World Health Organ. 80:806-12 (2002).

152. Brown A.R., George D.W., Matteson D.K. Vaccinator device for delivering propellant-driven aerosols of Streptococcus suis bacterin into the respiratory tracts of swine. Vaccine. 15:1165-73 (1997).

153. Cohn M.L., Davis C.L., Middlebrook G. Airborne immunization against tuberculosis. Science. 128:1282-3 (1958).

154. Lefford M.J. Induction and expression of immunity after BCG immunization. Infect Immun. 18:646-53 (1977).

155. Ganguly R., Ogra P.L., Regas S., Waldman R.H. Rubella immunization of volunteers via the respiratory tract. Infect Immun. 8:497-502 (1973).

156. Melnick J.L. Thermostability of poliovirus and measles vaccines. Dev Biol Stand. 87:155-60 (1996).

157. Schwarz L.A., Johnson J.L., Black M., Cheng S.H., Hogan M.E., Waldrep J.C. Delivery of DNA-cationic liposome complexes by small-particle aerosol. Hum Gene Ther. 7:731-41 (1996).

158. Coates A.L., Tipples G., Leung K., Gray M., Louca E. How many infective viral particles are necessary for successful mass measles immunization by aerosol? Vaccine. 24:1578-85 (2006).

159. Degen W.G., Jansen T., Schijns V.E. Vaccine adjuvant technology: from mechanistic concepts to practical applications. Expert Rev Vaccines. 2:327-35 (2003).

160. Seong S.Y., Matzinger P. Hydrophobicity: an ancient damage-associated molecular pattern that initiates innate immune responses. Nat Rev Immunol. 4:469-78 (2004).

161. Marciani D.J. Vaccine adjuvants: role and mechanisms of action in vaccine immunogenicity. Drug Discov Today. 8:934-43 (2003).

162. Lu D., Hickey A.J. Liposomal dry powders as aerosols for pulmonary delivery of proteins. AAPS PharmSciTech. 6:E641-8 (2005).

163. Tyagi P., Wu P.C., Chancellor M., Yoshimura N., Huang L. Recent advances in intravesical drug/gene delivery. Mol Pharm. 3:369-79 (2006).

164. Skalko-Basnet N., Pavelic Z., Becirevic-Lacan M. Liposomes containing drug and cyclodextrin prepared by the one-step spray-drying method. Drug Dev Ind Pharm. 26:1279-84 (2000).

165. Niven R.W., Speer M., Schreier H. Nebulization of liposomes. II. The effects of size and modeling of solute release profiles. Pharm Res. 8:217-21 (1991).

166. Niven R.W., Schreier H. Nebulization of liposomes. I. Effects of lipid composition. Pharm Res. 7:1127-33 (1990).

167. Niven R.W., Carvajal T.M., Schreier H. Nebulization of liposomes. III. The effects of operating conditions and local environment. Pharm Res. 9:515-20 (1992).

168. de Haan A., Tomee J.F., Huchshorn J.P., Wilschut J. Liposomes as an immunoadjuvant system for stimulation of mucosal and systemic antibody responses against inactivated measles virus administered intranasally to mice. Vaccine. 13:1320-4 (1995).

169. Bot A.I., Smith D.J., Bot S., Dellamary L., Tarara T.E., Harders S., Phillips W., Weers J.G., Woods C.M. Receptor-mediated targeting of spray-dried lipid particles coformulated with immunoglobulin and loaded with a prototype vaccine. Pharm Res. 18:971-9 (2001).

170. Crotts G., Park T.G. Protein delivery from poly(lactic-co-glycolic acid) biodegradable microspheres: release kinetics and stability issues. J Microencapsul. 15:699-713 (1998).

171. Shoyele S.A. Controlling the release of proteins/peptides via the pulmonary route. Methods Mol Biol. 437:141-8 (2008).

172. Allison S.D. Analysis of initial burst in PLGA microparticles. Expert Opin Drug

Deliv. 5:615-28 (2008).

173. Kirby D.J., Rosenkrands I., Agger E.M., Andersen P., Coombes A.G., Perrie Y. PLGA microspheres for the delivery of a novel subunit TB vaccine. J Drug Target. 16:282-93 (2008).

174. Jiang G., Joshi S.B., Peek L.J., Brandau D.T., Huang J., Ferriter M.S., Woodley W.D., Ford B.M., Mar K.D., Mikszta J.A., Hwang C.R., Ulrich R., Harvey N.G., Middaugh C.R., Sullivan V.J. Anthrax vaccine powder formulations for nasal mucosal delivery. J Pharm Sci. 95:80-96 (2006).

175. Gupta G.A., Hickey A.J. Contemporary approaches in aerosolized drug delivery to the lung. J. Control. Release. 17:127-147 (1991).

176. Cleland J.L. Design and production of single-immunization vaccines using polylactide polyglycolide microsphere systems. Pharm Biotechnol. 6:439-62 (1995).

177. Hadinoto K., Zhu K., Tan R.B. Drug release study of large hollow nanoparticulate aggregates carrier particles for pulmonary delivery. Int J Pharm. 341:195-206 (2007).

178. Hadinoto K., Phanapavudhikul P., Kewu Z., Tan R.B. Dry powder aerosol delivery of large hollow nanoparticulate aggregates as prospective carriers of nanoparticulate drugs: effects of phospholipids. Int J Pharm. 333:187-98 (2007).

179. Hadinoto K., Cheow W.S. Hollow spherical nanoparticulate aggregates as potential ultrasound contrast agent: shell thickness characterization. Drug Dev Ind Pharm. 35:1167-79 (2009).

180. Hadinoto K. Mechanical stability of hollow spherical nano-aggregates as ultrasound contrast agent. Int J Pharm. 374:153-61 (2009).

181. Lamprecht A., Ubrich N., Hombreiro Perez M., Lehr C., Hoffman M., Maincent P. Biodegradable monodispersed nanoparticles prepared by pressure homogenization-emulsification. Int J Pharm. 184:97-105 (1999).

182. Bivas-Benita M., Romeijn S., Junginger H.E., Borchard G. PLGA-PEI nanoparticles for gene delivery to pulmonary epithelium. Eur J Pharm Biopharm. 58:1-6 (2004).

183. Bivas-Benita M., van Meijgaarden K.E., Franken K.L., Junginger H.E., Borchard G., Ottenhoff T.H., Geluk A. Pulmonary delivery of chitosan-DNA nanoparticles enhances the immunogenicity of a DNA vaccine encoding HLA-A*0201-restricted T-cell epitopes of Mycobacterium tuberculosis. Vaccine. 22:1609-15 (2004).

184. Chao P., Deshmukh M., Kutscher H.L., Gao D., Rajan S.S., Hu P., Laskin D.L., Stein S., Sinko P.J. Pulmonary targeting microparticulate camptothecin delivery system: anticancer evaluation in a rat orthotopic lung cancer model. Anticancer Drugs. 21:65-

185. Louey M.D., Stewart P.J. Particle interactions involved in aerosol dispersion of ternary interactive mixtures. Pharm Res. 19:1524-31 (2002).

186. Steckel H., Bolzen N. Alternative sugars as potential carriers for dry powder inhalations. Int J Pharm. 270:297-306 (2004).

187. Martin A.N., Bustamante P. Physical pharmacy: physical chemical principles in the pharmaceutical sciences. Lea & Febiger, Philadelphia, 1993.

188. Hinds W.C. Aerosol technology: properties, behavior and measurement of airborne particles. J. Wiley, New York, 1999.

189. Yang Y., Bajaj N., Xu P., Ohn K., Tsifansky M.D., Yeo Y. Development of highly porous large PLGA microparticles for pulmonary drug delivery. Biomaterials. 30:1947-53 (2009).

190. Chan H.K. What is the role of particle morphology in pharmaceutical powder aerosols? Expert Opin Drug Deliv. 5:909-14 (2008).

191. Shi S., Hickey A.J. PLGA Microparticles in Respirable Sizes Enhance an In Vitro T Cell Response to Recombinant Mycobacterium Tuberculosis Antigen TB10.4-Ag85B. Pharm Res. (2009).

192. Shi S., Ashley E.S., Alexander B.D., Hickey A.J. Initial characterization of micafungin pulmonary delivery via two different nebulizers and multivariate data analysis of aerosol mass distribution profiles. AAPS PharmSciTech. 10:129-37 (2009).

193. Lodge J.P., Chan T.L. Cascade impactor: sampling and data analysis. American industrial hygiene association, 1986.

194. Christopher D., Adams W.P., Lee D.S., Morgan B., Pan Z., Singh G.J., Tsong Y., Lyapustina S. Product Quality Research Institute evaluation of cascade impactor profiles of pharmaceutical aerosols: part 2--evaluation of a method for determining equivalence. AAPS PharmSciTech. 8:5 (2007).

195. Christopher D., Adams W., Amann A., Bertha C., Byron P.R., Doub W., Dunbar C., Hauck W., Lyapustina S., Mitchell J., Morgan B., Nichols S., Pan Z., Singh G.J., Tougas T., Tsong Y., Wolff R., Wyka B. Product Quality Research Institute evaluation of cascade impactor profiles of pharmaceutical aerosols. Part 3. Final report on a statistical procedure for determining equivalence. AAPS PharmSciTech. 8:E90 (2007).

196. Adams W.P., Christopher D., Lee D.S., Morgan B., Pan Z., Singh G.J., Tsong Y.,

Lyapustina S. Product Quality Research Institute evaluation of cascade impactor profiles of pharmaceutical aerosols, part 1: background for a statistical method. AAPS PharmSciTech. 8:4 (2007).

197. Daffe M. The mycobacterial antigens 85 complex - from structure to function and beyond. Trends Microbiol. 8:438-40 (2000).

198. Wiker H.G., Harboe M. The antigen 85 complex: a major secretion product of Mycobacterium tuberculosis. Microbiol Rev. 56:648-61 (1992).

199. Olsen A.W., van Pinxteren L.A., Okkels L.M., Rasmussen P.B., Andersen P. Protection of mice with a tuberculosis subunit vaccine based on a fusion protein of antigen 85b and esat-6. Infect. Immun. 69:2773 (2001).

200. Renshaw P.S., Lightbody K.L., Veverka V., Muskett F.W., Kelly G., Frenkiel T.A., Gordon S.V., Hewinson R.G., Burke B., Norman J., Williamson R.A., Carr M.D. Structure and function of the complex formed by the tuberculosis virulence factors CFP-10 and ESAT-6. Embo J. 24:2491-8 (2005).

201. Skjot R.L., Brock I., Arend S.M., Munk M.E., Theisen M., Ottenhoff T.H., Andersen P. Epitope mapping of the immunodominant antigen TB10.4 and the two homologous proteins TB10.3 and TB12.9, which constitute a subfamily of the esat-6 gene family. Infect Immun. 70:5446-53 (2002).

202. Bae K., Choi J., Jang Y., Ahn S., Hur B. Innovative vaccine production technologies: the evolution and value of vaccine production technologies. Arch Pharm Res. 32:465-80 (2009).

203. Chawla A., Midha S., Bhatnagar R. Efficacy of recombinant anthrax vaccine against Bacillus anthracis aerosol spore challenge: preclinical evaluation in rabbits and Rhesus monkeys. Biotechnol J. 4:391-9 (2009).

204. Song L., Nakaar V., Kavita U., Tussey L. Efficacious Recombinant Influenza Vaccines Produced by High Yield Bacterial Expression: A Solution to Global Pandemic and Seasonal Needs. PLoS ONE. 3:e2257 (2008).

205. Shi C.H., Fan X.L., Xu Z.K., Li Y., Bai Y.L., Xue Y. Mycobacterium tuberculosis secreting protein Ag85B-ESAT6 fused expression and purification. Zhonghua Jie He He Hu Xi Za Zhi. 27:89-92 (2004).

206. Lakey D.L., Voladri R.K., Edwards K.M., Hager C., Samten B., Wallis R.S., Barnes P.F., Kernodle D.S. Enhanced production of recombinant Mycobacterium tuberculosis antigens in Escherichia coli by replacement of low-usage codons. Infect Immun. 68:233-8 (2000).

207. Baneyx F., Mujacic M. Recombinant protein folding and misfolding in Escherichia

coli. Nat Biotechnol. 22:1399-408 (2004).

208. Mitraki A., King J. Protein Folding Intermediates and Inclusion Body Formation. Nat Biotechnol. 7:690-697 (1989).

209. Adler S., Modrich P. T7-induced DNA polymerase. Requirement for thioredoxin sulfhydryl groups. J Biol Chem. 258:6956-62 (1983).

210. Mukherjee A., Martin S.G. The thioredoxin system: a key target in tumour and endothelial cells. Br J Radiol. 81 Spec No 1:S57-68 (2008).

211. Hall A., Parsonage D., Horita D.A., Karplus P.A., Poole L.B., Barbar E.J. Redox Dependent Dynamics of a Dual Thioredoxin-Fold Protein: Evolution of Specialized Folds. Biochemistry. (2009).

212. LaVallie E.R., DiBlasio E.A., Kovacic S., Grant K.L., Schendel P.F., McCoy J.M. A thioredoxin gene fusion expression system that circumvents inclusion body formation in the E. coli cytoplasm. Biotechnology (N Y). 11:187-93 (1993).

213. Bayer M.E. Areas of adhesion between wall and membrane of Escherichia coli. J Gen Microbiol. 53:395-404 (1968).

214. Cai S., He F., Samra H.S., de la Maza L.M., Bottazzi M.E., Joshi S.B., Middaugh C.R. Biophysical and stabilization studies of the Chlamydia trachomatis mouse pneumonitis major outer membrane protein. Mol Pharm. 6:1553-61 (2009).

215. Clark E.D.B. Protein refolding for industrial processes. Current Opinion in Biotechnology. 12:202-207 (2001).

216. Khan M.A., Sadaf S., Sajjad M., Akhtar M.W. Production enhancement and refolding of caprine growth hormone expressed in Escherichia coli. Protein Expr Purif. (2009).

217. Khalili-Shirazi A., Quaratino S., Londei M., Summers L., Collinge J. Protein Conformation Significantly Influences Immune Responses to Prion Protein. The Journal of Immunology. 174:3256-3263 (2005).

218. Sinha S., Surolia A. Oligomerization Endows Enormous Stability to Soybean Agglutinin: A Comparison of the Stability of Monomer and Tetramer of Soybean Agglutinin. Biophysical Journal. 88:4243-4251 (2005).

219. St John R.J., Carpenter J.F., Randolph T.W. High pressure fosters protein refolding from aggregates at high concentrations. Proc Natl Acad Sci U S A. 96:13029-33 (1999).

220. Seefeldt M.B., Kim Y.S., Tolley K.P., Seely J., Carpenter J.F., Randolph T.W. High-pressure studies of aggregation of recombinant human interleukin-1 receptor

antagonist: thermodynamics, kinetics, and application to accelerated formulation studies. Protein Sci. 14:2258-66 (2005).

221. Lu J.M., Wang X., Marin-Muller C., Wang H., Lin P.H., Yao Q., Chen C. Current advances in research and clinical applications of PLGA-based nanotechnology. Expert Rev Mol Diagn. 9:325-41 (2009).

222. Okada H. One- and three-month release injectable microspheres of the LH-RH superagonist leuprorelin acetate. Adv Drug Deliv Rev. 28:43-70 (1997).

223. Okada H., Toguchi H. Biodegradable microspheres in drug delivery. Crit Rev Ther Drug Carrier Syst. 12:1-99 (1995).

224. Hamishehkar H., Emami J., Najafabadi A.R., Gilani K., Minaiyan M., Mahdavi H., Nokhodchi A. The effect of formulation variables on the characteristics of insulin-loaded poly(lactic-co-glycolic acid) microspheres prepared by a single phase oil in oil solvent evaporation method. Colloids Surf B Biointerfaces. 74:340-9 (2009).

225. Han Y., Tian H., He P., Chen X., Jing X. Insulin nanoparticle preparation and encapsulation into poly(lactic-co-glycolic acid) microspheres by using an anhydrous system. Int J Pharm. 378:159-66 (2009).

226. Kim B.S., Oh J.M., Hyun H., Kim K.S., Lee S.H., Kim Y.H., Park K., Lee H.B., Kim M.S. Insulin-Loaded Microcapsules for In Vivo Delivery. Mol Pharm. (2009).

227. Watts P.J., Davies M.C., Melia C.D. Microencapsulation using emulsification/solvent evaporation: an overview of techniques and applications. Crit Rev Ther Drug Carrier Syst. 7:235-59 (1990).

228. Wu X.S. Preparation, characterization, and drug delivery applications of microspheres based on biodegradable lactide/glycolide polymers. In: Wise (eds.), Encyclopedic handbook of biomaterials and bioengineering, Marcel Dekker, New York, 1995, p. 1151-1200.

229. Vehring R. Pharmaceutical particle engineering *via* spray drying. Pharm Res. 25:999-1021 (2007).

230. Arshaday R. Preparation of biodegradable microspheres and microcapsules: 2. Polylactides and releated polyesters. J. Control. Release. 17:1-22 (1991).

231. Cohen-Sela E., Teitlboim S., Chorny M., Koroukhov N., Danenberg H.D., Gao J., Golomb G. Single and double emulsion manufacturing techniques of an amphiphilic drug in PLGA nanoparticles: formulations of mithramycin and bioactivity. J Pharm Sci. 98:1452-62 (2009).

232. Morlock M., Kissel T., Li Y.X., Koll H., Winter G. Erythropoietin loaded

microspheres prepared from biodegradable LPLG-PEO-LPLG triblock copolymers: protein stabilization and in-vitro release properties. J Control Release. 56:105-15 (1998).

233. Pean J.M., Venier-Julienne M.C., Boury F., Menei P., Denizot B., Benoit J.P. NGF release from poly(D,L-lactide-co-glycolide) microspheres. Effect of some formulation parameters on encapsulated NGF stability. J Control Release. 56:175-87 (1998).

234. Hickey A.J., Mansour H.M., Telko M.J., Xu Z., Smyth H.D., Mulder T., McLean R., Langridge J., Papadopoulos D. Physical characterization of component particles included in dry powder inhalers. II. Dynamic characteristics. J Pharm Sci. 96:1302-19 (2007).

235. Hickey A.J., Mansour H.M., Telko M.J., Xu Z., Smyth H.D., Mulder T., McLean R., Langridge J., Papadopoulos D. Physical characterization of component particles included in dry powder inhalers. I. Strategy review and static characteristics. J Pharm Sci. 96:1282-301 (2007).

236. Telko M.J., Hickey A.J. Critical assessment of inverse gas chromatography as means of assessing surface free energy and acid-base interaction of pharmaceutical powders. J Pharm Sci. 96:2647-54 (2007).

237. Carr R.L. Evaluating flow properties of solids. Chem. Eng. 72:163-168 (1965).

238. Wells J.I. Pharmaceutical preformulation: the physicochemical properties of drug substances. Wiley, New York, 1988.

239. Stolnik S., Garnett M.C., Davies M.C., Illum L. The colloidal properties of surfactant-free biodegradable nanospheres from poly(β-malic acid-co-benzyl malate)s and poly(lactic acid-co-glycolide). Colloids and Surfaces A. 97:235-245 (1995).

240. Hirota K., Hasegawa T., Hinata H., Ito F., Inagawa H., Kochi C., Soma G., Makino K., Terada H. Optimum conditions for efficient phagocytosis of rifampicin-loaded PLGA microspheres by alveolar macrophages. J Control Release. 119:69-76 (2007).

241. O'Hara P., Hickey A.J. Respirable PLGA microspheres containing rifampicin for the treatment of tuberculosis: manufacture and characterization. Pharm Res. 17:955-61 (2000).

242. Shi S., Hickey A.J. Multivariate Data Analysis as a Semi-quantitative Tool for Interpretive Evaluation of Comparability or Equivalence of Aerodynamic Particle Size Distribution Profiles. AAPS PharmSciTech. (2009).

243. Dos Santos D.F., Nicolete R., de Souza P.R., Bitencourt C.D., Dos Santos Junior R.R., Bonato V.L., Silva C.L., Faccioli L.H. Characterization and in vitro activities of cell-

free antigens from Histoplasma capsulatum-loaded biodegradable microspheres. Eur J Pharm Sci. (2009).

244. Wang C., Muttil P., Lu D., Beltran-Torres A.A., Garcia-Contreras L., Hickey A.J. Screening for potential adjuvants administered by the pulmonary route for tuberculosis vaccines. Aaps J. 11:139-47 (2009).

245. Nastasovic A.B., Onjia A.E. Determination of glass temperature of polymers by inverse gas chromatography. J Chromatogr A. 1195:1-15 (2008).

246. Surana R., Randall L., Pyne A., Vemuri N.M., Suryanarayanan R. Determination of glass transition temperature and in situ study of the plasticizing effect of water by inverse gas chromatography. Pharm Res. 20:1647-54 (2003).

247. Jones B.G., Dickinson P.A., Gumbleton M., Kellaway I.W. Lung surfactant phospholipids inhibit the uptake of respirable microspheres by the alveolar macrophage NR8383. J Pharm Pharmacol. 54:1065-72 (2002).

248. Evora C., Soriano I., Rogers R.A., Shakesheff K.N., Hanes J., Langer R. Relating the phagocytosis of microparticles by alveolar macrophages to surface chemistry: the effect of 1,2-dipalmitoylphosphatidylcholine. J Control Release. 51:143-52 (1998).

249. Jones B.G., Dickinson P.A., Gumbleton M., Kellaway I.W. The inhibition of phagocytosis of respirable microspheres by alveolar and peritoneal macrophages. Int J Pharm. 236:65-79 (2002).

250. Sugiyama K., Mitsuno S., Shiraishi K. Adsorption of protein on the surface of thermosensitive poly(methyl methacrylate) microspheres modified with the N-(2-hydroxypropyl)methacrylamide and 2-(methacryloyloxy)ethyl phosphorylcholine moieties. J. Polymer. Sci: Part A: Polymer Chem. 35:3349-3357 (1996).

251. Dye C., Lonnroth K., Jaramillo E., Williams B.G., Raviglione M. Trends in tuberculosis incidence and their determinants in 134 countries. Bull World Health Organ. 87:683-91 (2009).

252. Sousa A.O., Mazzaccaro R.J., Russell R.G., Lee F.K., Turner O.C., Hong S., Van Kaer L., Bloom B.R. Relative contributions of distinct MHC class I-dependent cell populations in protection to tuberculosis infection in mice. Proc Natl Acad Sci U S A. 97:4204-8 (2000).

253. D'Souza C.D., Cooper A.M., Frank A.A., Ehlers S., Turner J., Bendelac A., Orme I.M. A novel nonclassic beta2-microglobulin-restricted mechanism influencing early lymphocyte accumulation and subsequent resistance to tuberculosis in the lung. Am J Respir Cell Mol Biol. 23:188-93 (2000).

254. Rolph M.S., Raupach B., Kobernick H.H., Collins H.L., Perarnau B., Lemonnier F.A.,

Kaufmann S.H. MHC class Ia-restricted T cells partially account for beta2-microglobulin-dependent resistance to Mycobacterium tuberculosis. Eur J Immunol. 31:1944-9 (2001).

255. van Pinxteren L.A., Cassidy J.P., Smedegaard B.H., Agger E.M., Andersen P. Control of latent Mycobacterium tuberculosis infection is dependent on CD8 T cells. Eur J Immunol. 30:3689-98 (2000).

256. Canaday D.H., Gehring A., Leonard E.G., Eilertson B., Schreiber J.R., Harding C.V., Boom W.H. T-cell hybridomas from HLA-transgenic mice as tools for analysis of human antigen processing. J Immunol Methods. 281:129-42 (2003).

257. Kerr M.C., Teasdale R.D. Defining macropinocytosis. Traffic. 10:364-71 (2009).

258. Eyles J.E., Carpenter Z.C., Alpar H.O., Williamson E.D. Immunological aspects of polymer microsphere vaccine delivery systems. J Drug Target. 11:509-14 (2003).

259. Westwood A., Healey G.D., W.E. D., Eyles J.E. Activation of dendritic cells after microparticulate uptake. Proceedings of the 30th Annual Meeting of the Controlled Release Society. 30:4 (2003).

260. Hickey A.J. Pulmonary Drug Delivery-Pharmaceutical Chemistry and Aerosol Technology. In B. Wang, T. Siahaan, and R. Soltero, eds. Delivery Issues in Drug Discovery. John Wiley and Sons, New York. (2005).

261. Hickey A.J., Kazantseva M., Garcia-Contreras L. Debugging the lungs: the use of therapeutic aerosols in the treatment of pulmonary infectious diseases. In S.R. Smith, F. Paul-Aviles, and J. Liu, eds. Pharmaceutical Approaches to Infectious Disease Therapy. Davis Horwood International, Godalming, UK. 67-93 (2002).

262. Hickey A.J. Summary of common approaches to pharmaceutical aerosol administration. In A.J. Hickey, ed. Pharmaceutical Inhalation Aerosol Technology, 2nd ed. Marcel Dekker, New York. 385-421 (2004).

263. Tsong Y. Statistical comparison of particle size distribution profiles. 2004; Available at: http://pqri.org/commworking/minutes/pdfs/dptc/psdpcwg/Addl/DC01-475116-v2-Yi_Tsong_Statistical_Archive_PQRI_Profile_Comparisons.DOC. Accessed June 22, 2007.

264. DeLuca P.P., Lyapustina, S. Product Quality Research Institute reports. AAPS PharmSciTech [serial online]. 2007;8:article 6.

265. Eriksson L., Johansson E., Kettaneh-Wold N., Trygg J., Wikstrom C., Wold S. Multi- and Megavariate Data Analysis. Part 1. Basic Principles and Applications. Second Revised and Enlarged Edition. Umetrics Academy. 2006.

266. Rochfort S. Metabolomics reviewed: a new "omics" platform technology for systems biology and implications for natural products research. J Nat Prod. 68:1813-20 (2005).

267. van den Berg R.A., Hoefsloot H.C., Westerhuis J.A., Smilde A.K., van der Werf M.J. Centering, scaling, and transformations: improving the biological information content of metabolomics data. BMC Genomics. 7:142 (2006).

268. Noda I. Scaling techniques to enhance two-dimensional correlation spectra. Journal of Molecular Structure. 883:216-227 (2008).